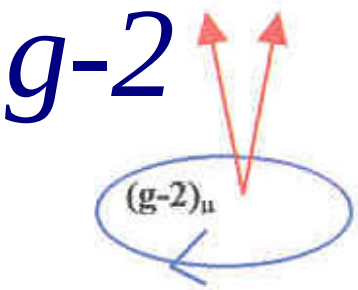

Brookhaven National Laboratory

Brookhaven Science Associates

Upton, New York 11973

Muon g-2 Note No. 388

Title: **ν_a Analysis of the 1999 Data**

Author(s): **Alexei Trofimov**

Affiliation: **Boston University**

Date: **January 15, 2001**

ω_a Analysis of the 1999 Data

Alexei Trofimov
Boston University
January 15, 2001

Abstract

This note describes the ω_a analysis of the data taken during the 1999 run, mainly focusing on the results of the fit with a 17-parameter function. The data selection process, correction for energy scale changes, fitting and other relevant procedures are summarized. The results are compared for different energy cuts, forms of fitting function, with and without pile-up subtraction. The final value of R is given as $143.25 \pm 1.24 \pm 0.22$ ppm.

1 Introduction

This note is an overview of my work on the analysis of the 1999 data (`g2off` version). Most results given here were presented at the collaboration meetings at BNL in September and November,2000.

The principal difference between this and other analyses is that, for the most studies presented here no pile-up subtraction had been applied, which required increasing the number of parameters in the fitting function. Also, most systematic studies and some of the data selection procedures were performed independently from other analyses.

In section 2, I describe the data selection process. Section 3 outlines the fitting procedure. The fit results are given in section 4, and the systematic errors are discussed in section 5. The last section summarizes the results and conclusions. Appendices A and B contain an overview of my pile-up and energy scale change studies with real and simulated data.

2 Data Selection

2.1 Run and Spill Selection

The data runs used in this analysis were selected by Ernst Sichtermann. All runs with laser, LED, high "flashlet" contamination, early-to-late time instabilities in positron energy and decay spectra etc. were eliminated from the available run list. In total, 806 runs between run number 3813 and 5093 met the selection criteria. Detectors 2 and 20, notorious for their hardware problems, were not used in this analysis. At Ernst's suggestion, a number of runs were dropped from the selection for individual detectors: 18 (runs 3903 - 4139 dropped) and 14 (4790 - 4796). The data used were produced with `g2off` at BNL and stored in the form of standard ntuples [1].

Within the selected range of runs, cuts were applied to every data spill (corresponding to a single-time beam injection into the g-2 storage ring). A spill would be dropped if a quadrupole trace was not read out, or the trace was shorter than 780 μs (a possible spark), or the difference between medium- and late-time or early- and medium-time amplitudes was greater than 15 counts (another indication of a spark). An entire "event" (all 6 spills from the same AGS cycle) would be dropped if t0 counter signal was not read out, or had an insufficient amplitude (misfired injection, causing higher "flashlet" contamination in subsequent spills) in any spill, aka "`T0STAT` cut".

Losses due to these cuts were: 1.6% of the total number of spills for the t0 cut, and 0.4% for the quad cut. A large fraction of spill losses was due to t0 or quad read-out problems in a small number of runs (Fig.1). Runs afflicted by read-out trouble were dropped (5024, 5025 had no t0, runs 3857, 3908-3911 and 4810 had no QUAD information). In addition to this, 4% of the spills contained no data. (Cenap included these into his calculation of losses due to the t0-cut [2]).

It was also found that beginning with run 4567, the last (6^{th}) spill was often missing from the ntuples for detectors 1 through 8. This caused a 4.5% difference in the number of good spills between detectors 1-8 and 9-24 (the numbers were respectively 2.57 and 2.69 million spills).

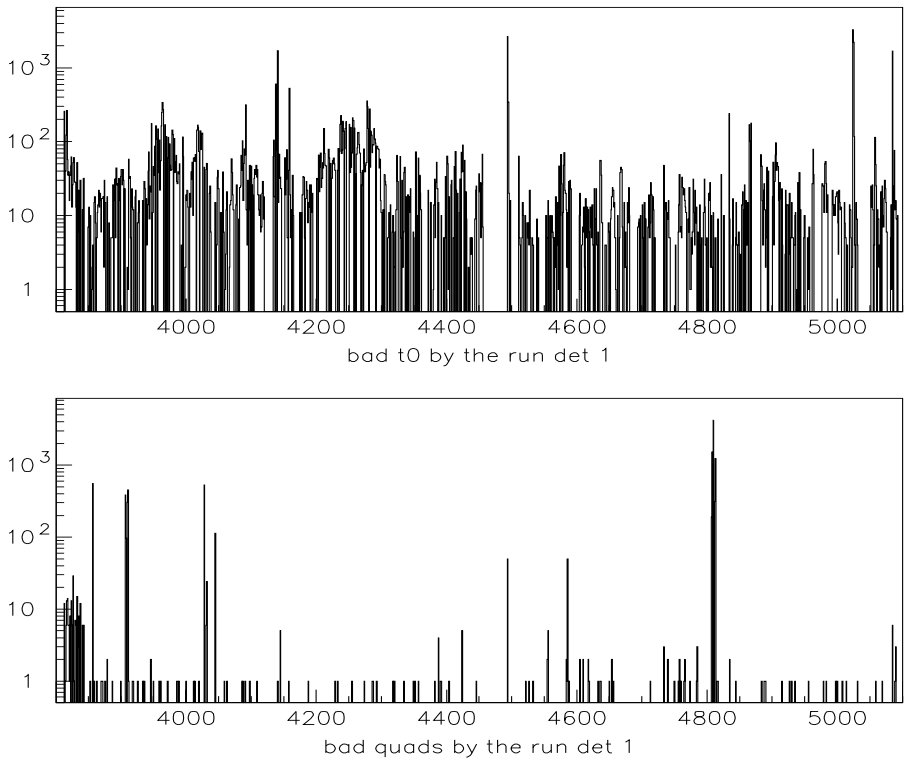

Fig.1. Number of fills with t0 (top) and quadrupole (bottom) problems, by the run. About 2% of all fills with data were dropped due to these cuts.

2.2 Energy Calibration

The end-points of the energy distribution were fitted individually for every detector in each of the selected runs. A section of the energy-distribution slope was fitted to a straight line. The linear fitted section was chosen individually for each detector due to differences in the form of the energy spectrum. It was usually a section corresponding to the positron energies between 70% and 93% of the pre-fitted spectrum energy maximum (or between 2.2 and 2.9 GeV). The crossing of the fit-line with x-axis, the end-point was assumed to correspond to positron energy of 3.1 GeV. This technique was used in the 1998 ω_a analysis [3], with its validity established in a simulation. An example is given on Fig.2.

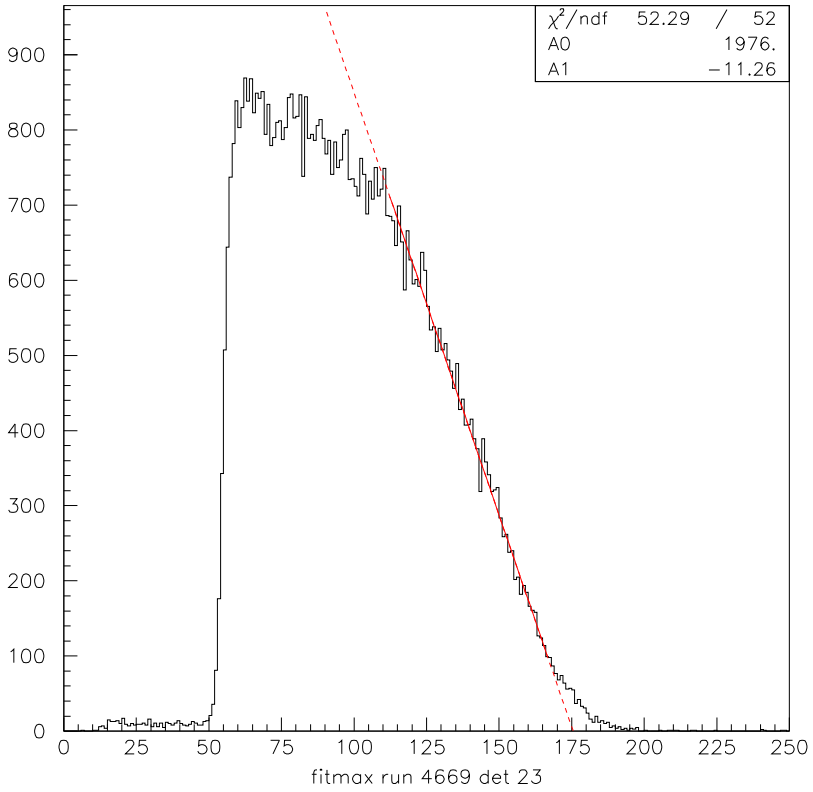

Fig.2. An example of endpoint fitting (detector 23 in run 4669): x-axis is positron energy in WFD-counts.

The energy spectra for end-point fitting were taken at late time (at least 100 μs after the injection) in order to minimize the effects of pile-up and energy-scale changes (caused by PMT and "off-line" reconstruction instabilities) at earlier time. The end-point values for each detector were then averaged over groups of runs, as illustrated in figures 4 ("stable" detector 8) and 5 (detector 1, which had been recalibrated during the run).

For this analysis, only the positrons with energies greater than 1.8 GeV (58.1% of the endpoint energy) were used. Most detectors required subdivision into only 2-3 groups, except for detector 9, which had 9 groups due to instability of the energy scale (Fig.3).

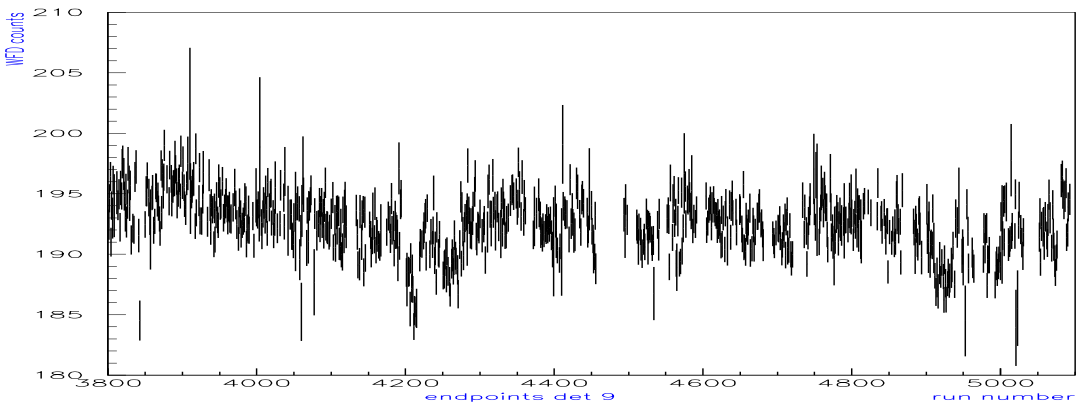

Fig.3. End-points for detector 9 drifted around a lot.

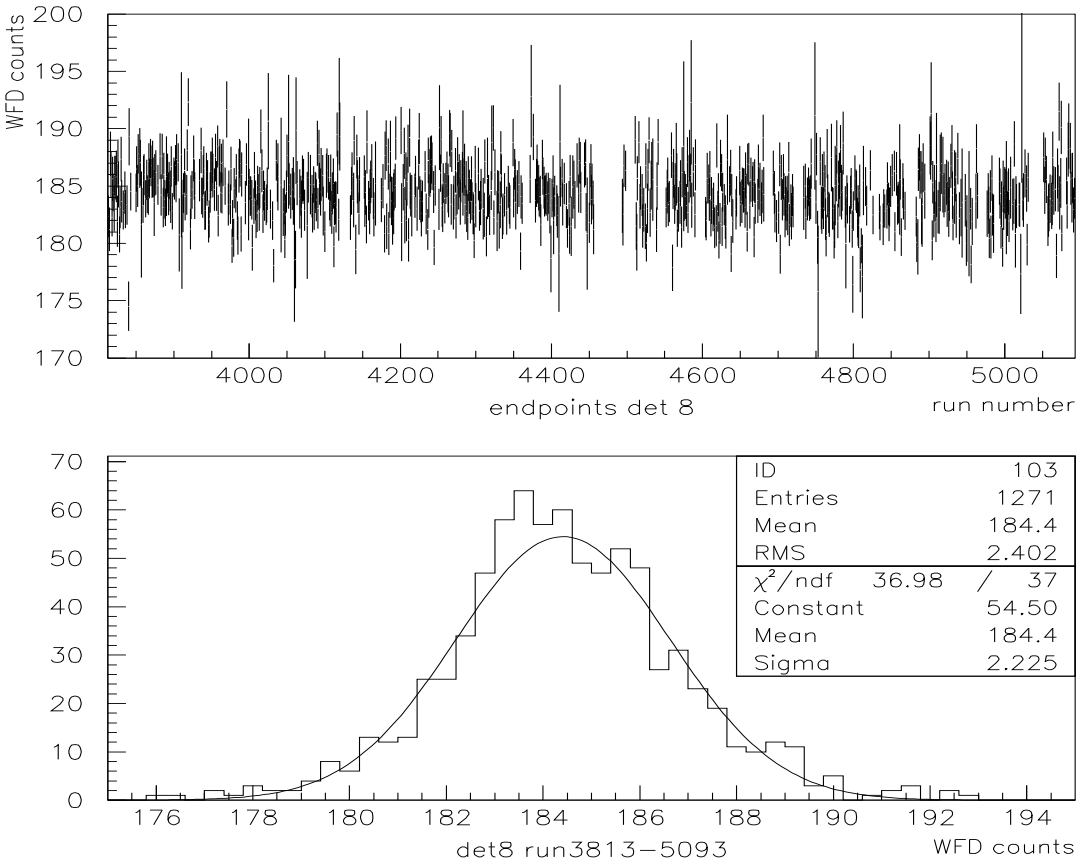

Fig.4. Detector 8 shows very little run-to-run instability in energy scale: (top) End-point values (in WFD-counts) for detector 8 by run number (given with errors: occasional large error bars come from runs with low statistics) ; (bottom) the distribution of end-points has a gaussian form.

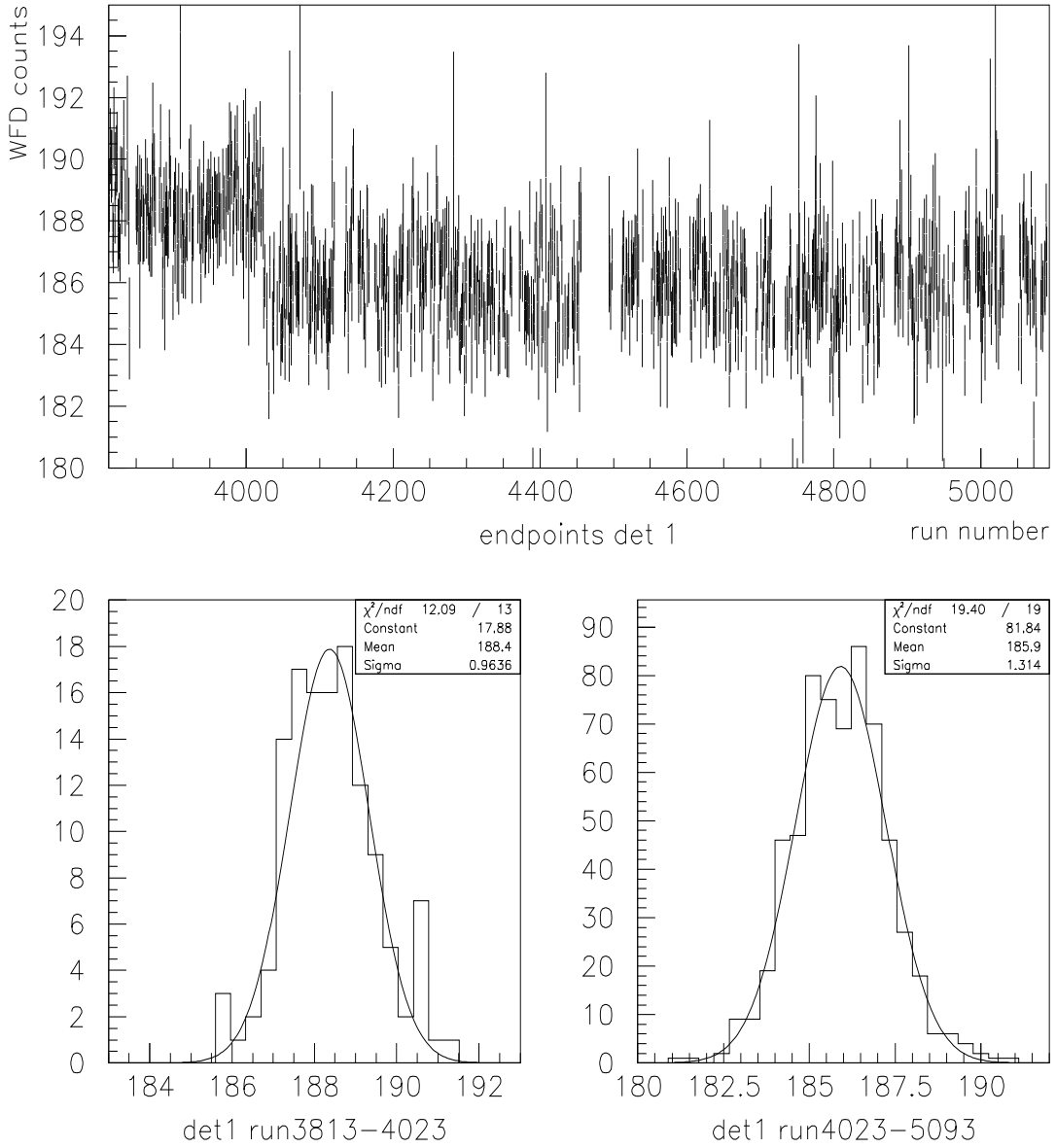

Fig.5. Detector 1 had a 2% step in the energy scale after run 4023: (top) End-point values (in WFD-counts) for detector 1 by run number (given with errors: occasional large error bars come from runs with low statistics) ; the distribution of end-points has a gaussian form for both groups of runs, before (bottom left) and after (bottom right) the recalibration occurred.

2.3 Correction for Energy Scale Change (ESC)

Time-dependent ESC was investigated by looking at the time-dependent change in the average of the energy distribution. The procedure is described in Appendix A.

Only 6 detectors were found to have E-scale of the order of 0.1% or higher at 30 μs (see Fig.6a). In another group consisting of 8 detectors (those shown in Fig.6b and also dets 18,21), the scale change was less than 0.1% by 25 μs after the injection. Detectors 3, 6, 7, 10, 13-15, and 17 had no visible effect. The evolution of energy scale change with time could be described as an exponentially decreasing function, except for in the case of detectors 1 and 4, which required an additional gaussian-like term:

$$f_e(t) = g \cdot e^{-\frac{t}{\tau_g}} + a_g e^{-\frac{1}{2}(\frac{t-t_0}{\sigma})^2} \quad (1)$$

The results of these studies are summarized in Table 1.

Table 1. Results of ESC studies. Columns 2-6 contain parameter values from fit with a function (1). The number in column 7 is the amplitude of ESC at 30 μs. And $t_{0.1\%}$ (column 8) is the time after injection, when ESC becomes smaller than 0.1%. A "Y" in the last column signifies that a time-variable energy cut was used in the pulse selection process for that detector, to compensate for the changes in the energy scale.

Det	g (%)	τ_g (μs)	a_g(%)	t_0(μs)	σ(μs)	shift at 30 μs (%)	$t_{0.1\%}$, μs,	"bad"?
1*	-2.629	28.17	1.601	25.61	9.411	0.530	92.1	Y
3	N/A							
4*	-5.45	14.36	0.183	44.52	9.84	-0.613	42.7	Y
5	-1.133	15.21				-0.158	37.0	Y
6	N/A							
7	N/A							
8	1.540	15.49				0.222	42.4	Y
9	1.984	7.48				0.036	22.4	
10	N/A							
11	1.121	9.67				0.050	23.4	
12	0.907	13.50				0.098	29.8	Y
13	N/A							
14	N/A							
15	N/A							
16	0.729	7.81				0.015	15.6	
17	N/A							
18	1.047	10.12				0.054	23.8	
19	0.714	9.00				0.025	17.7	
21	1.702	5.64				0.008	16.0	
22	1.403	8.52				0.041	22.5	
23	1.271	7.92				0.028	20.2	
24	1.959	9.93				0.095	29.6	Y

* Detectors 1 and 3 were fitted to a 5-parameter function (Eq.1).

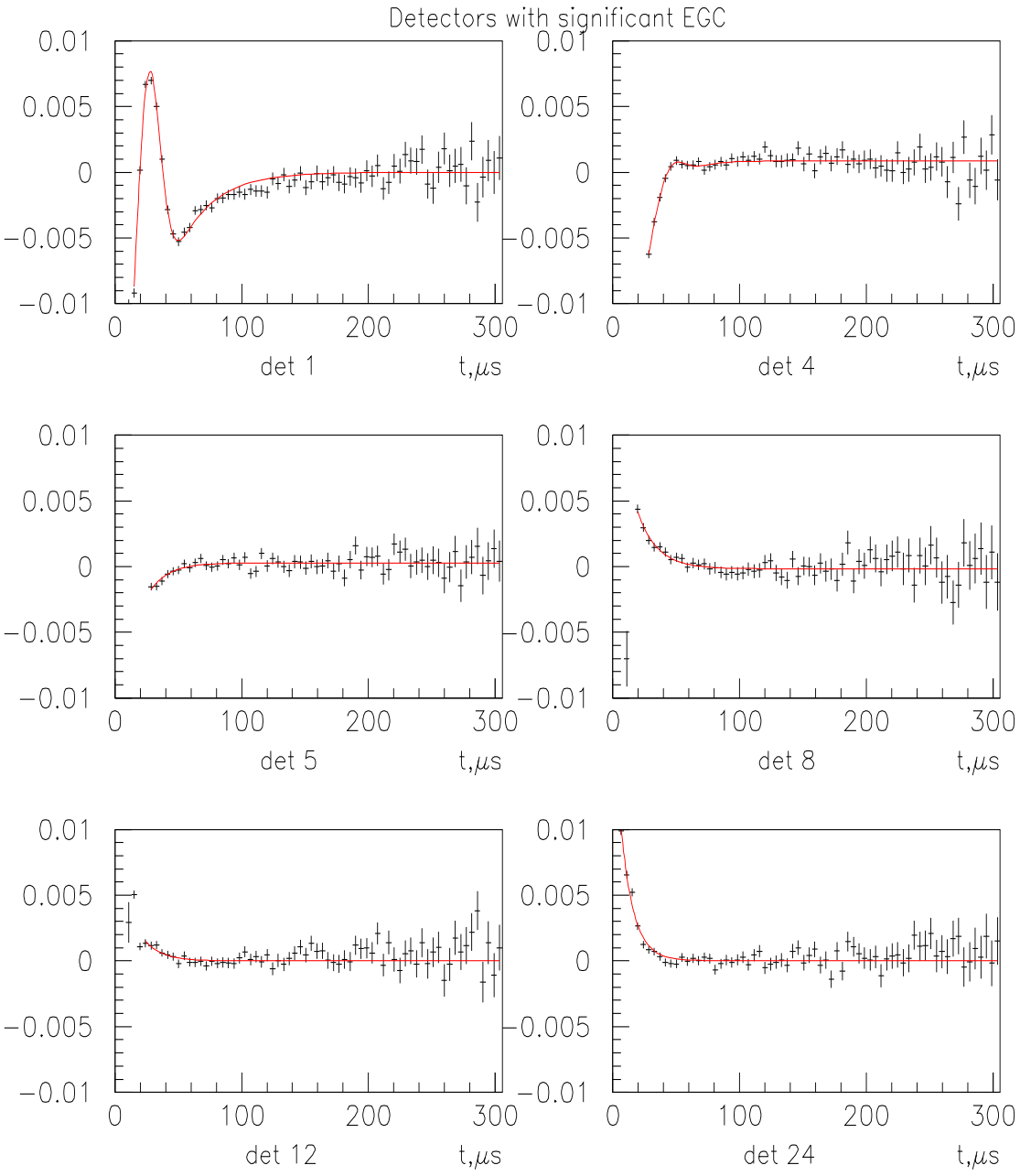

Fig.6a. Detectors 1,4,5,8,12,24 all show significant ESC effect at 30 μs. On the y-axis: relative change in the energy scale (0.01 corresponds to 1%)

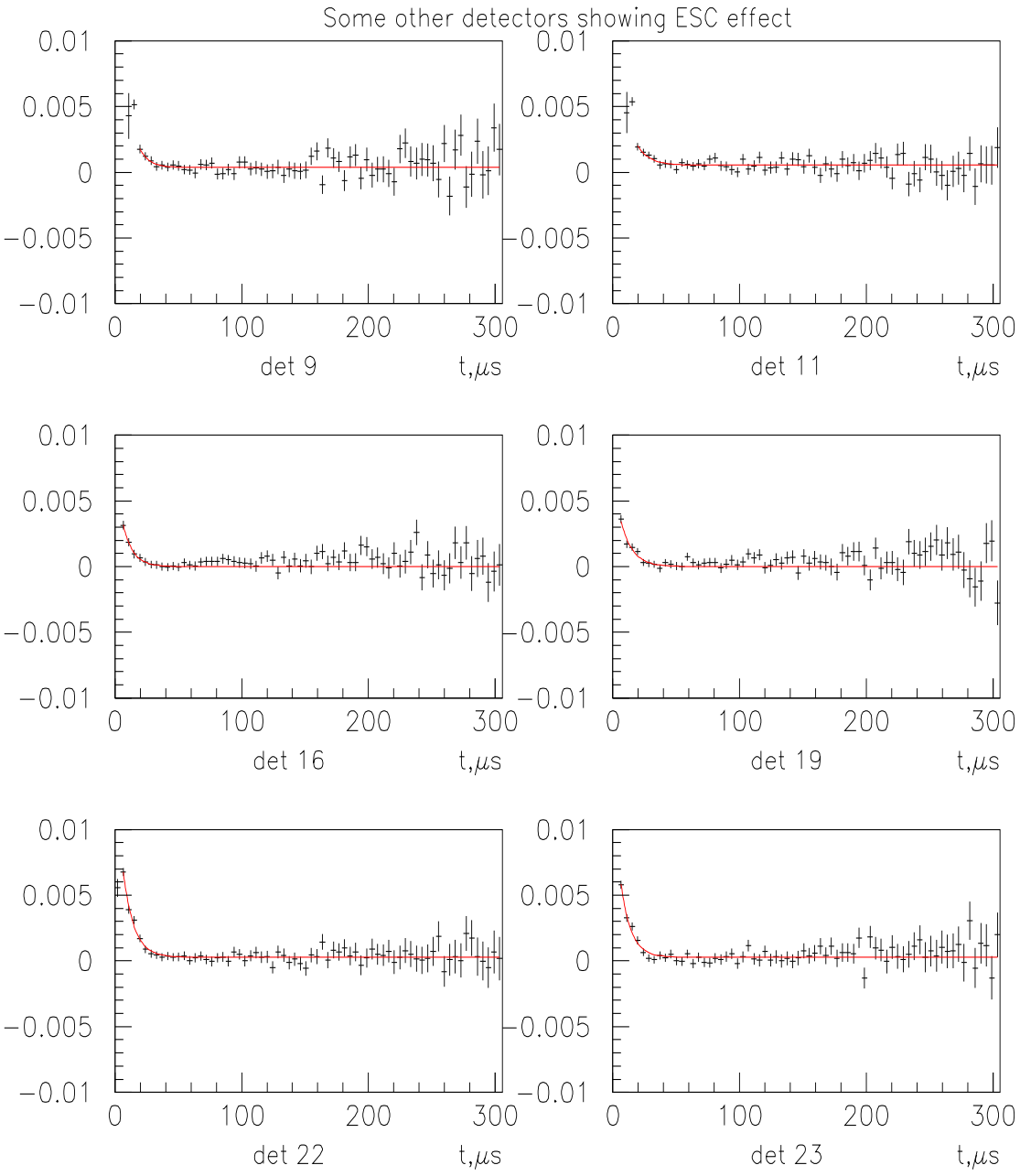

Fig.6b. Some other detectors are obviously affected by ESC, but the effect is less than 0.1% after 25 μs. On the y-axis: relative change in the energy scale (0.01 corresponds to 1%)

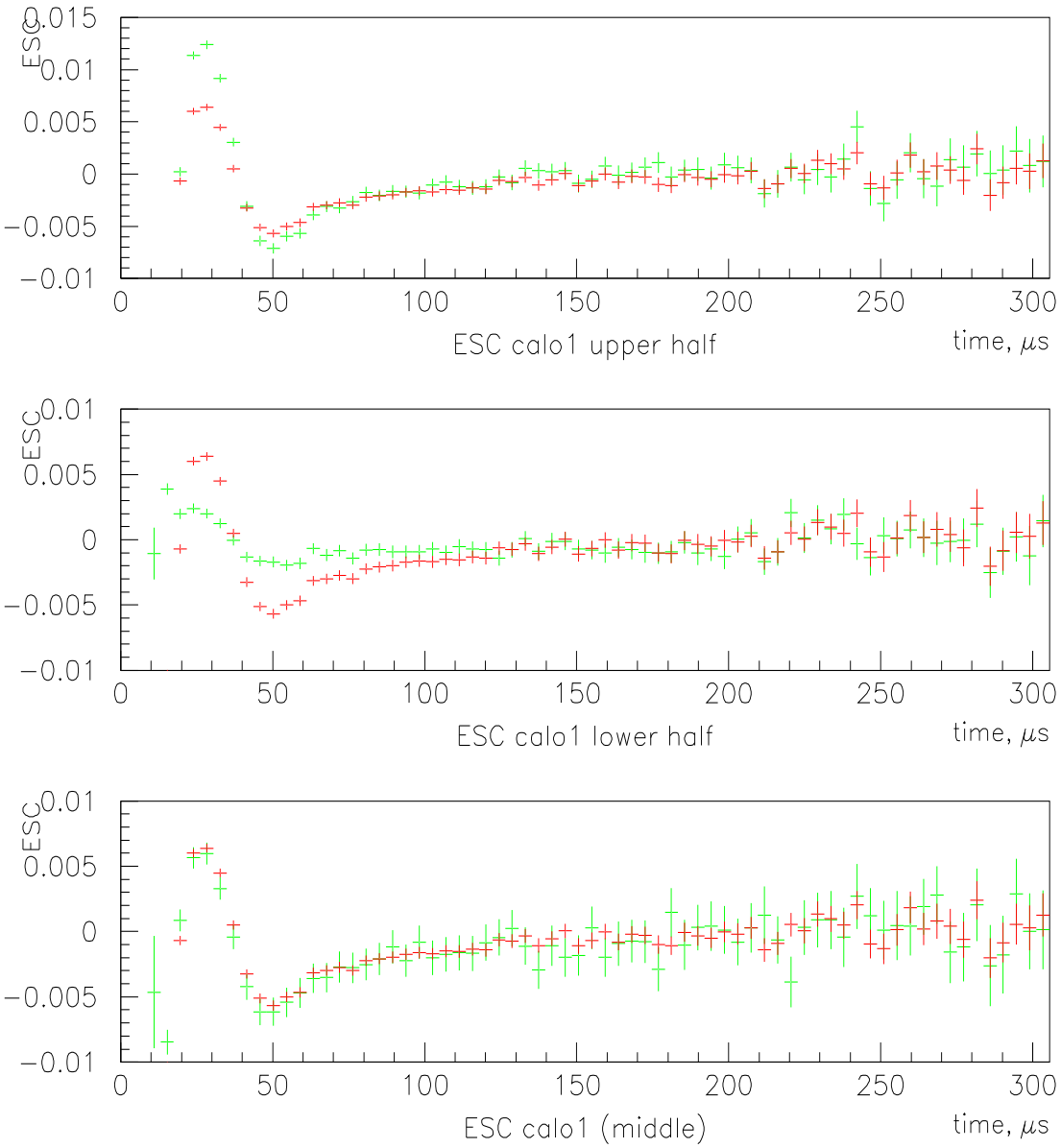

Fig.7a. More ESC studies for detector 1. In green, the energy scale change is plotted for three different groups of pulses: those that produced a trigger only in the upper half quadrants of the calorimeter (top plot), only in the lower half quadrants (middle plot), and both (bottom plot). In red, the result is given for all pulses together. This study confirms that the observed ESC came from a single "Özben" calorimeter tube, corresponding to the front upper-half quadrant. The residual "Özben-wiggle" is still present in the data from the lower half due to the limitations in the trigger-cut efficiency.

As was established recently, the ESC in detector 1 was mainly due to a single calorimeter tube. A more detailed ESC study for this detector (Fig.7a.) shows that the upper half of the calorimeter was seeing about twice the average energy scale change, while the effect was very small in the lower half. As will be shown in Sections 4.2, 5.3. The average ESC still can be a good approximation, even if the effect is different for different calorimeter quadrants.

In detector 4, another one showing a big ESC effect, the difference between the upper and lower parts was statistically insignificant. (Fig.7b.)

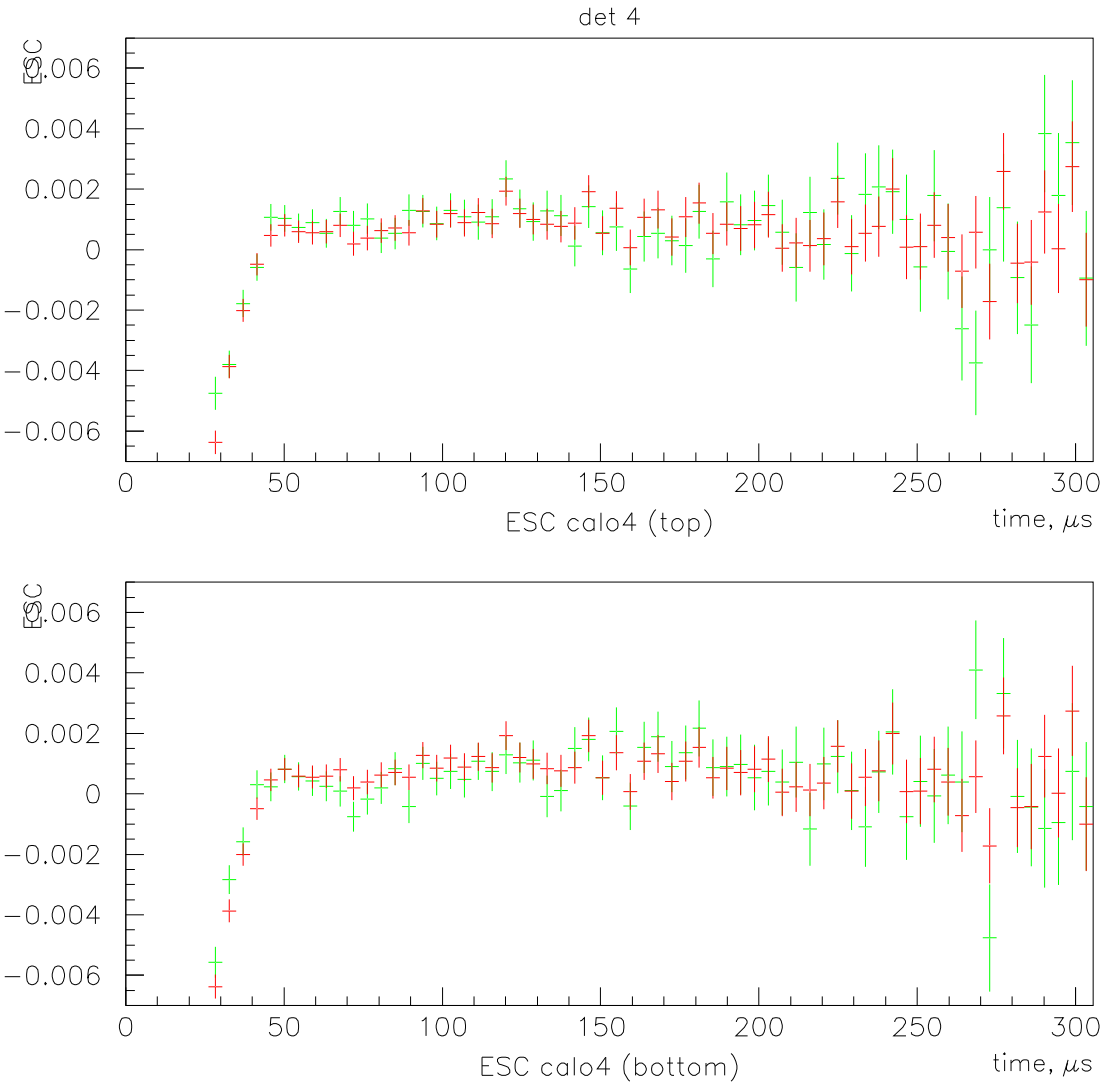

Fig.7b. In detector 4, there is no significant difference in the energy scale change between the upper and lower halfs of the calorimeter. The results for the halfs separately are plotted in green, and the average over the detector is in red.

2.4 Histograms

The g-2 time spectrum histograms had 5000 bins each, with a bin width of 149.185 ns.

The histograms were filled in for two different energy thresholds: 1.8 and 2 GeV (or $0.581 \cdot E_{max}$ and $0.645 \cdot E_{max}$). Double precision description of pulse times was used to minimize the effects of rounding of histogram bin boundaries in PAW.

For detectors 1, 4, 5, 8, 12, 24 a time-variable threshold was used, to minimize the effect of energy scale change (Fig.8).

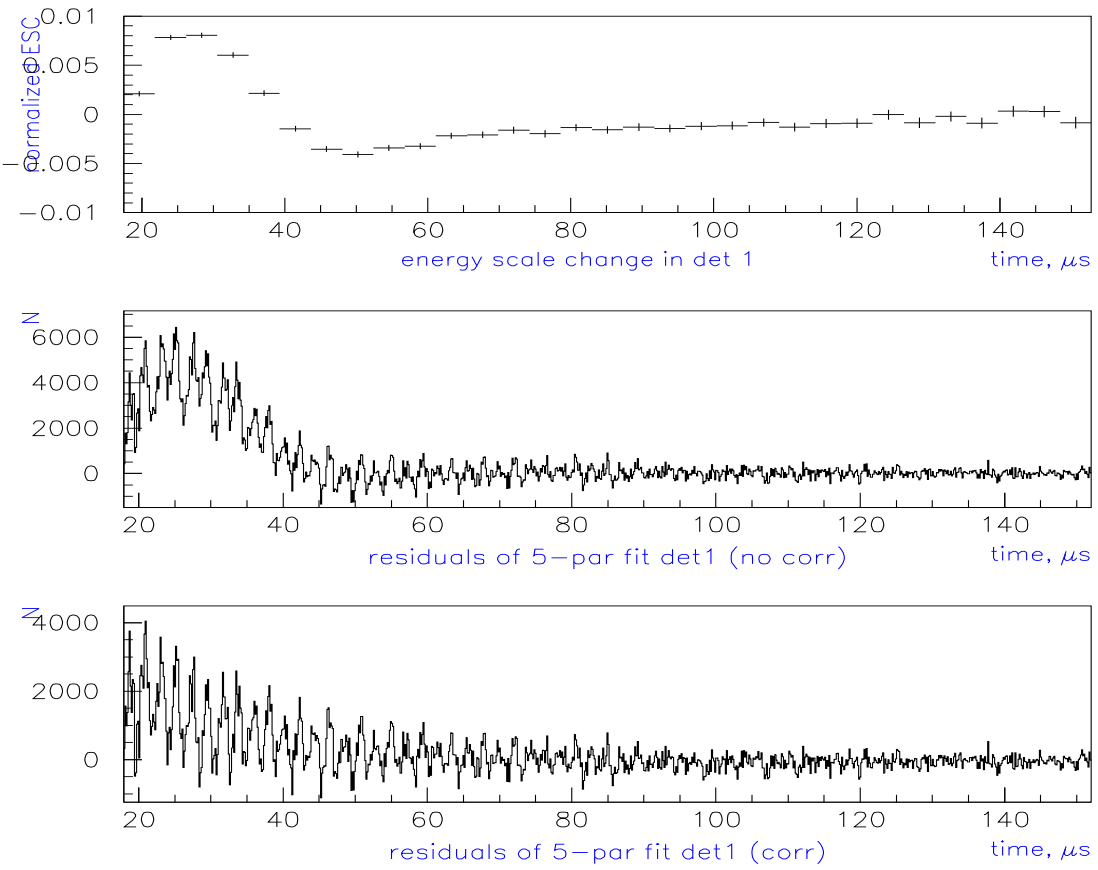

Fig.8. Application of a time-variable threshold removes the effect of the energy scale change. Top: ESC in detector 1 (from ESC studies). Middle: Spectrum of 5-parameter fit residuals before the correction was applied. Bottom: after the ESC correction was applied, the residuals are mostly contributed to by the coherent betatron oscillation, muon losses and pile-up.

Injection time for each spill was randomized within the bin width, to minimize the effect of fast rotation [3,4]. 10 different random seeds were used (10 time spectra created).

Detector phases were aligned within ± 2 ns (at 50 μs) after these phases were determined from fit. In other words, each detector had a different time offset with respect to the injection time to compensate for differences in cable lengths etc. The offsets were calculated with respect to detector 16, and varied between -3.4 ns (det.21) and 17.7 ns (det.5).

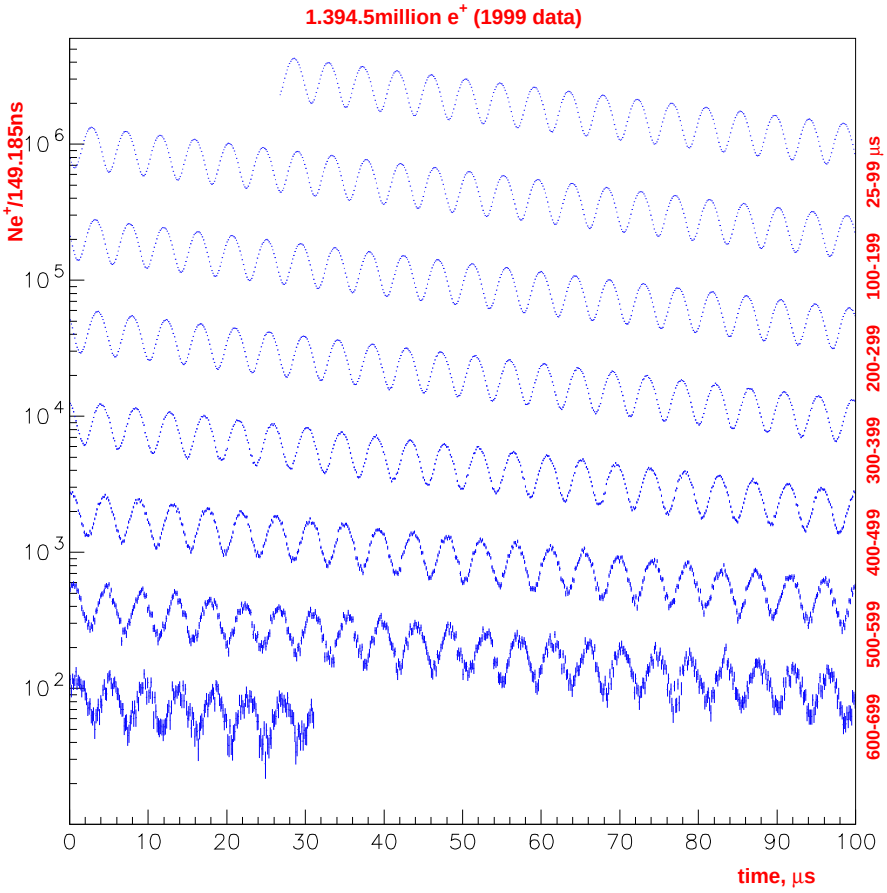

Fig.9. G-2 time spectrum for positrons with E>1.8 GeV (1999 data).

3 Fitting Procedure

To perform the fits, I used a modification of the `FORTRAN/MINUIT` program developed by Jörg Pretz for his 1998 analysis [4], which included successive fitting with packages `MIGRAD`, `HESSE`, `IMPROVE` and `MINOS`. `MIGRAD` is a χ^2 minimization algorithm, using Davidon-Fletcher-Powell variable-metric technique. `HESSE` is called by `MIGRAD` to recalculate the error matrices at the minimum. `IMPROVE` attempts to find a new local minimum in the vicinity of the one found by `MIGRAD`. And `MINOS` performs a better evaluation of fitting errors, taking into account possible non-linearities around the minimum [5]. All fits were performed using the square root of the bin value (first step), and then the square root of fitting function (all subsequent steps) as an error estimate.

3.1 Fitting Function

The data were fitted to a 17 parameter function of the form:

$$N(t) = N_0 \cdot \left(e^{-\lambda t} \cdot (1 + A \cdot \cos[\omega_a t + \phi]) + e^{-2\lambda t} \cdot f_p(t) \cdot f_{fr}(t)\right) \cdot f_{CBO}(t) \cdot f_X(t) \qquad (2)$$

where $\omega_a = 2\pi f_0\left(1 - (R - \Delta) * 10^{-6}\right)$, with f_0 = 229.1 kHz, and the offset of Δ; the

term describing the pile-up contribution is:

$$f_p(t) \;=\; n_p \;+\; A_p \cdot \cos(\omega_a t \;+\; \phi \;+\; \Delta\phi_p) \qquad (3)$$

multiplied by a fast rotation correction to pile-up of the form:

$$f_{fr}(t) \qquad = \qquad 1 \;+\; a_p \;\cdot\; e^{-\frac{1}{2}(\frac{t}{\tau_p})^2} \qquad (4)$$

Coherent betatron oscillation (CBO) correction:

$$f_{CBO}(t) = 1+A_B\cdot\cos(\omega_B t+\phi_B)\cdot e^{-(\frac{t-t_{0B}}{\tau_B})^2} \qquad (5)$$

And a correction for lost particles and other background:

$$f_X(t) \qquad = \qquad 1 \;+\; a_X \;\cdot\; e^{-\frac{1}{2}(\frac{t}{\tau_X})^2} \qquad (6)$$

$$\left(or \quad f_X(t) \;=\; 1 \;+\; a_X \;\cdot\; e^{-\frac{t}{\tau_X}}\right) \qquad (6a)$$

Four parameters out of 17 were fixed at all times:

- the difference between the g-2 and pile-up phases, $\Delta\phi_p$ = 0 (some $\Delta\phi_p$ estimates from pile-up subtracted spectra were used as well);
- parameters of pile-up amplification due to fast rotation: a_p = 0.72, τ_p=12.7 μs (from simulation and fits to real data: see appendices A and B).
- $t_{0B} = 0$, the mean time of the CBO packet.

Letting $\Delta\phi_p$ vary increases the error on R two-fold [6]. And the parameters describing the fast rotation correction to pile-up, if let vary freely, cause fit instabilities due to small size and short life time of this correction.

For the purposes of making the multi-parameter fit more stable at late start times, some parameters were allowed to vary at earlier start times only. These include: a_X and τ_B fixed after 50 μs, τ_X after 70 μs, and f_B ($= \frac{2\pi}{\omega_B}$) fixed after 80 μs.

For the new term in the fitting function, describing muon and proton losses, and possibly other background, both forms shown in equation 6 and 6a were tested. Both functions are very close in the region of interest (after 30 μs), but the correction of a gaussian form (eq. 6) produces more stable and consistent results (Fig.10). Other advantages of the "gaussian" correction will be discussed in Section 4.7.

Letting the start time of the CBO packet vary brings an interesting result (Fig.11): the amplitude A_B, width τ_B and start time t_{0B} of the CBO packet change linearly with the fit start time, which means that the shape of the packet is not exactly gaussian. At early times (30-40 μs), the packet is centered at 0. Also, the time when the amplitude of the packet falls by 2.7 ($\simeq e$) , $(\tau_B + t_{0B})$ remains stable at around 140 μs, the same as the one obtained from a fit with t_{0B} fixed at 0 μs (Fig.12). The difference in R between the two forms of the fitting function is relatively insignificant.

Parameter correlation coefficients are given in table 2 (generated by `MINUIT`).

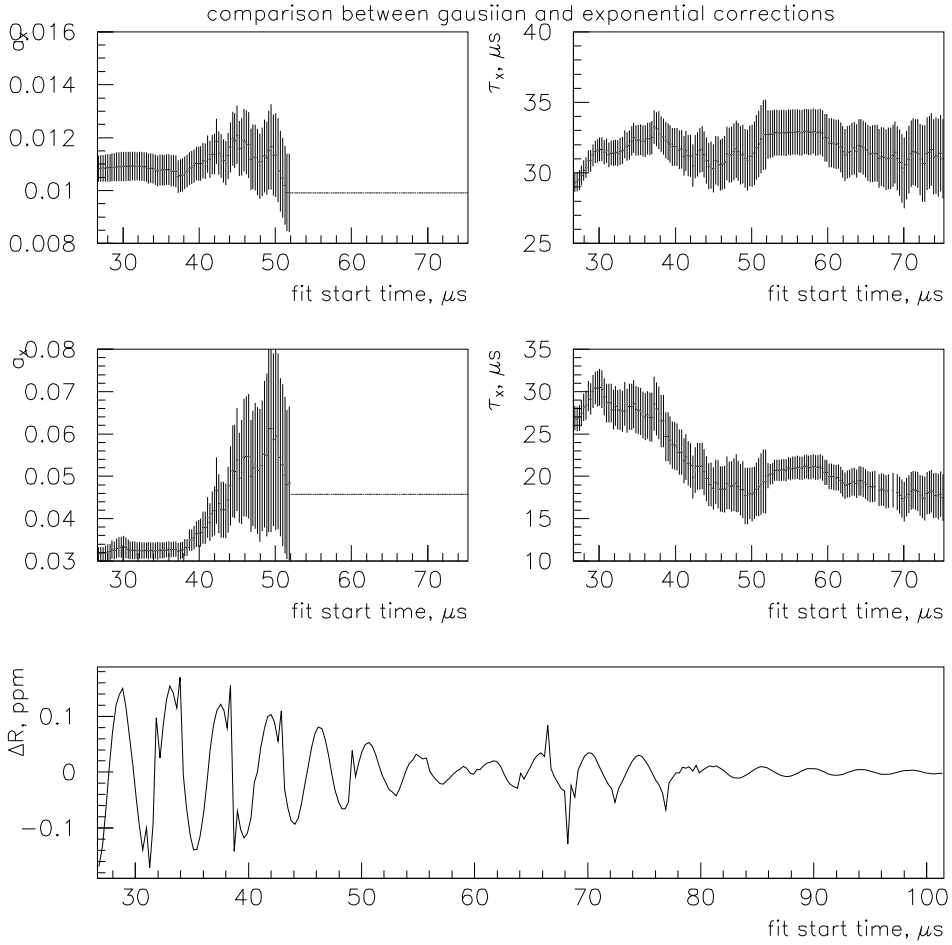

Fig.10. Comparison between fit parameters for different forms of the "muon loss" correction. Top: a_x and τ_B as a function of fit start time when a gaussian form is used (Eq. 4); parameters are stable with respect to the fit start time (a_x is fixed after 50 μs). Middle: similar plots for the case when an exponential correction (Eq. 4a) was used. Bottom: relative phase pulling on R for two forms of "muon correction"; phase pulling is minimal at the zero-crossings of g-2 precession.

Table 2. Fit parameter correlation table. Correlation coefficients are shown for 13 free parameters. Some coefficients are shown for the case when pile-up phase, $\Delta\phi_p$ was let vary (last line).

NAME	NO.	GLOBAL	1	2	3	4	5	6	7	8	9	10	11	12	13
N	1	0.99663	1.000	-0.972	0.005	0.001	0.002	-0.945	-0.798	0.004	-0.005	0.546	0.004	-0.029	0.003
λ	2	0.98641	-0.972	1.000	-0.004	-0.001	-0.002	0.869	0.733	-0.003	0.004	-0.460	-0.004	0.055	-0.002
A	3	0.86655	0.005	-0.004	1.000	0.005	0.006	-0.009	-0.468	0.009	0.009	0.032	-0.008	0.048	0.005
R	4	0.87630	0.001	-0.001	0.005	1.000	0.876	-0.003	-0.006	0.012	-0.025	0.010	0.021	0.017	0.009
ϕ	5	0.87645	0.002	-0.002	0.006	0.876	1.000	-0.004	-0.009	0.016	-0.034	0.014	0.029	0.023	0.013
n_p	6	0.99688	-0.945	0.869	-0.009	-0.003	-0.004	1.000	0.848	-0.006	0.009	-0.727	-0.007	-0.106	-0.004
A_1	7	0.96453	-0.798	0.733	-0.468	-0.006	-0.009	0.848	1.000	-0.013	-0.001	-0.640	0.001	-0.133	-0.008
A_B	8	0.80905	0.004	-0.003	0.009	0.012	0.016	-0.006	-0.013	1.000	-0.108	0.017	0.116	0.024	0.809
ϕ_B	9	0.95827	-0.005	0.004	0.009	-0.025	-0.034	0.009	-0.001	-0.108	1.000	-0.026	0.958	0.039	0.137
τ_X	10	0.99211	0.546	-0.460	0.032	0.010	0.014	-0.727	-0.640	0.017	-0.026	1.000	0.022	0.718	0.012
f_B	11	0.95834	0.004	-0.004	-0.008	0.021	0.029	-0.007	0.001	0.116	-0.958	0.022	1.000	0.033	0.147
a_X	12	0.97569	-0.029	0.055	0.048	0.017	0.023	-0.106	-0.133	0.024	-0.039	0.718	0.033	1.000	0.018
τ_B	13	0.81067	0.003	-0.002	0.005	0.009	0.013	-0.004	-0.008	0.809	-0.137	0.012	0.147	0.018	1.000
$\Delta\phi_p$	-	0.96758	-0.178	0.164	-0.090	-0.843	-0.933	0.188	-0.045	-0.015	-0.030	-	0.021	-0.181	-

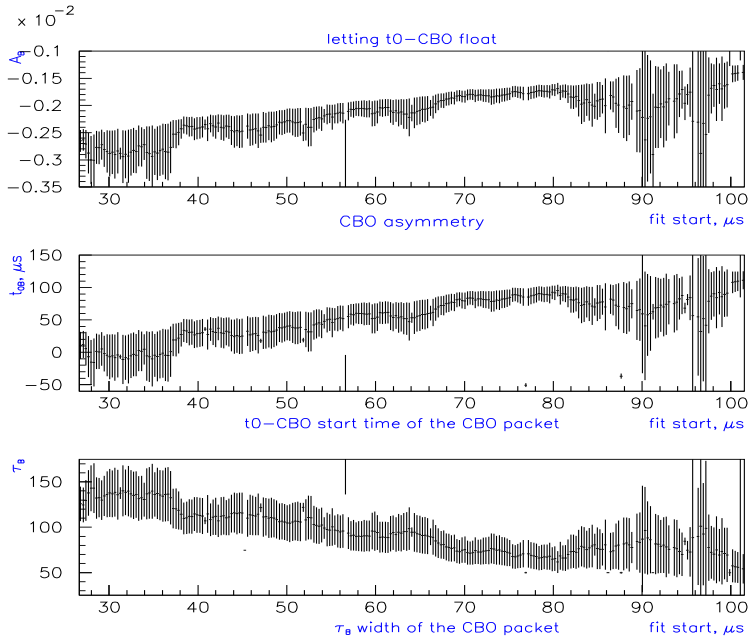

Fig.11. If the start time of the CBO packet t_{0B} is treated as a free parameter, the values of A_B, τ_B and t_{0B} are changing linearly from early to late time. The time when the amplitude of the packet falls by the value of $e \simeq 2.71$, $(\tau_B + t_{0B})$ remains stable at around 140 μs.

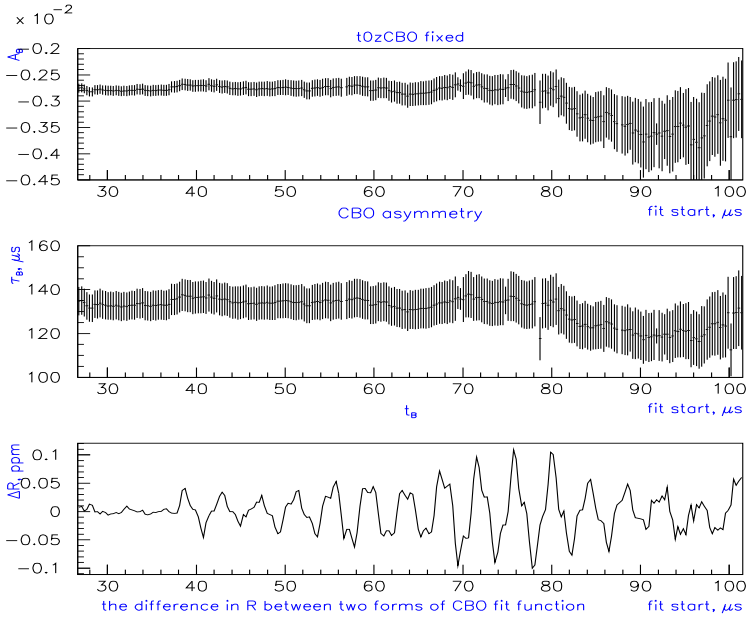

Fig.12. For this test, the start time of the CBO packet t_{0B} was fixed at 0 μs. Both, the amplitude A_B (top) and the packet width τ_B (middle) are stable. The CBO phase (not shown) is not affected by fixing t_{0B}. On the bottom plot: the difference of the values of R between the two fits (with t_{0B} fixed and floating): the phase pulling is of the order of 40 ppb for the start times up to 60 μs (for the later start times the discrepancy is increased due to the errors caused by fixing other parameters).

4 Fit Results

Fits were performed for different energy cuts and for each individual detector.

4.1 Detectors Combined (With Pile-up Phase Fixed at 0)

The results of fitting to the time-distribution of the positrons for three different energy cuts: E>1.8 GeV , E>2 GeV and 1.8 GeV < E <3.1 GeV are shown in Figs.13-15(a,b,c). Start time of the fit varied between 27 and 100 μs, with the end time fixed at 599.7 μs (bin 4020).

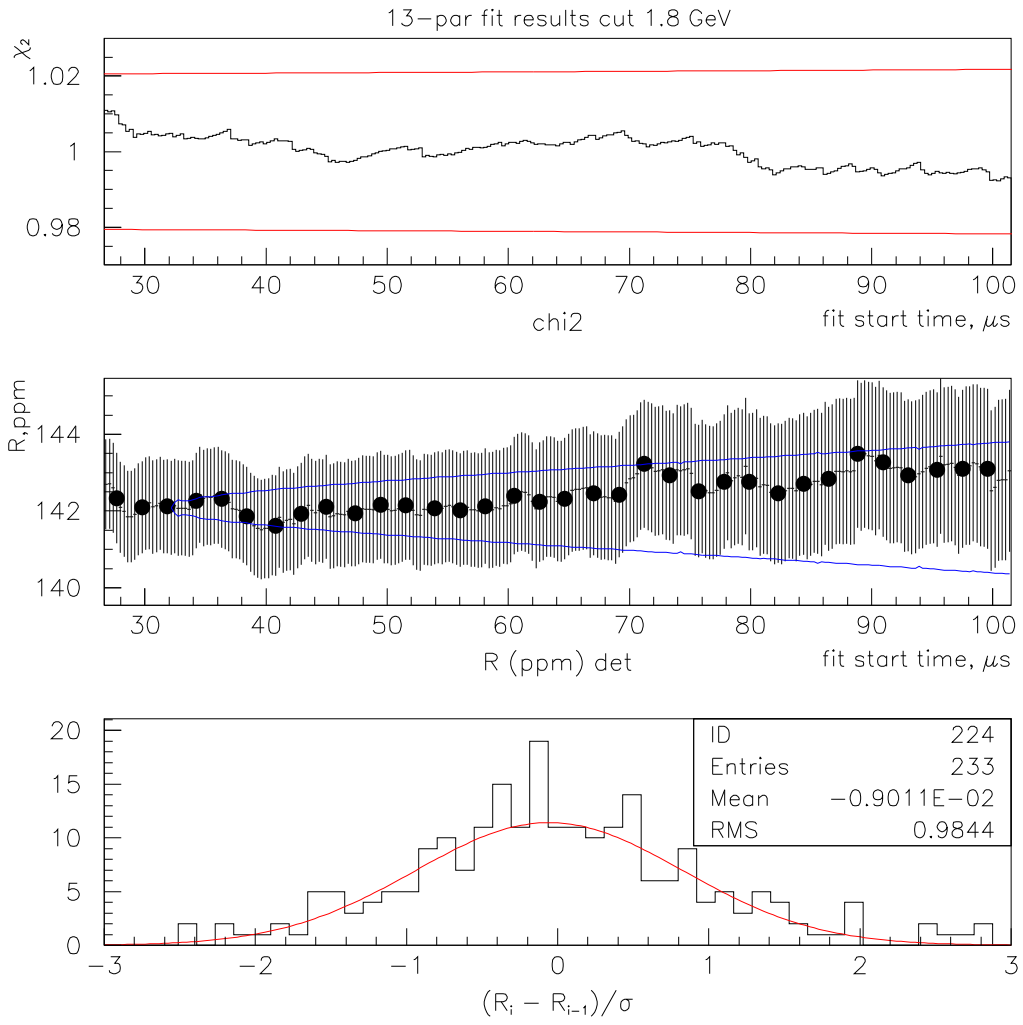

Fig.13a. Fit results for cut 1.8 GeV (one random seed only). Top: χ^2 as a function of fit start time, acceptable at all start times. Middle: R vs fit start time (black dots are the zero-crossings of g-2 precession). Allowed variation limits given by Kawall formula [7] are shown with respect to the start time of 32 μs. Bottom: distribution of the step-by-step variation in fitted R values: $\frac{R_i - R_{i-1}}{\sigma(i,i-1)}$, with $\sigma(i,i-1) = \sqrt{\sigma_i^2 - \sigma_{i-1}^2}$.

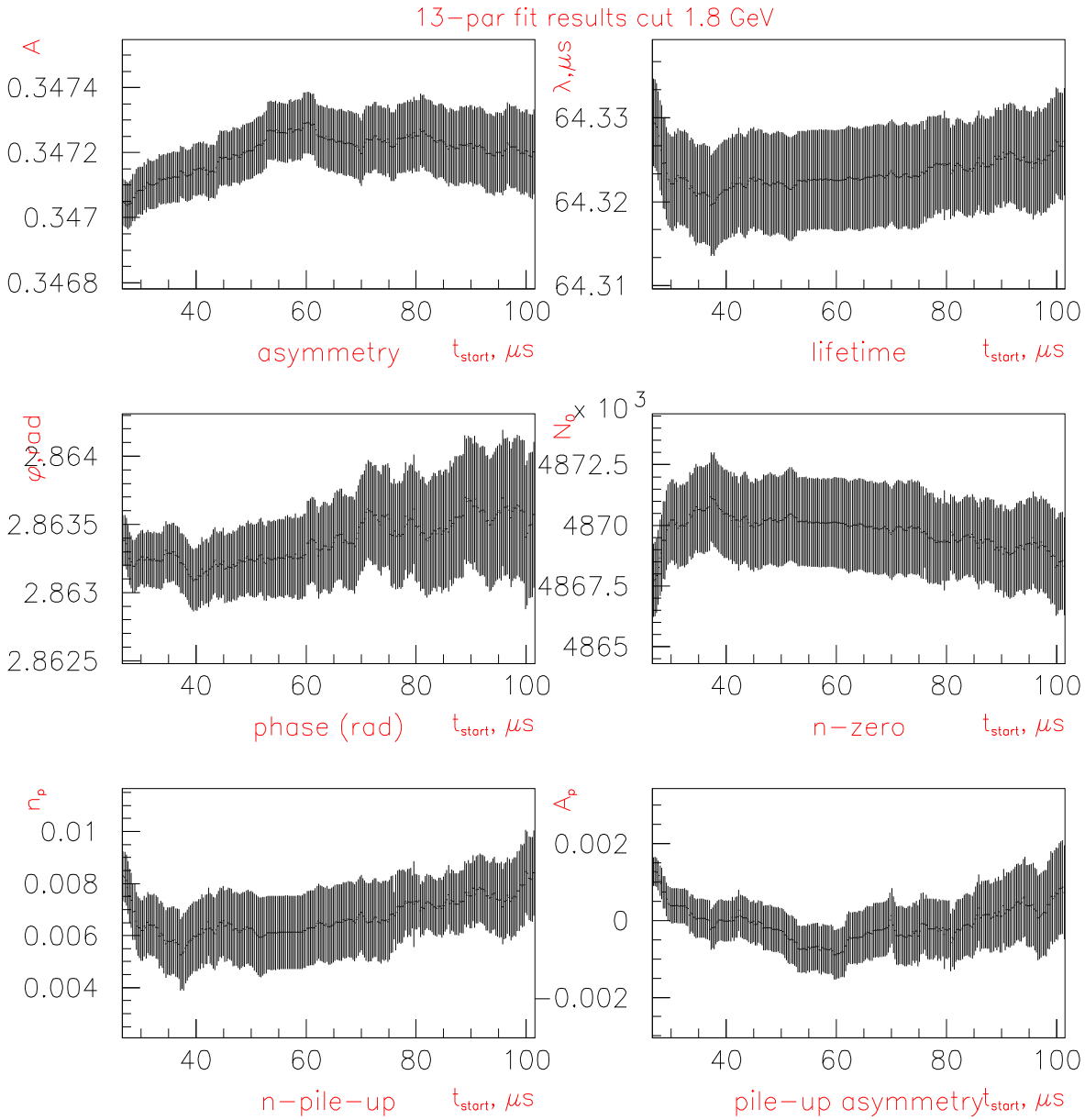

Fig.13b. Fit results for cut 1.8 GeV: fit parameters as a function of start time. Top left to bottom right: A, $1/\lambda$, ϕ, N_0, n_p, A_p. After 32 μs all parameters vary within the limits allowed by Kawall formula.

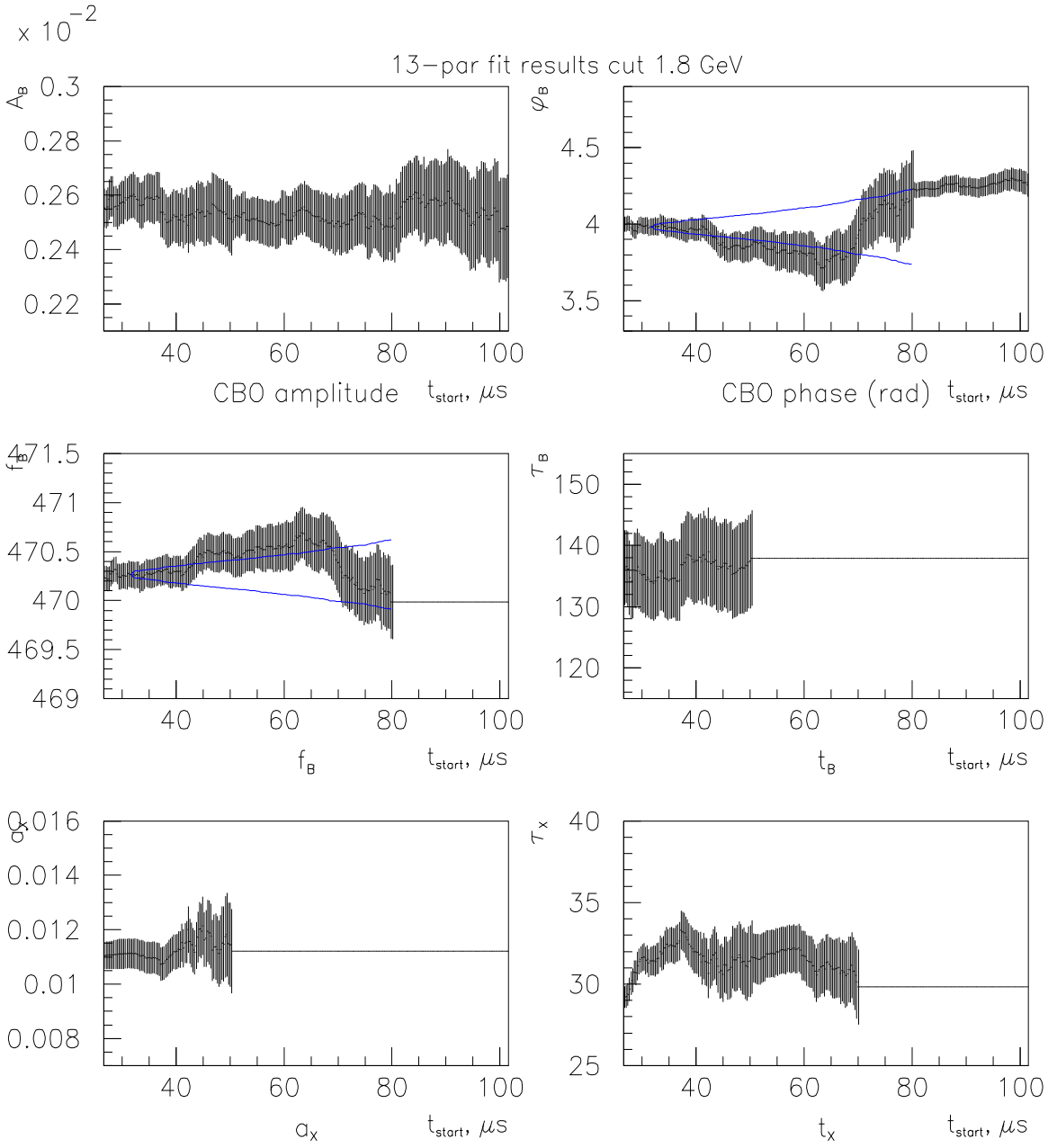

Fig.13c. Fit results for cut 1.8 GeV: fit parameters as a function of start time. Top left to bottom right: betatron oscillation parameters A_B, ϕ_B (in μs), f_b (in kHz), τ_B (μs), and "muon loss" parameters, a_X and τ_X (μs). 4 latter parameters were fixed after 50, 70 or 80 μs. ϕ_B shows a significant decrease of statistical error after f_B was fixed. After 32 μs all parameters vary within the limits allowed by Kawall formula (shown for ϕ_B, f_B).

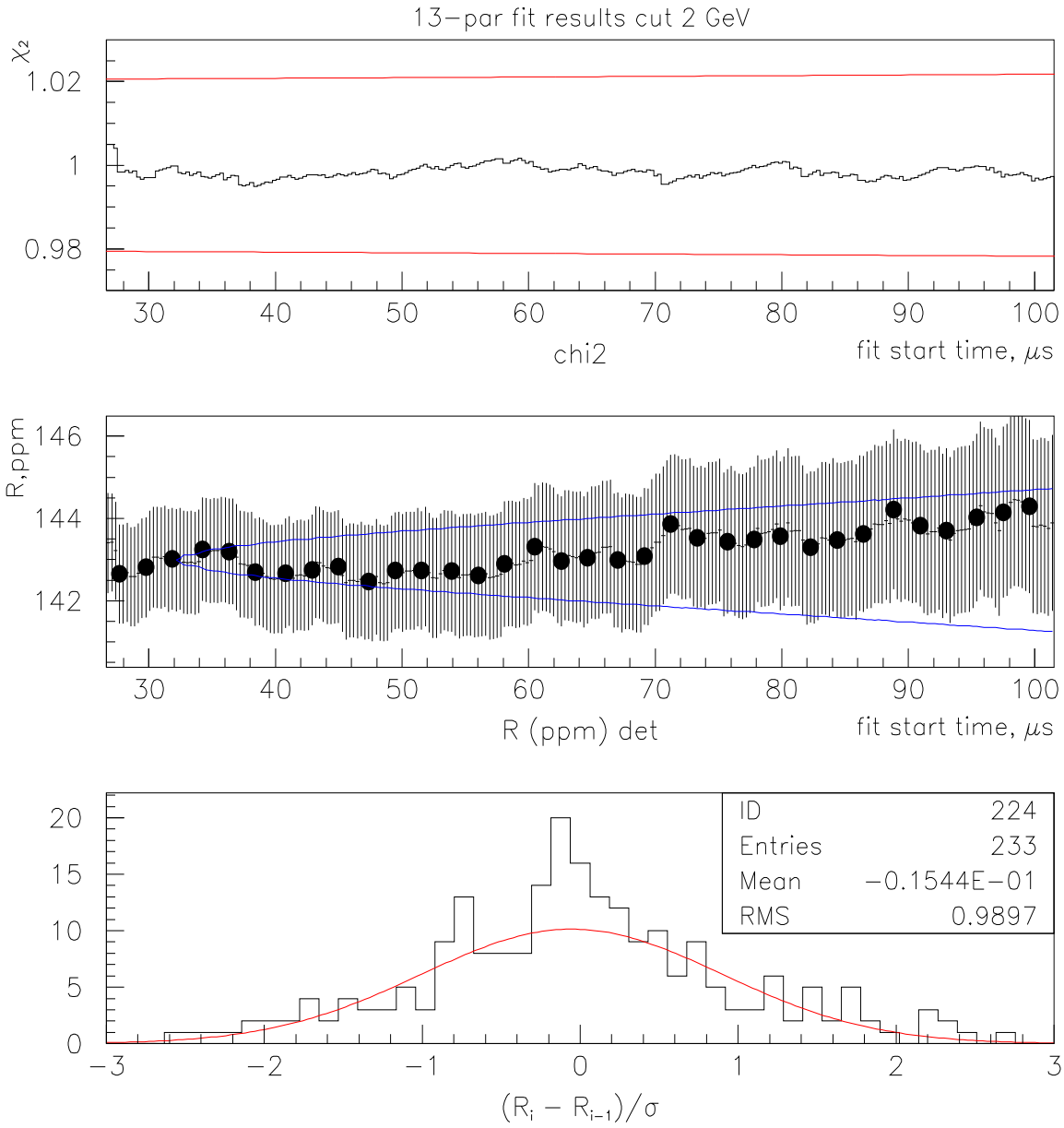

Fig.14a. Fit results for cut 2 GeV (one random seed only). Top: χ^2 as a function of fit start time, acceptable at all start times. Middle: R vs fit start time (black dots are the zero-crossings of g-2 precession). Allowed variation limits given by Kawall formula are shown with respect to the start time of 32 μs. Bottom: distribution of the step-by-step variation in fitted R values: $\frac{R_i - R_{i-1}}{\sigma(i,i-1)}$

.

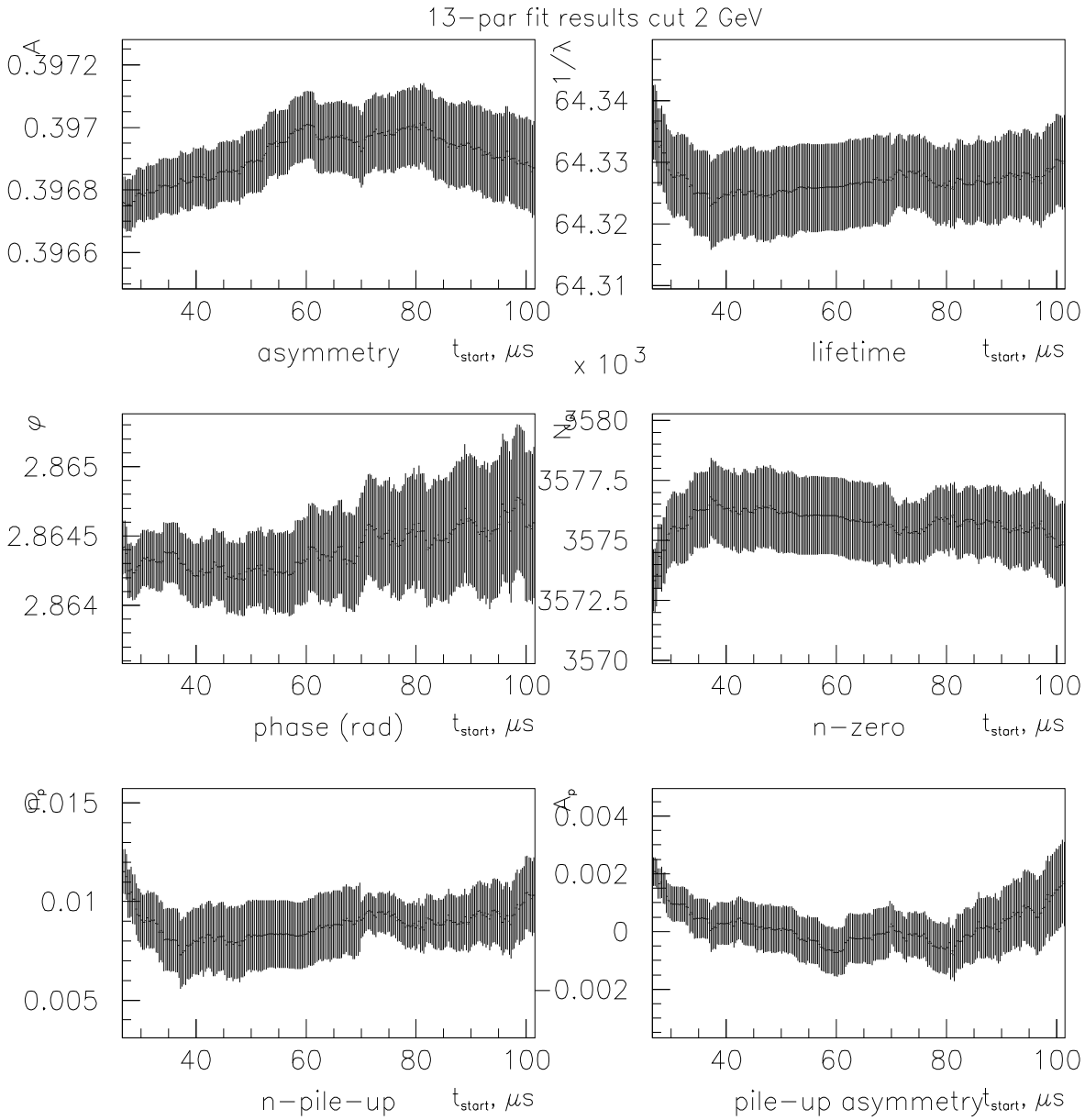

Fig.14b. Fit results for cut 2 GeV: fit parameters as a function of start time. Top left to bottom right: A, $1/\lambda$, ϕ, N_0, n_p, A_p. After 32 μs all parameters vary within the limits allowed by Kawall formula.

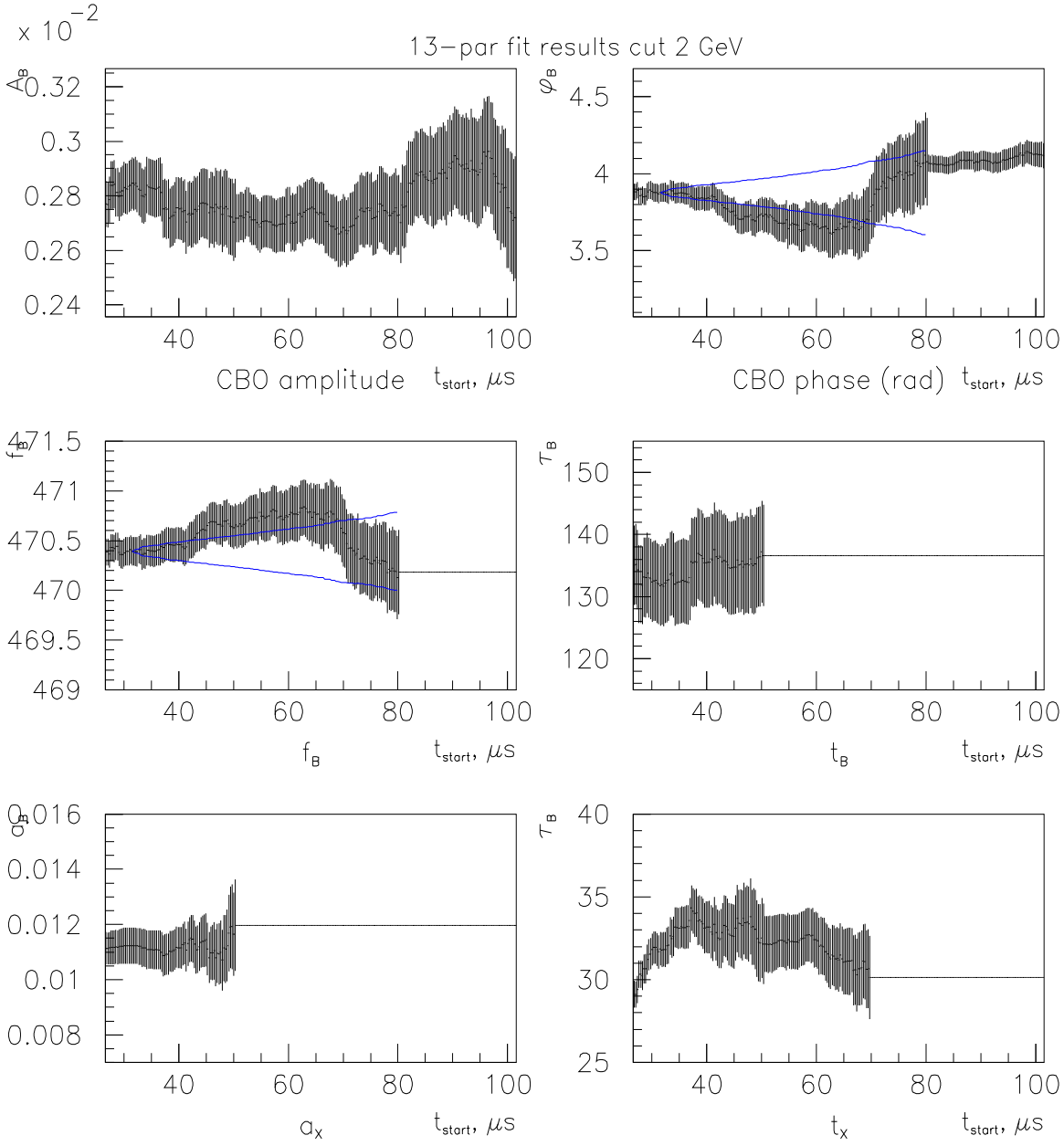

Fig.14c. Fit results for cut 2 GeV: fit parameters as a function of start time. Top left to bottom right: betatron oscillation parameters A_B, ϕ_B (in μs), f_b (in kHz), τ_B (μs), and "muon loss" parameters, a_X and τ_X (μs). 4 latter parameters were fixed after 50, 70 or 80 μs. After 32 μs all parameters vary within the limits allowed by Kawall formula (shown for ϕ_B, f_B).

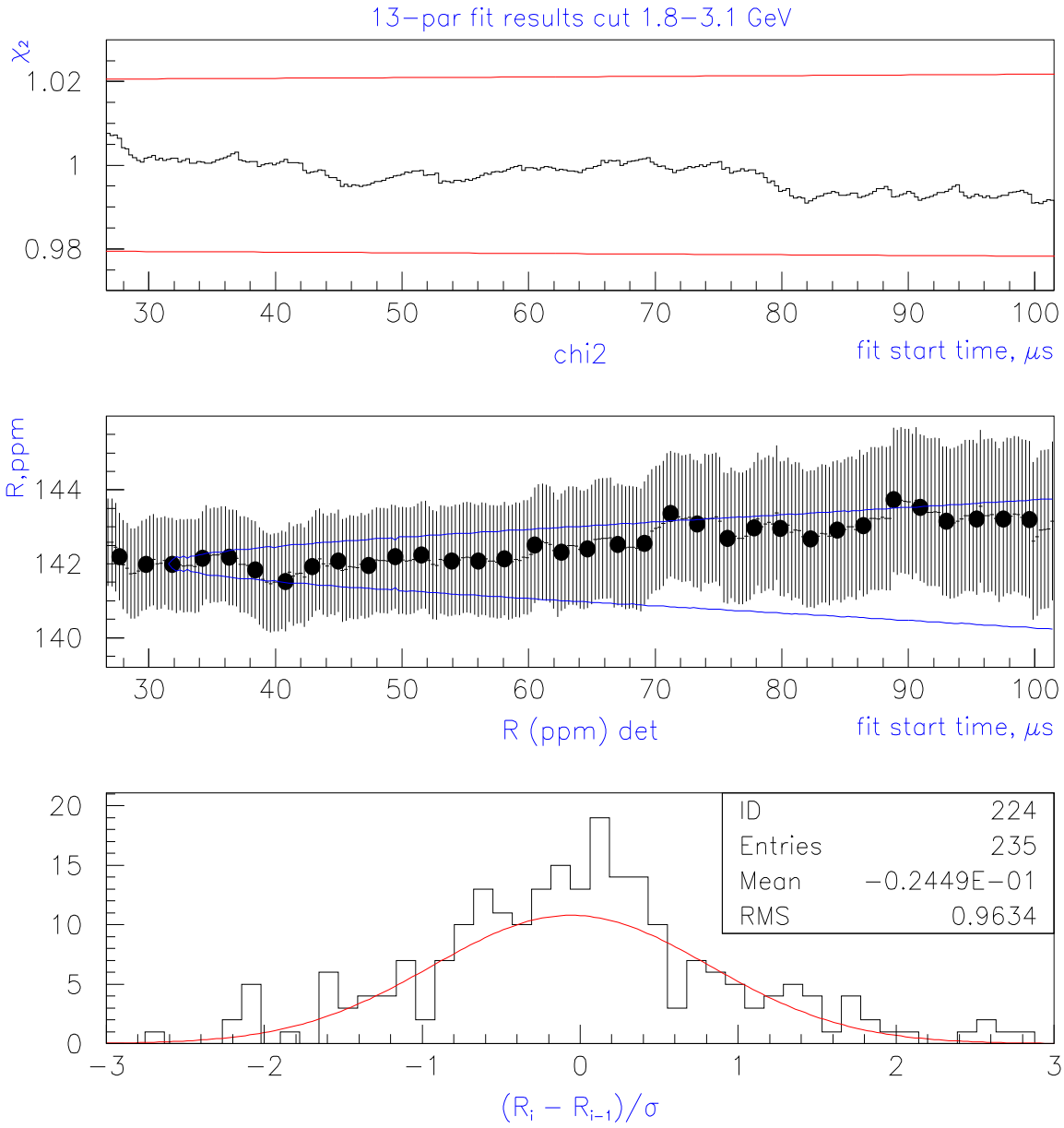

Fig.15a. Fit results for cut 1.8-3.1 GeV (one random seed only). Top: χ^2 *as a function of fit start time, acceptable at all start times. Middle: R vs fit start time (black dots are the zero-crossings of g-2 precession). Allowed variation limits given by Kawall formula are shown with respect to the start time of 32* μ*s. Bottom: distribution of the step-by-step variation in fitted R values:* $\frac{R_i - R_{i-1}}{\sigma(i,i-1)}$.

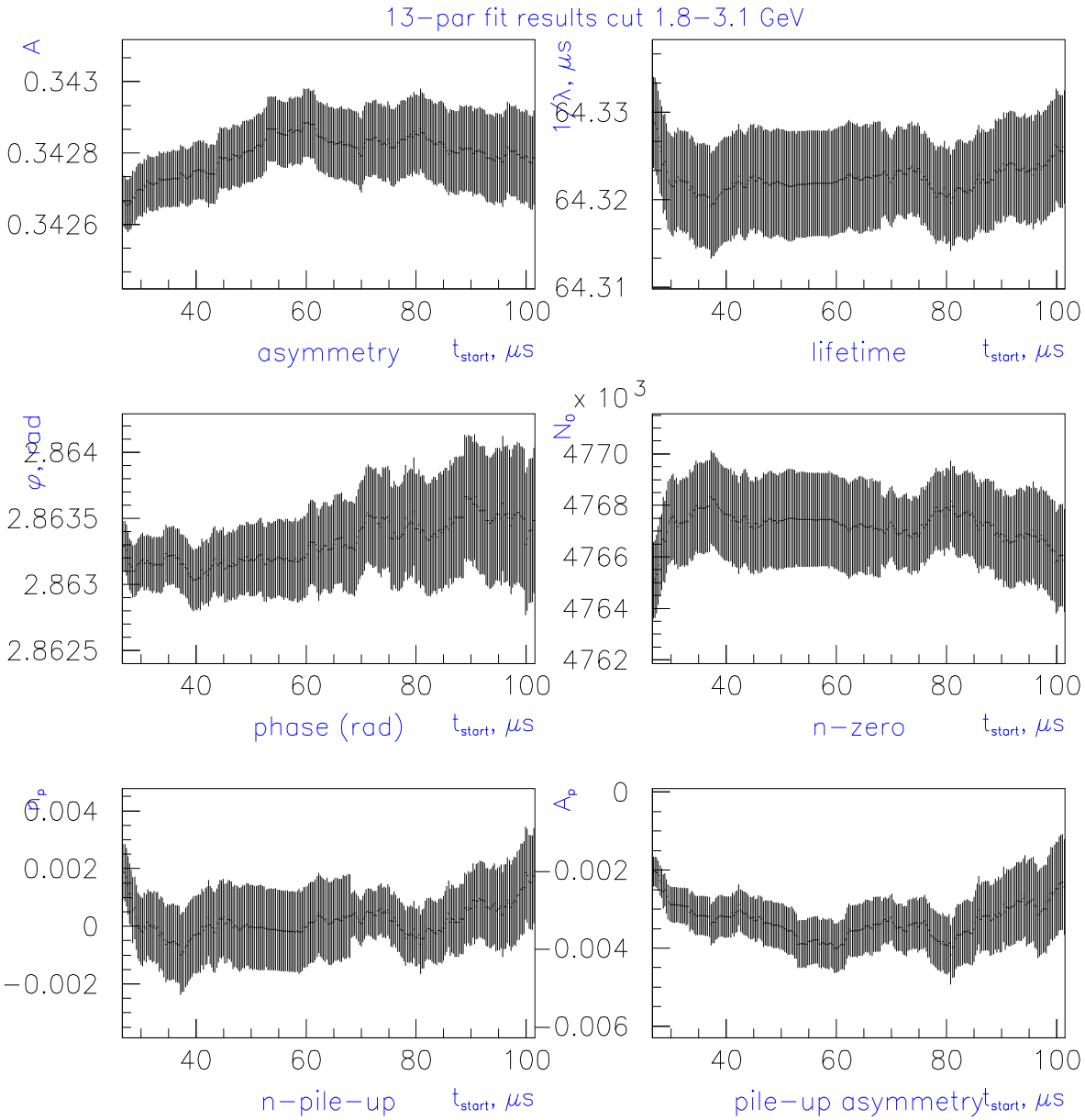

Fig.15b. Fit results for cut 1.8-3.1 GeV: fit parameters as a function of start time. Top left to bottom right: A, $1/\lambda$, ϕ, N_0, n_p, A_p. After 32 μs all parameters vary within the limits allowed by Kawall formula.

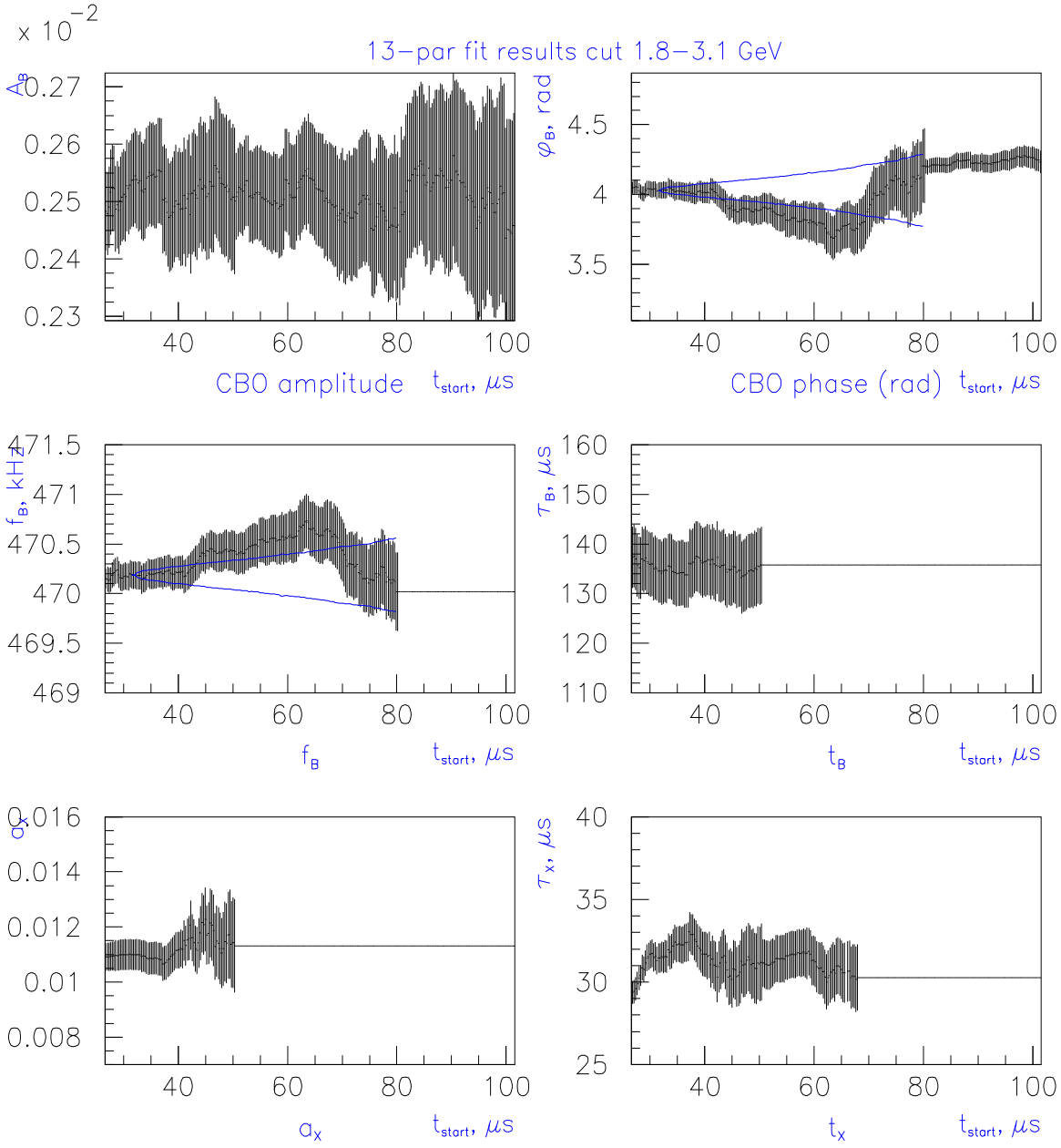

Fig.15c. Fit results for cut 1.8-3.1 GeV: fit parameters as a function of start time. Top left to bottom right: betatron oscillation parameters A_B, ϕ_B (in μs), f_b (in kHz), τ_B (μs), and "muon loss" parameters, a_X and τ_X (μs). 4 latter parameters were fixed after 50, 70 or 80 μs. After 32 μs all parameters vary within the limits allowed by Kawall formula (shown for ϕ_B, f_B).

For the fit to the data from all detectors combined, normalized χ^2 was found acceptable for all fit start times after 30 μs, with the value of R varying within the limits allowed by Kawall formula (Figs. 13a, 14a, 15a).

Other fit parameters showed reasonable early-to-late time stability and consistency as well (Figs. 13-15, parts b and c).

It was encouraging to find that fitted values for some new parameters were consistent with their prediction. The frequency of coherent betatron oscillation could be estimated using Fourier transform of the data from e.g detectors 8 and 9, which showed the most pronounced effect. The fit errors on f_B were generally much smaller than one would obtain from fast Fourier transform studies, but the results agree very well within the errors (Fig.16a). Fitted values of pile-up fraction for different cuts were consistent from early to late fit start times and agreed very well with the simulation result (Fig.16b, and Fig.B4 in appendix B).

On the other hand, the results for R differed between the 2-GeV and 1.8-GeV cuts by about 0.6-1 ppm for all fit start times (Fig.17, Tables 3-5). The source of this discrepancy will be discussed in Section 4.5. Besides R, only the values of the asymmetry and pile-up parameters n_p and A_p differed significantly for different cuts, as expected (Table 6).

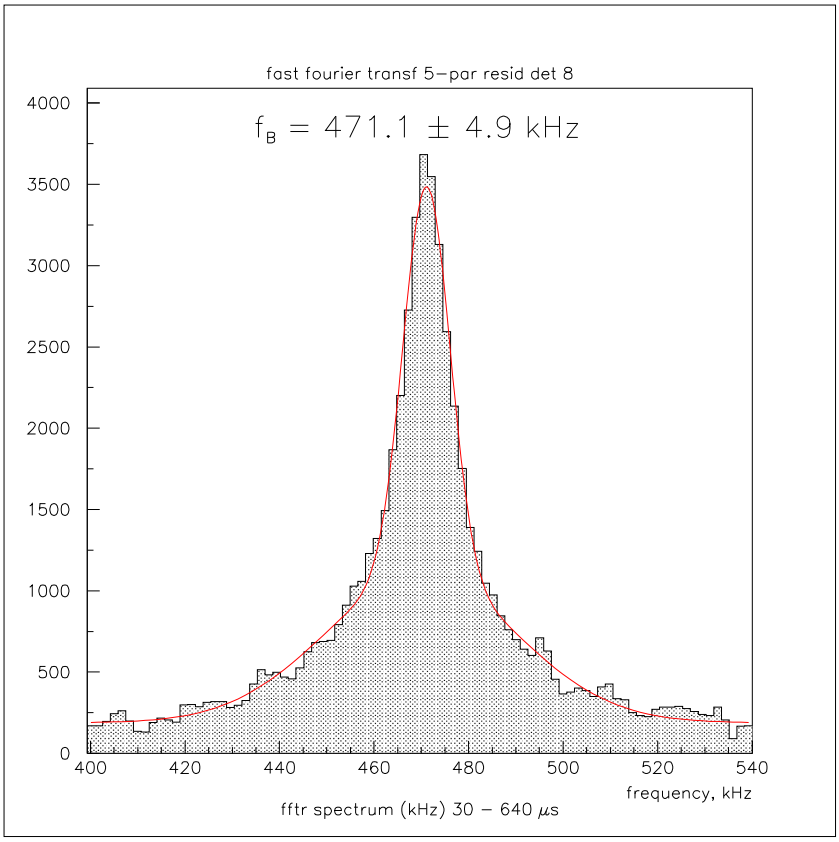

Fig.16a. The result of fitting to CBO frequency using Fourier transform agrees well with fit results. Shown here is a Fourier transform of 5-parameter fit residuals to the data from detector 8. Fit to the data brings $f_B \simeq 470.4 \pm 0.2$ KHz (at 32 μs after the injection).

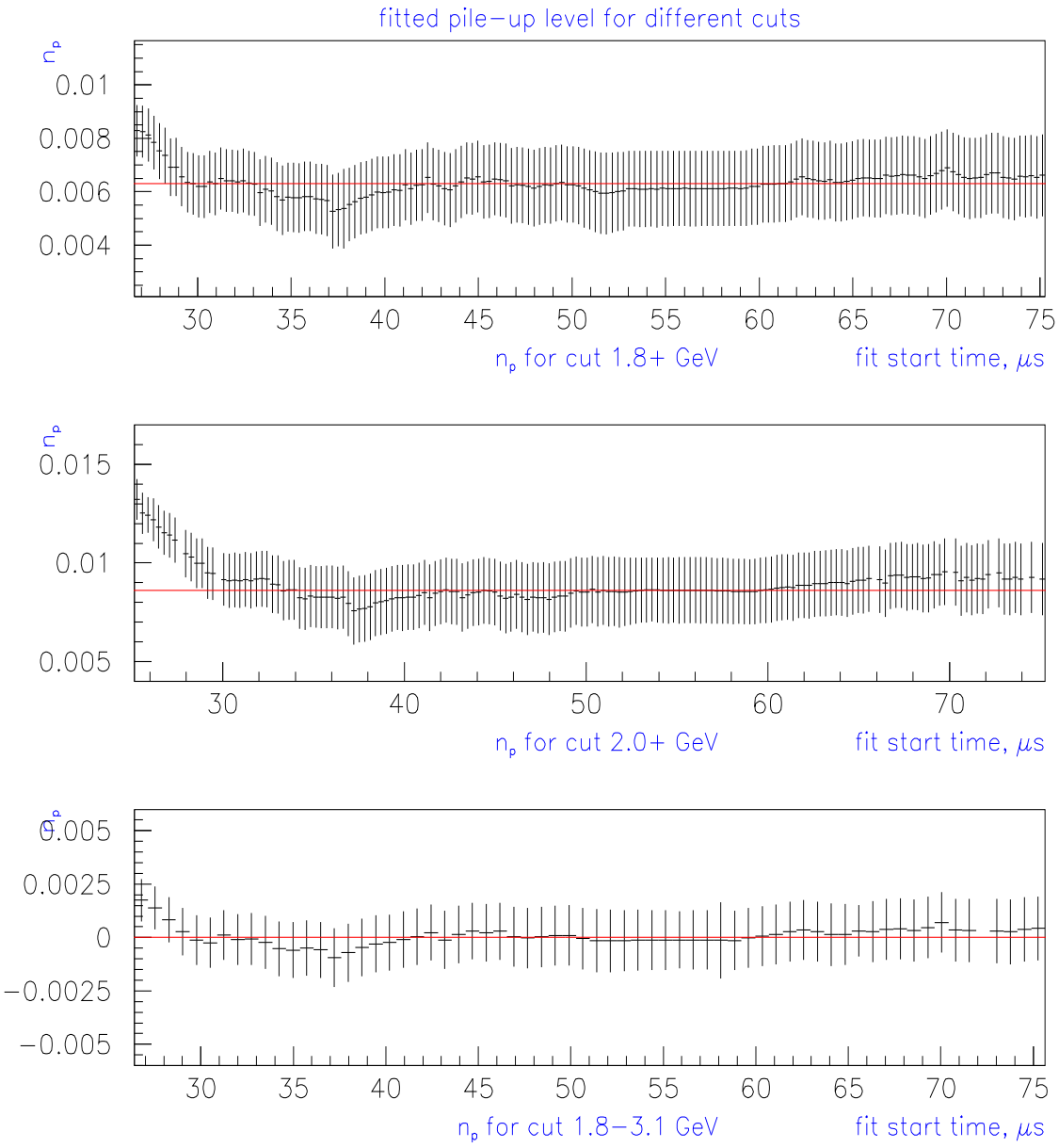

Fig.16b. Fitted pile-up levels for different cuts agreed well with the simulation results. Top to bottom: cuts E>1.8 GeV, E>2 GeV and 1.8<E<3.1 GeV. Horizontal lines represent levels predicted by a simulation. The simulation is described in appendix B.

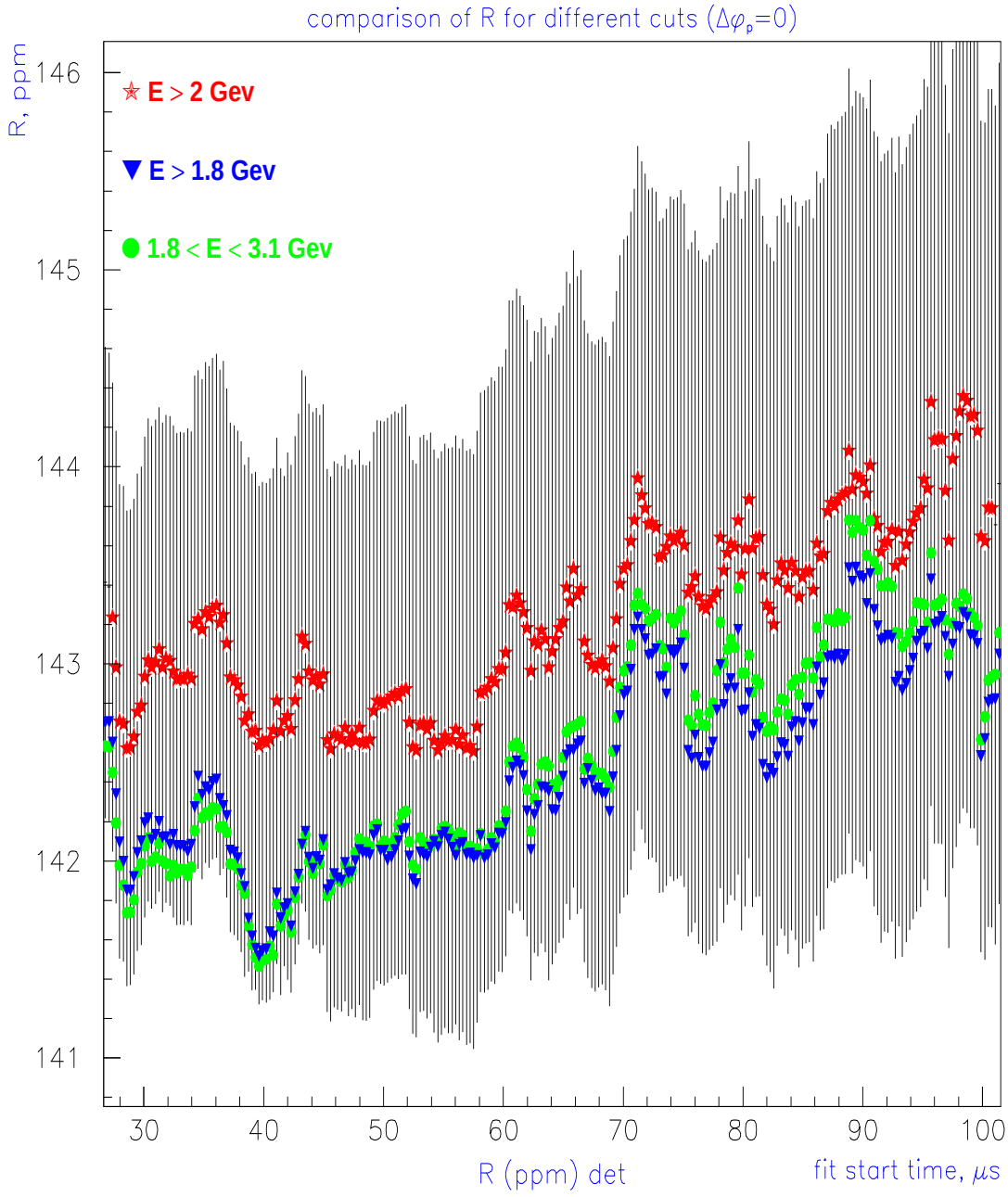

Fig.17. Comparison of fitted values of R for different cuts **with $\Delta\phi_p = 0$ fixed for each of the cuts**. *The errors are given for the results from the cut 2 GeV only. There is a shift of 0.6-1 ppm between the values of R from the 2-GeV and 1.8 GeV cuts. The results for the 1.8-GeV and 1.8-3.1 cuts are very close.*

Table 3. Summary of fit results for cut 1.8 GeV ($\Delta\phi_p$ = 0). The numbers for the sum of detectors are averaged for 10 random seeds. The numbers for the detectors fitted separately are averaged over 22 detectors for a single random seed. The value of R contains an offset.

Start Time, μs	Ne^+, M	Dets summed		Dets separate	
		R	χ^2	R	χ^2
32	1279.0	142.17 ± 1.22	1.001	142.14 ± 1.23	1.007
40	1125.3	141.59 ± 1.30	0.996	141.49 ± 1.30	1.001
50	960.7	142.03 ± 1.42	0.996	141.84 ± 1.42	1.000
60	819.6	142.12 ± 1.52	0.997	141.97 ± 1.53	1.000
70	701.6	142.83 ± 1.65	0.996	142.63 ± 1.66	0.999
80	604.4	142.88 ± 1.79	0.992	142.76 ± 1.80	0.998

Table 4. Summary of fit results for cut 1.8-3.1 GeV ($\Delta\phi_p$ = 0) . The numbers for the sum of detectors are averaged for 10 random seeds.

Start Time, μs	Ne^+, M	Dets summed		Dets separate	
		R	χ^2	R	χ^2
32	1260.73	142.04 ± 1.25	0.999	141.94 ± 1.26	1.005
40	1109.5	141.56 ± 1.33	0.995	141.41 ± 1.34	1.001
50	947.5	142.10 ± 1.43	0.994	141.87 ± 1.45	1.000
60	808.5	142.16 ± 1.55	0.995	142.03 ± 1.56	1.000
70	692.2	142.99 ± 1.69	0.993	142.78 ± 1.70	0.999
80	596.4	143.08 ± 1.82	0.990	142.99 ± 1.83	0.998

Table 5. Summary of fit results for cut 2.0 GeV ($\Delta\phi_p$ = 0) . The numbers for the sum of detectors are averaged for 10 random seeds. For the detectors separate, averaging done over 10 seeds, 22 detectors.

Start Time, μs	Ne^+, M	Dets summed		Dets separate	
		R	χ^2	R	χ^2
32	948.9	143.00 ± 1.24	1.012	142.92 ± 1.25	1.012
40	834.6	142.59 ± 1.31	1.009	142.52 ± 1.32	1.008
50	712.5	142.67 ± 1.43	1.008	142.72 ± 1.43	1.007
60	607.3	142.94 ± 1.54	1.009	142.78 ± 1.55	1.006
70	520.0	143.36 ± 1.67	1.009	143.29 ± 1.68	1.006
80	448.2	143.43 ± 1.81	1.008	143.46 ± 1.83	1.005

As shown in Table 6, the values of muon lifetime obtained from fitting to two selections with different threshold cuts are in an excellent agreement with each other, and with the result of fitting individual detectors, both separately and combined, to a 5-parameter function at late times (Fig.18). The value of lifetime is about 0.1% lower than would be expected from theory, due to the presence of the muon loss fraction with a life time close to that of the muon, not accounted for in the fitting function. (This muon loss fraction has been seen in the studies of the FSD 3-fold coincidences [8,9].) An attempt to correct for it will be done in Section 4.7.

Table 6. The values of fit parameters for different cuts (fit from 32 to 600 μs, average over 10 random seeds, $\Delta\phi_p$ = 0).

Fit parameter	Cut 1.8-3.1 GeV	Cut 1.8-6.2 GeV	Cut 2.0-6.2 GeV
$1/\lambda$ (μs)	64.322 ± 0.006	64.324 ± 0.006	64.328 ± 0.007
A	0.34272 ± 0.00008	0.34711 ± 0.00008	0.39679 ± 0.00009
R, ppm	142.04 ± 1.25	142.17 ± 1.22	142.97 ± 1.24
ϕ (rad)	2.8630 ± 0.0002	2.8631 ± 0.0002	2.8641 ± 0.0002
N_0	(4.7673 ± 0.0017)·10^6	(4.8264 ± 0.0017)·10^6	(3.5755 ± 0.0014)·10^6
n_p	(0.02 ± 1.19)·10^{-3}	(6.45 ± 1.19)·10^{-3}	(9.05 ± 1.42)·10^{-3}
A_p	(-2.91 ± 0.45)·10^{-3}	(0.36 ± 0.46)·10^{-3}	(0.97 ± 0.60)·10^{-3}
A_B	(2.55 ± 0.08)·10^{-3}	(2.61 ± 0.08)·10^{-3}	(2.81 ± 0.10)·10^{-3}
ϕ_B (rad)	4.022 ± 0.058	3.975 ± 0.056	3.872 ± 0.061
f_B (kHz)	470.20 ± 0.14	470.28 ± 0.13	470.40 ± 0.15
τ_B (μs)	133.47 ± 6.34	133.24 ± 6.17	132.00 ± 6.50
a_X	(1.10 ± 0.06)·10^{-2}	(1.11 ± 0.06)·10^{-2}	(1.12 ± 0.07)·10^{-2}
τ_X (μs, **"gaussian"**)	31.45 ± 0.90	31.39 ± 0.89	31.81 ± 1.04

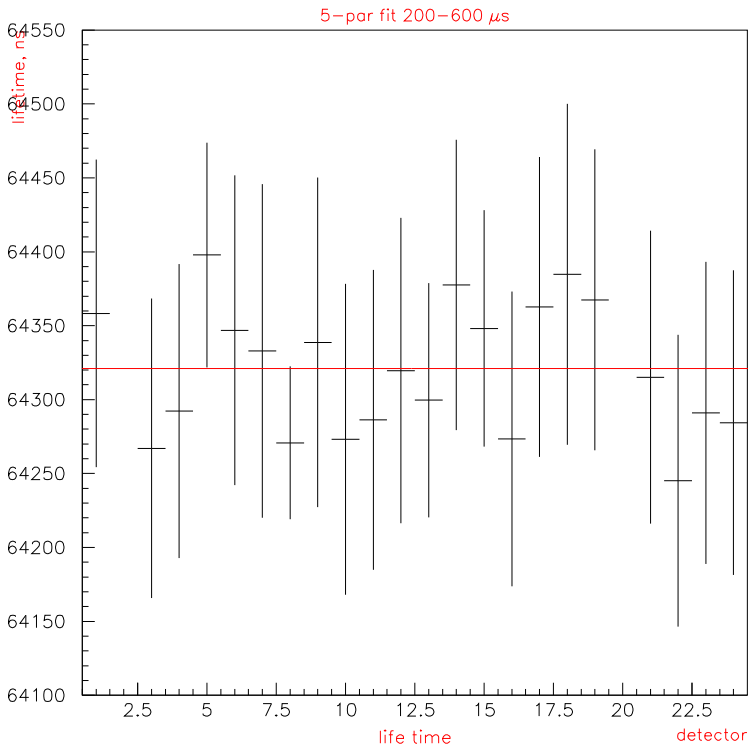

Fig.18. 5-parameter fit at late times (200-600 μs) brings a value of the muon lifetime, which is in a good agreement with the 13-parameter fit result at early time. On the figure: lifetime in ns vs detector number (fit starts at 200 μs); for the detectors together, 1/λ = (64,321.2 ± 13.5) ns.

4.2 Detectors Fitted Separately

The time spectra for each detector separately were fitted with the muon loss characteristic time, τ_X = 31.5 μs (gaussian notation) fixed for all fit start times. An example of the fit parameter evolution with start time is shown in Figs.19a,b (detector 9).

As shown in Fig.20, the energy-scale correction had a very positive effect on the parameter stability: it eliminated a strong phase pulling on R without introducing a bias.

For most detectors, fit χ^2 was acceptable for all start times after 30 μs and the values of R and other parameters varied within the limits given by Kawall formula (Figs. 21-24).

A good agreement was found between the values of R obtained by fitting the detectors separately and then averaging the result, and fitting the summed data from all detectors, with the difference of less than 0.2 ppm for each of the 3 cuts (Tables 3-5). Since all detectors have different levels of pile-up, to which factor this method is especially sensitive, the average over the results for individual detectors is not necessarily the same as for the sum.

In Figs.25a,b, the values of fit parameters vs detector number are shown for the start time of 32 μs. These values are in a good agreement with the ones obtained by fitting the data from all detectors added together

As in the case of the data from all detectors added together, the fitted value of R was found different for different cuts in some detectors (Fig.26). The offset between the values of R for cuts 1.8 and 2 GeV differed in both sign and size by the detector, which implied that factors other than the energy threshold were in play.

The pile-up phase $\Delta\phi_p$ was fixed at 0 for all detectors, and that might have been the source of the discrepancy in the results for R from different cuts.

4.3 Fit by the Energy Bin

Separate histograms were created for this study, which covered all of the selected range of the 1999 data. The energy spectrum between 0.46·E_{max} and 0.78·E_{max} was divided into 16 slices of the width equal to E_{max}/50 (approximately 60-MeV wide). For each of these slices, time spectra were created and then fitted. I used the function described in the Section 3.1, with CBO characteristic time τ_B = 135 μs, and the amplitude of the muon loss $a_X = 0.011$ fixed. Fixing these parameters was necessary for better fit convergence, since the amount of data in each slice was much smaller than the entire data set. The pile-up phase was fixed at 0 as well. The fit region went from approximately 40 to 525 μs. Fit results for selections covering different energy bins are shown in Figs. 27a,b.

These results are hard to interpret: the value of R undergoes a big jump at around 0.6·E_{max} (Fig.27a), the pile-up asymmetry is changing with the energy in a rather strange way, and a number of other parameters (muon lifetime, pile-up fraction et al.) are unstable. It is hard to judge how reliable these fit results are, and if they can be used for evaluation of the data quality, since the amount of data was comparably small and the pile-up phase was fixed at the same value for all energy bins. Making the pile-up phase a free parameter made the fit very unstable.

4.4 Fit to Selections With Different Lower Cuts

The results for selections with different lower cuts (no upper cut) are shown in Figs. 28a,b. This study was done for 16 values of lower cut, varying between 0.46 and 0.76·E_{max} with a step of E_{max}/50. For this study, the pile-up phase was kept fixed as well. Again, the value of R changed significantly for cuts between 0.56·E_{max} (1.74 GeV) and 0.64·E_{max} (1.98 GeV). Fitted pile-up levels are in a good agreement with the simulation result (see Appendix B, Fig.B4.). As in the case of fitting by the energy bin, the "muon loss" parameters varied little from cut to cut, whereas, the amplitude and phase of coherent betatron oscillation showed a strong cut-dependence.

Letting the pile-up phase vary (Fig.29) brings a result confirming that the swing in the value of R (in Fig.28a) occurs when pile-up asymmetry crosses zero and the uncertainty in the pile-up phase becomes very big. The result of the fit to real data shows a pile-up phase behavior in the vicinity of the asymmetry zero crossing, similar to the pattern predicted with a simulation (see Appendix B, Fig.B6).

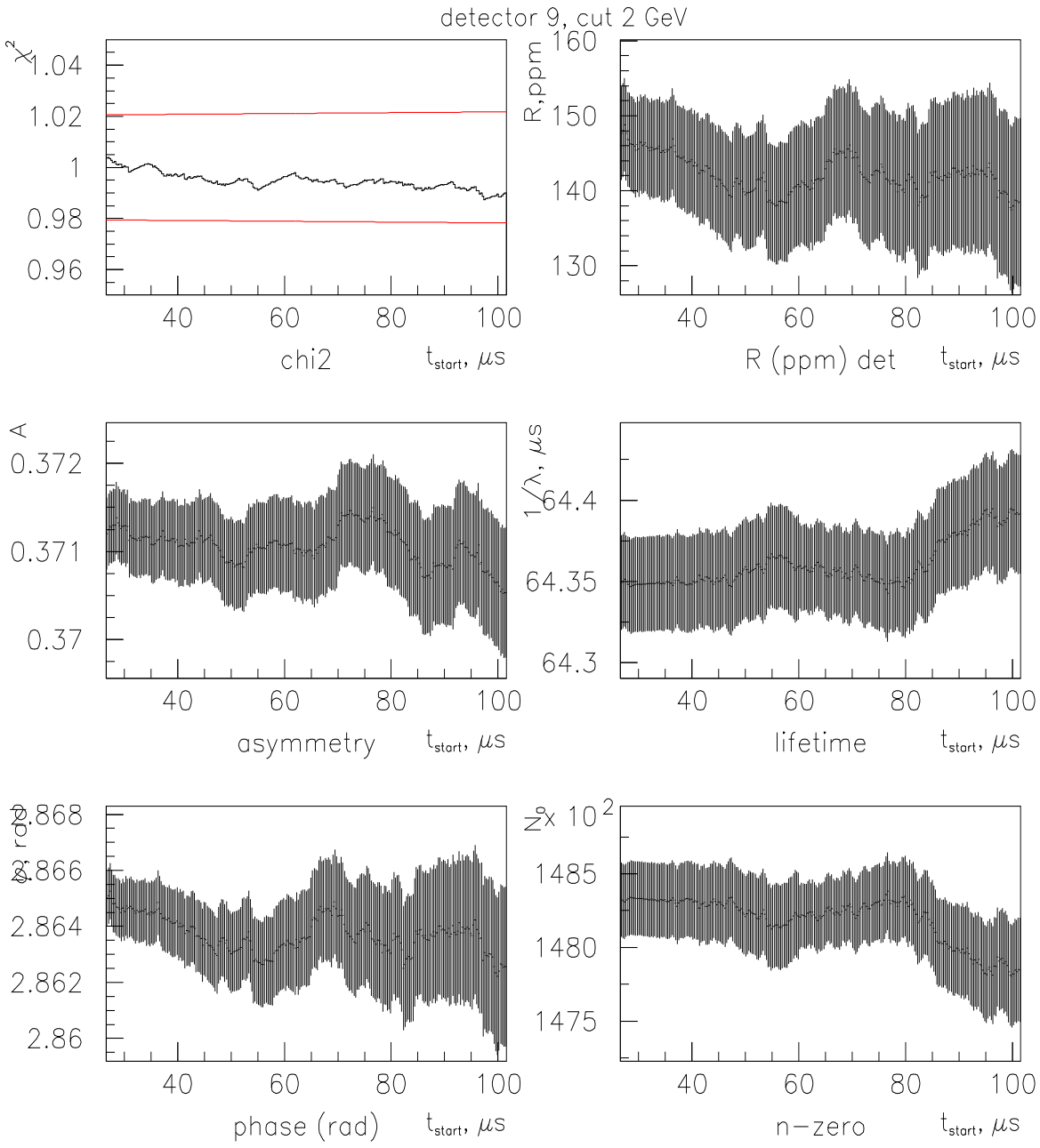

Fig.19a. Fit results for detector 9 (cut 2 GeV). Fit parameters are plotted as a function of the fit start time: χ^2, R, A, muon life time 1/λ, ϕ and N_0.

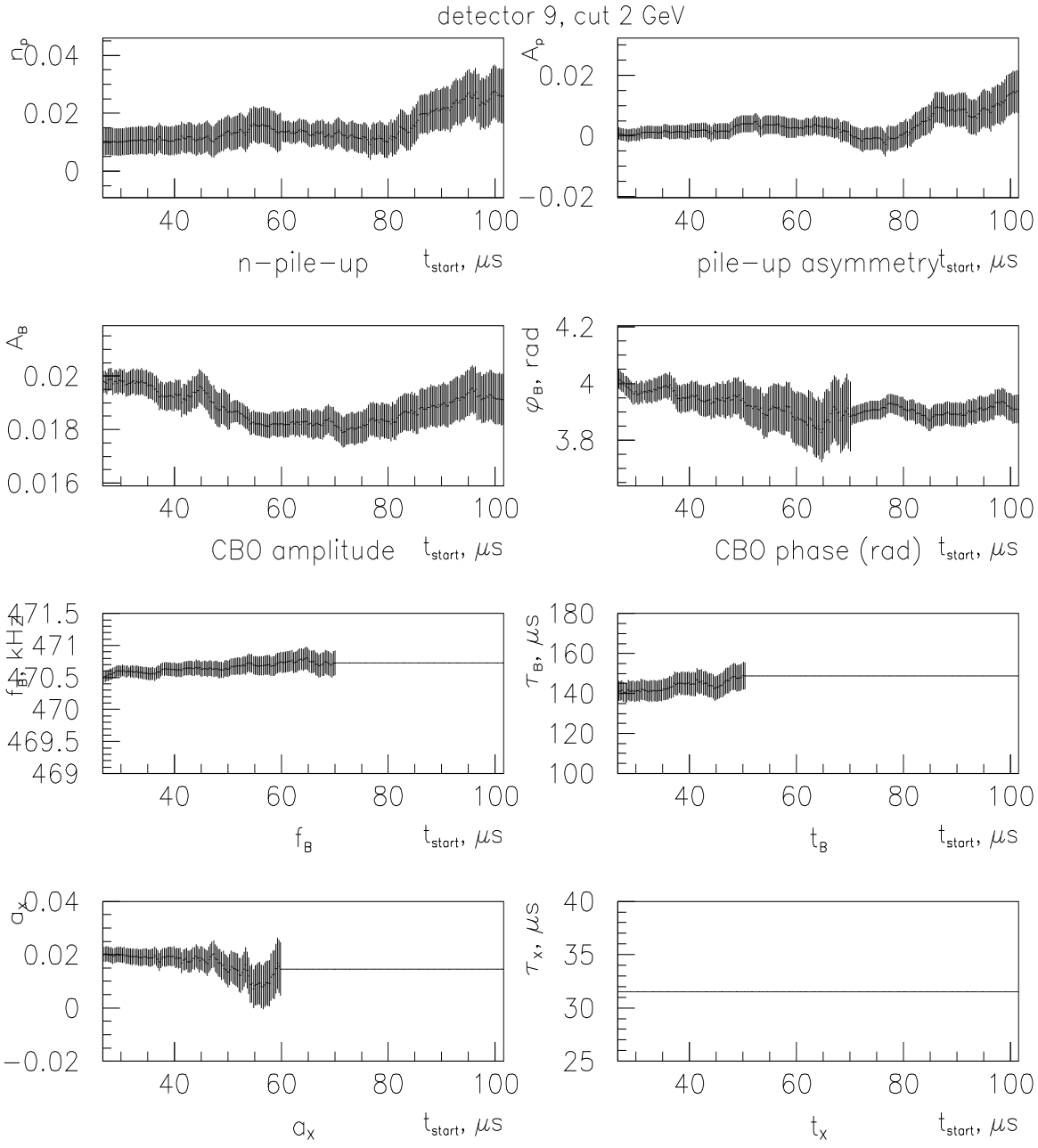

Fig.19b. Fit results for detector 9 (cut 2 GeV). Fit parameters are plotted as a function of the fit start time: pile-up parameters n_p and A_p, coherent betatron oscillation parameters A_B, ϕ_B, f_B and τ_B, and muon loss parameters a_X and τ_X (the latter was fixed at 31.5 μs for all start times).

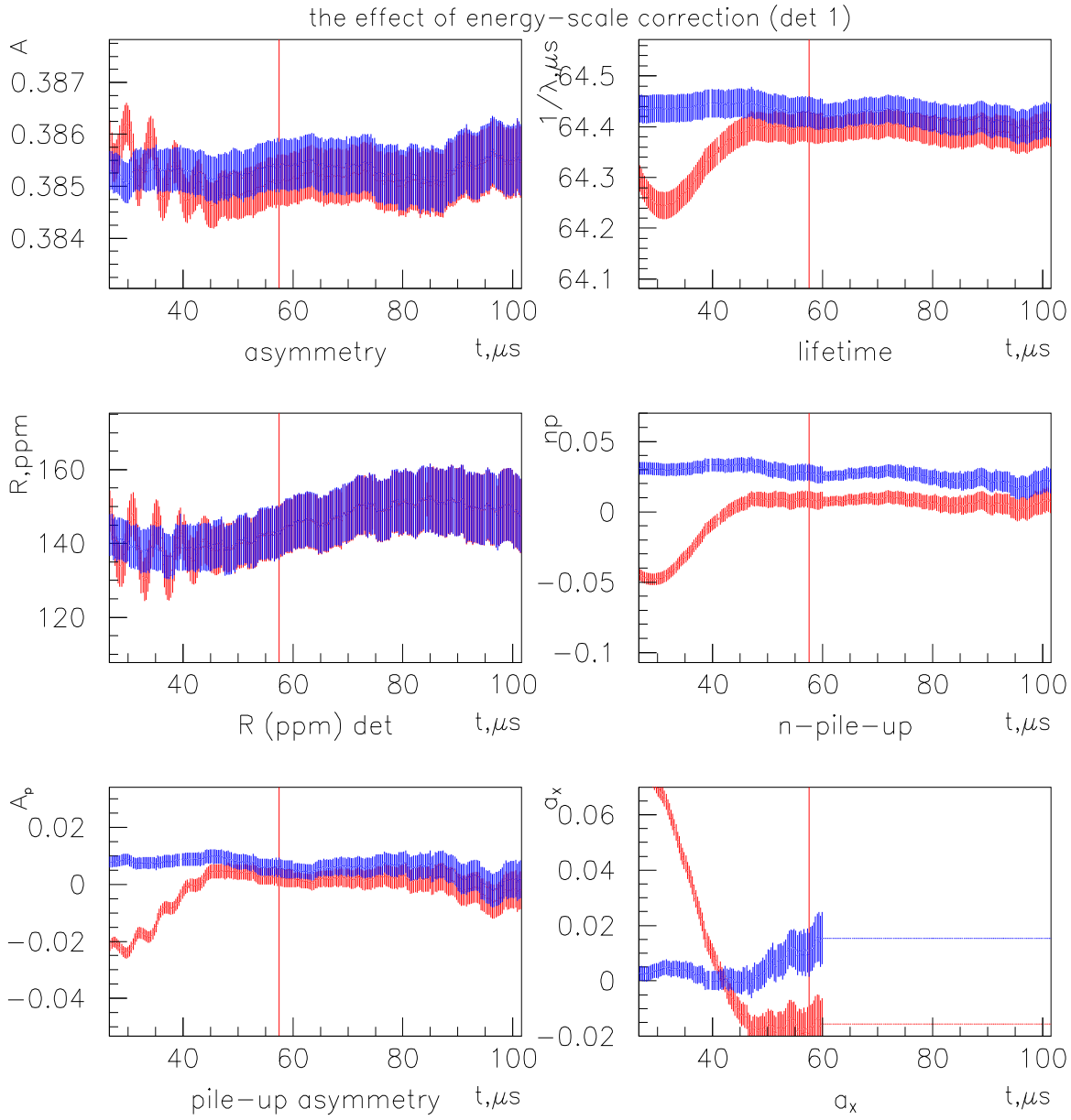

Fig.20. The effect of the energy-scale correction on fit parameters (e.g. detector 1). Some fit parameters are shown as a function of time before (red) and after (blue) the correction was applied. ES correction removed phase pulling on R and A at early times, without shifting the value of R at the zero crossings (more on that when we talk about the systematic errors); pile-up and "muon loss" parameters are stable from early to late time. Also, the unphysical "muon gain" (negative a_X after 40 μs) is no longer there after the correction is applied. (Oversized error bars at 58 μs are produced by a failed fit.)

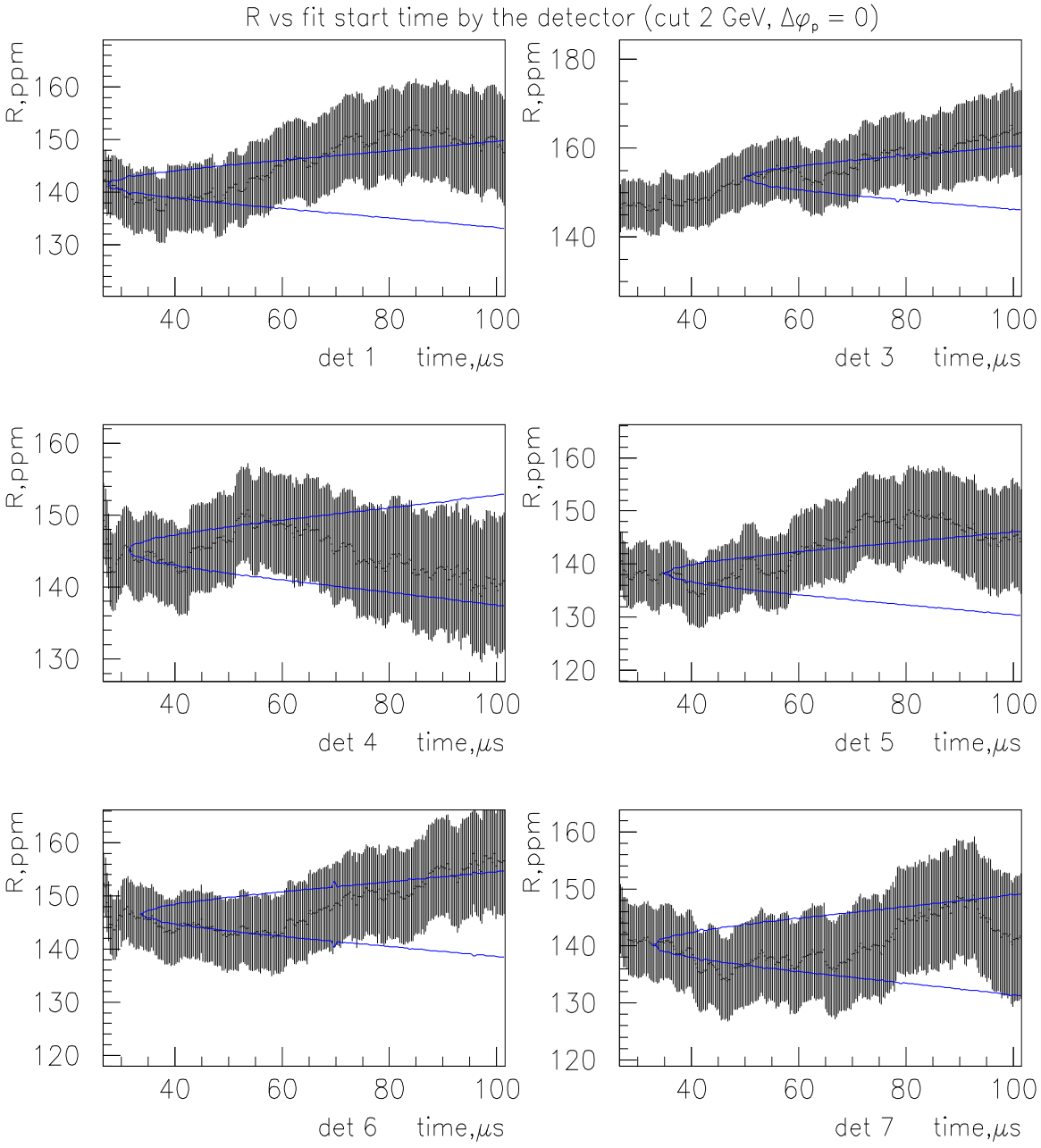

Fig.21a. Fitted R value as a function of fit start time for detectors 1-7, cut 2 GeV.

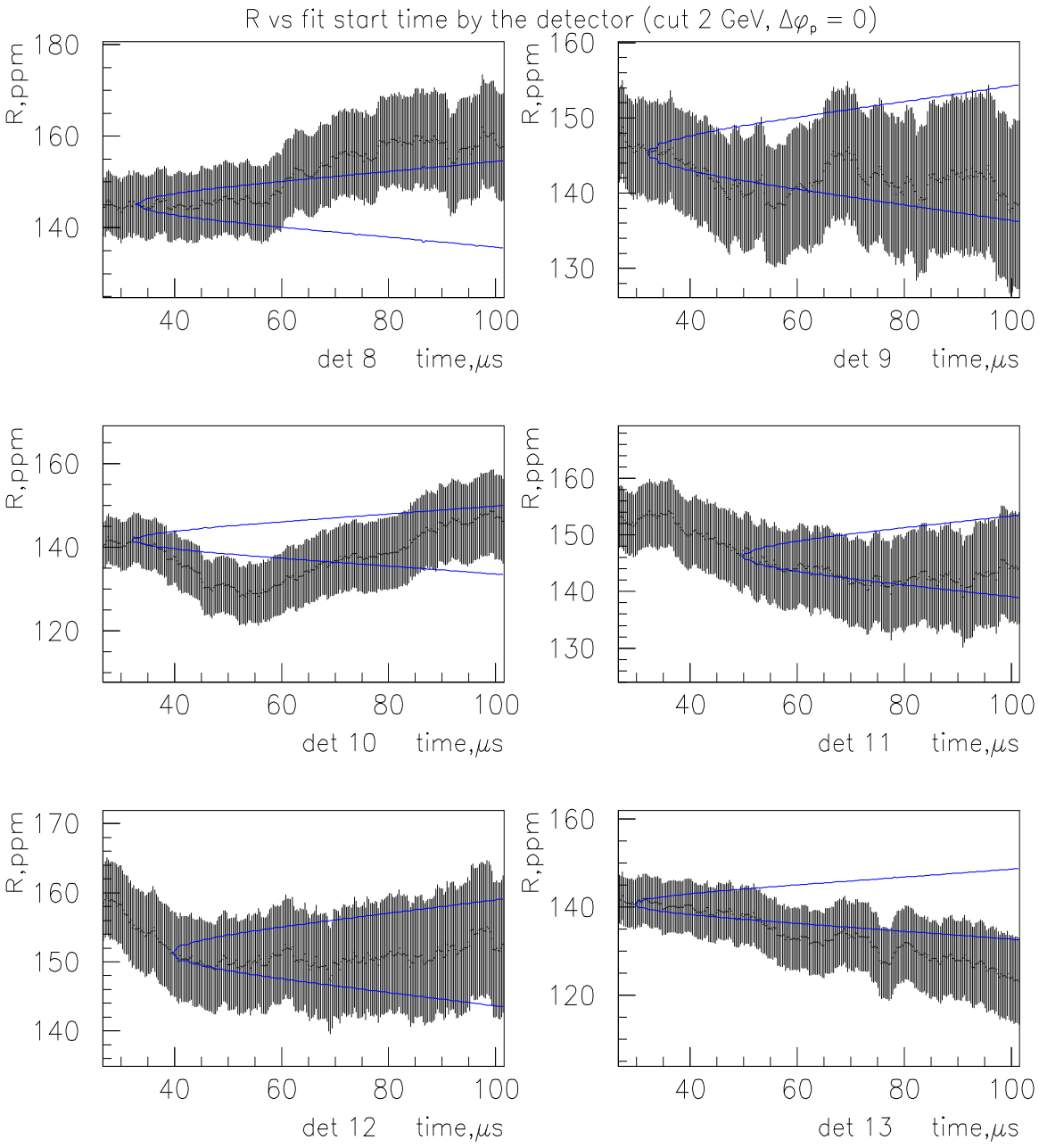

Fig.21b. Fitted R value as a function of fit start time for detectors 8-13, cut 2 GeV.

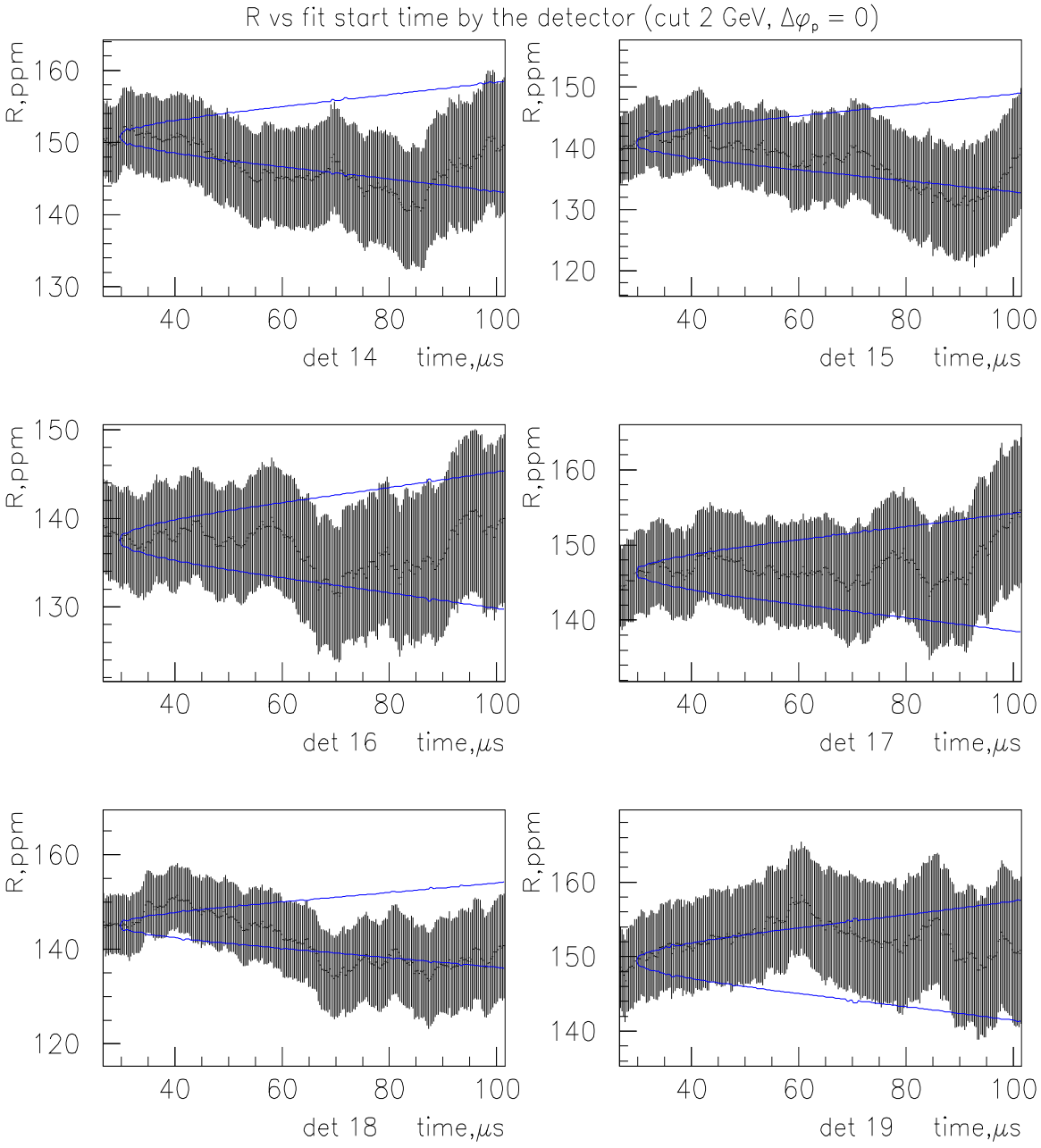

Fig.21c. Fitted R value as a function of fit start time for detectors 14-19, cut 2 GeV.

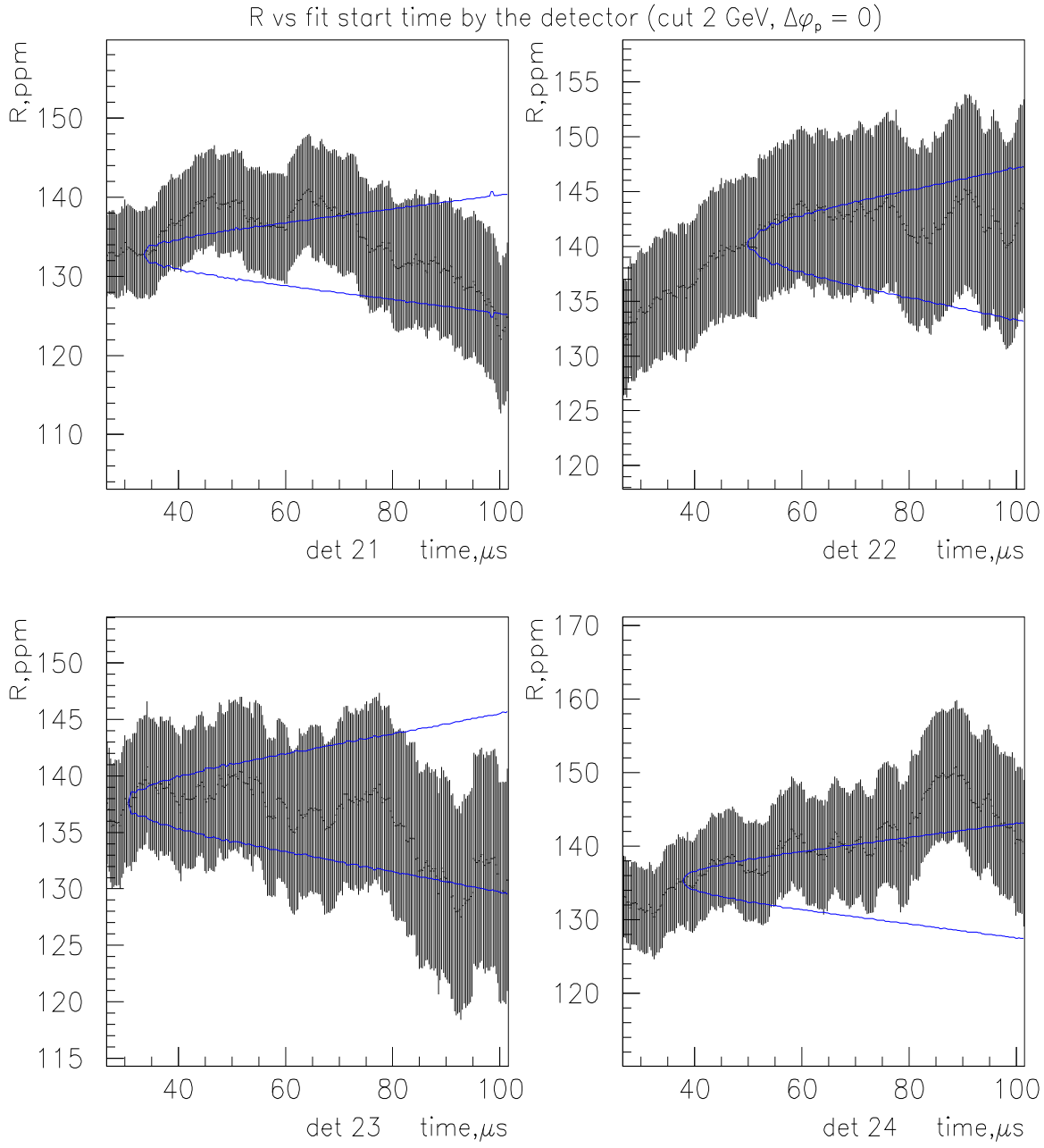

Fig.21d. Fitted R value as a function of fit start time for detectors 21-24, cut 2 GeV.

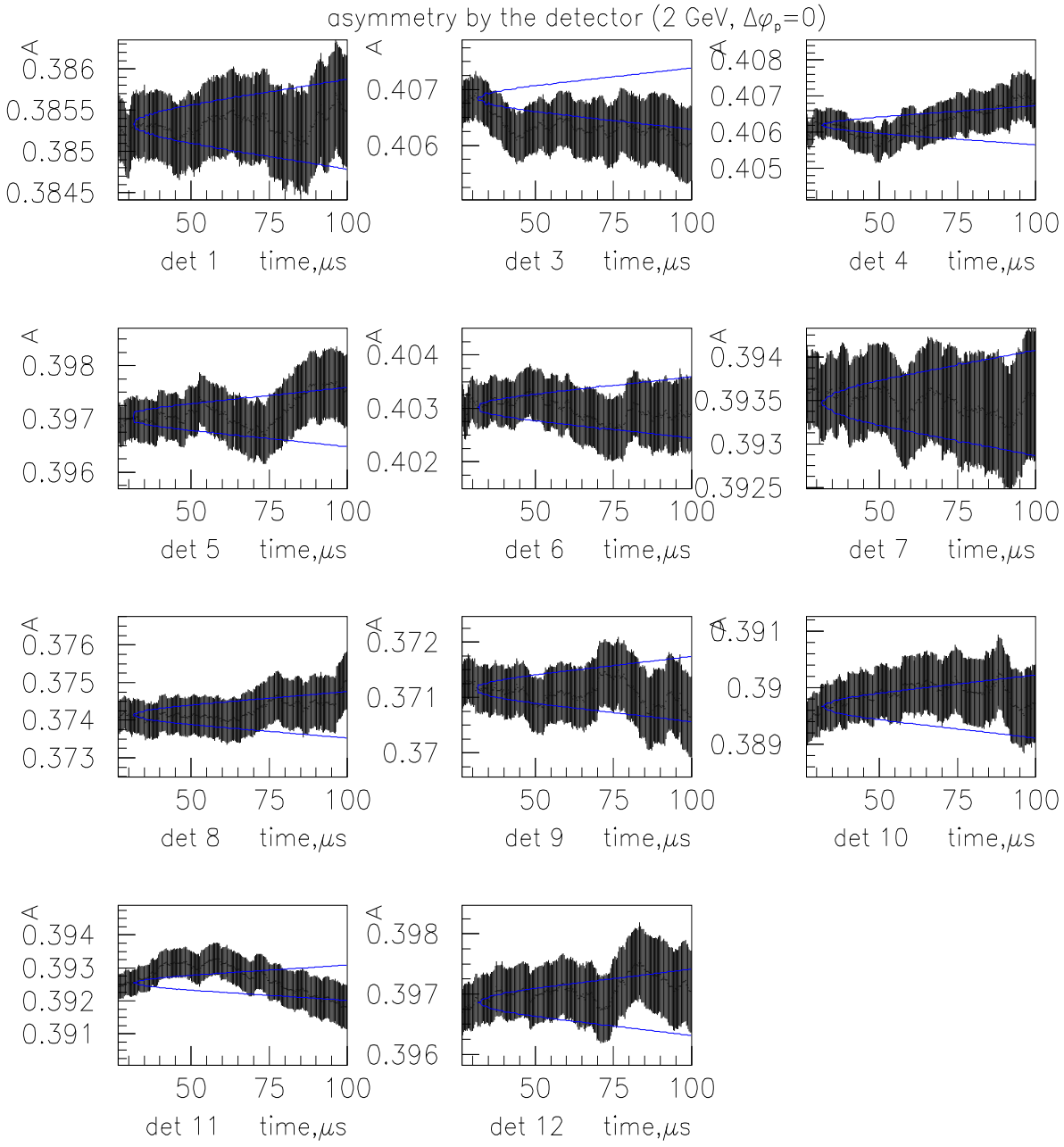

Fig.22a. Asymmetry as a function of fit start time for detectors 1-12, cut 2 GeV. "Kawall bounds" are shown with respect to the start time of 32 μs.

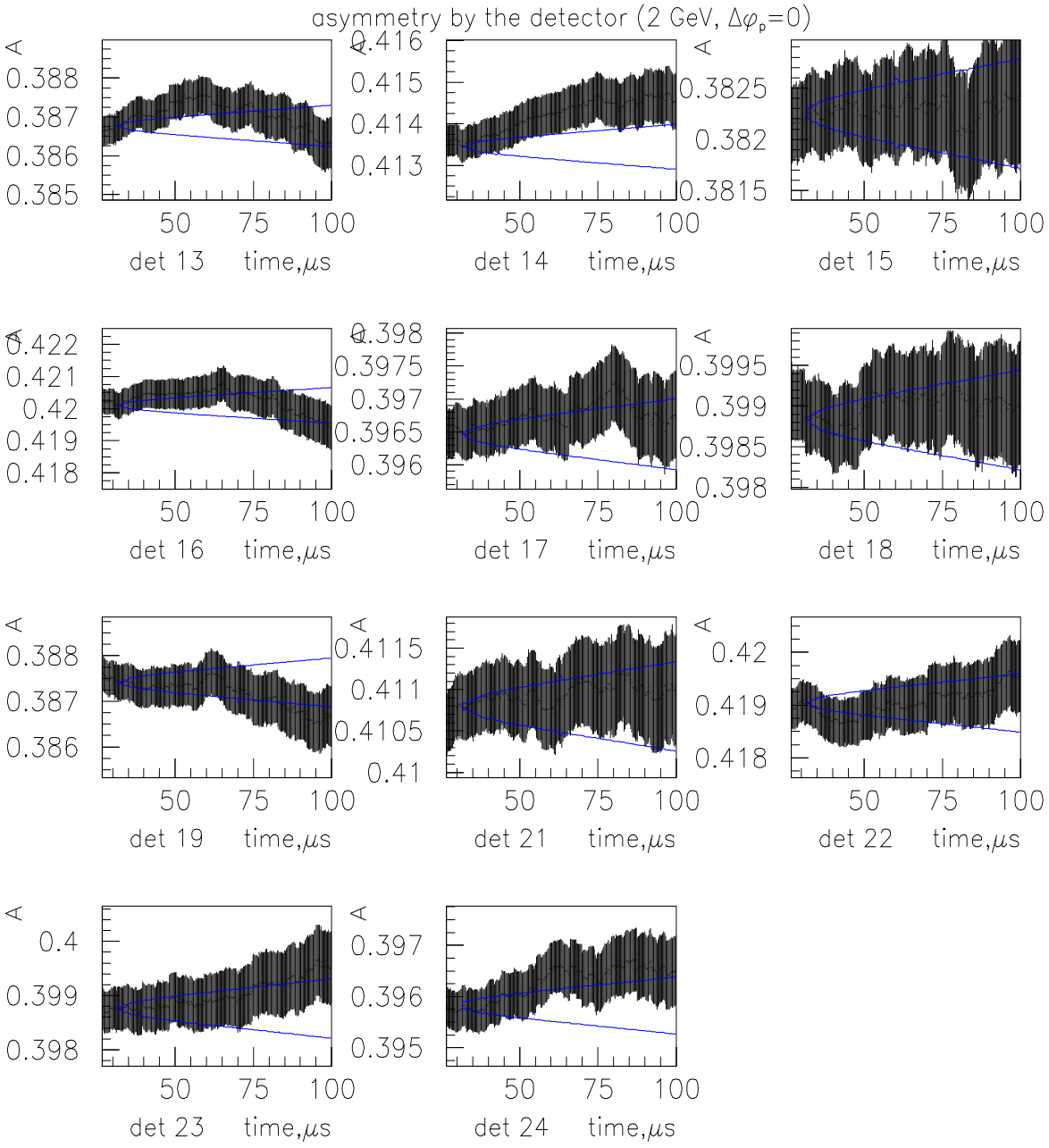

Fig.22b. Asymmetry as a function of fit start time for detectors 13-24, cut 2 GeV. "Kawall bounds" are shown with respect to the start time of 32 μs.

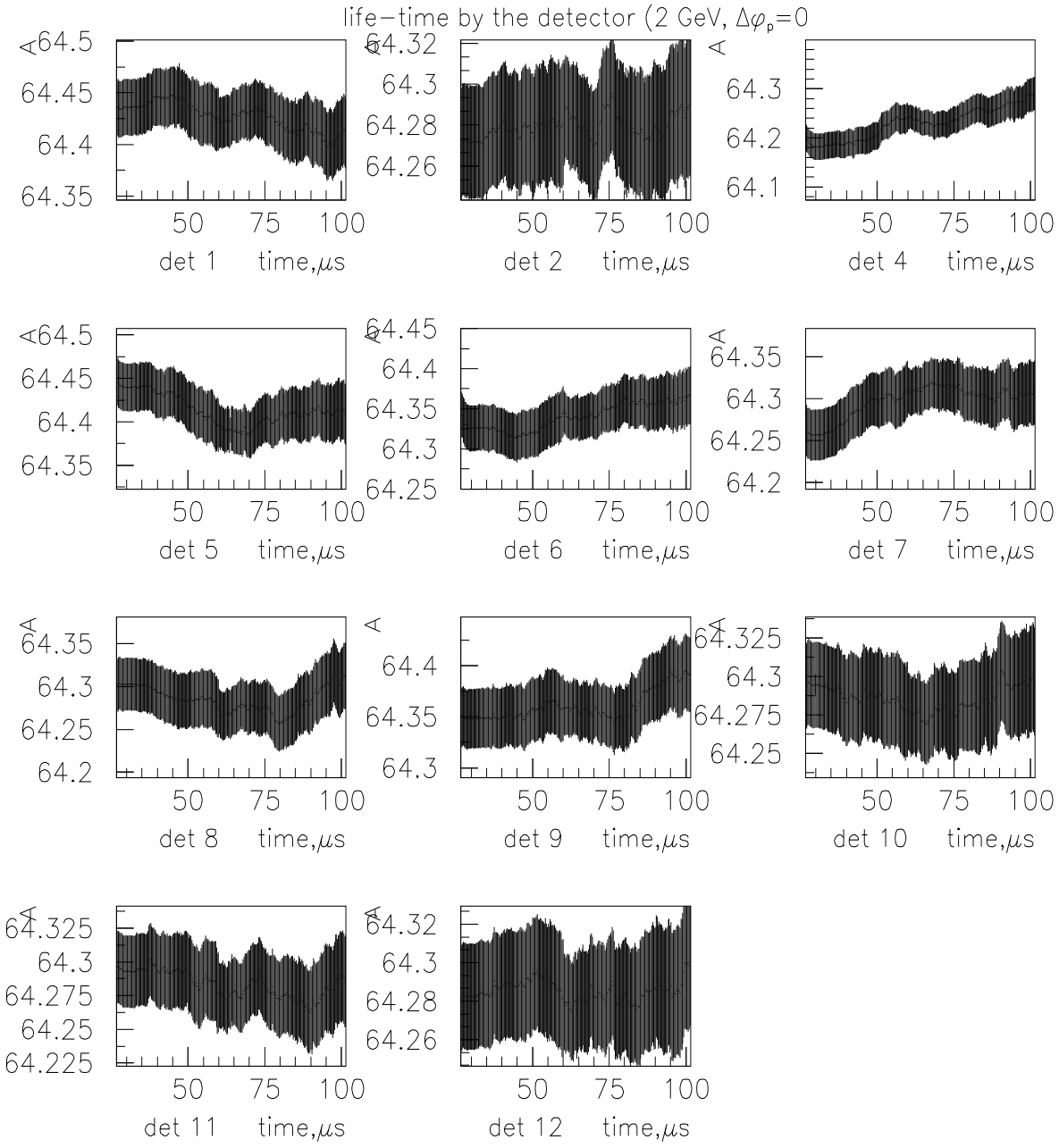

Fig.23a. Fitted muon lifetime (in μs) as a function of fit start time for detectors 1-12, cut 2 GeV. "Kawall bounds" are not shown, since the error on $1/\lambda$ is reduced significantly after some other parameters are fixed at 50 μs. Typos: the plot in the center of the top row is for detector 3; y-axis shows $1/\lambda$ in μs (not A).

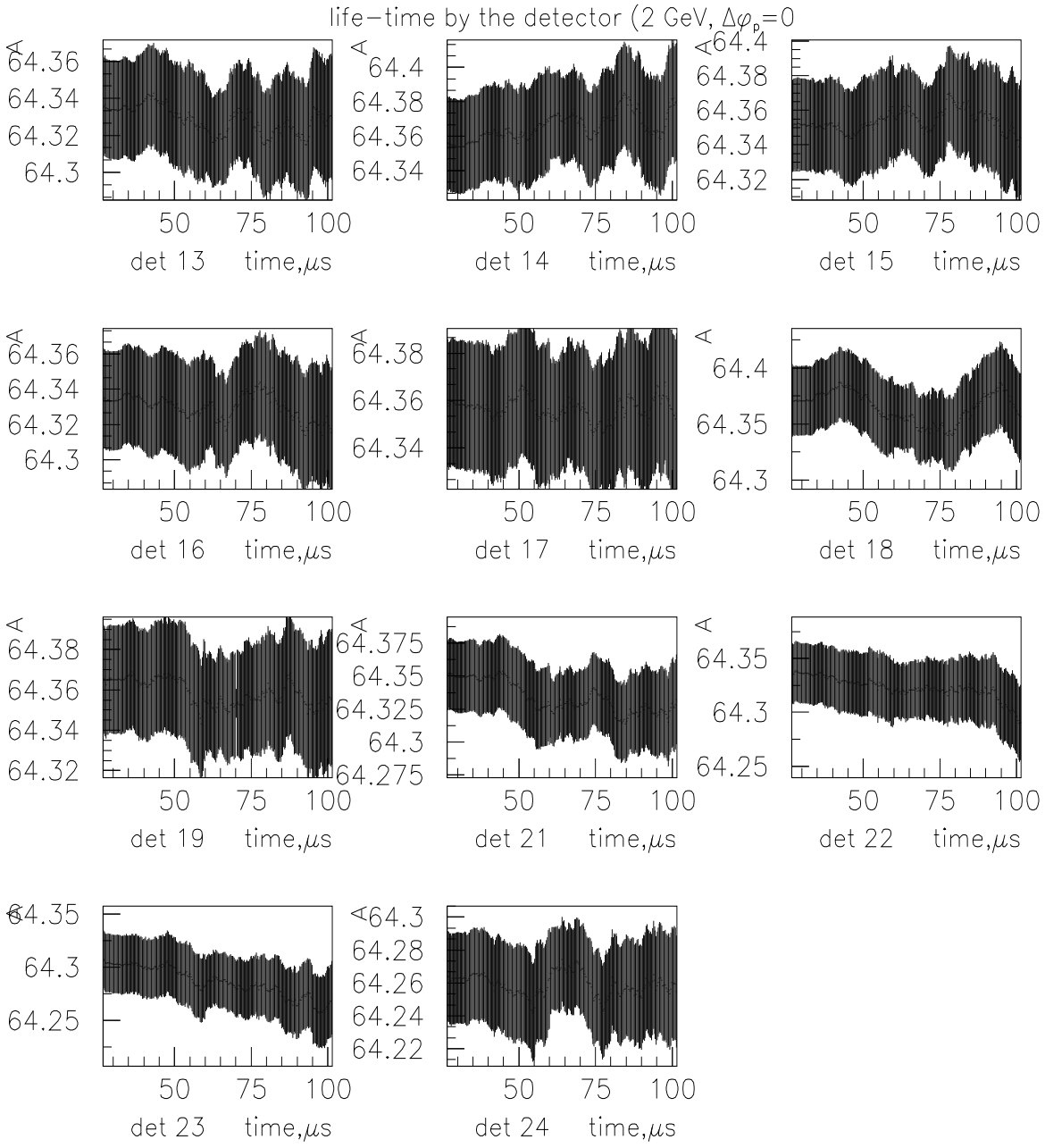

Fig.23b. Fitted muon lifetime (in μs) as a function of fit start time for detectors 13-24, cut 2 GeV. A typo: y-axis shows $1/\lambda$ *in μs (not A).*

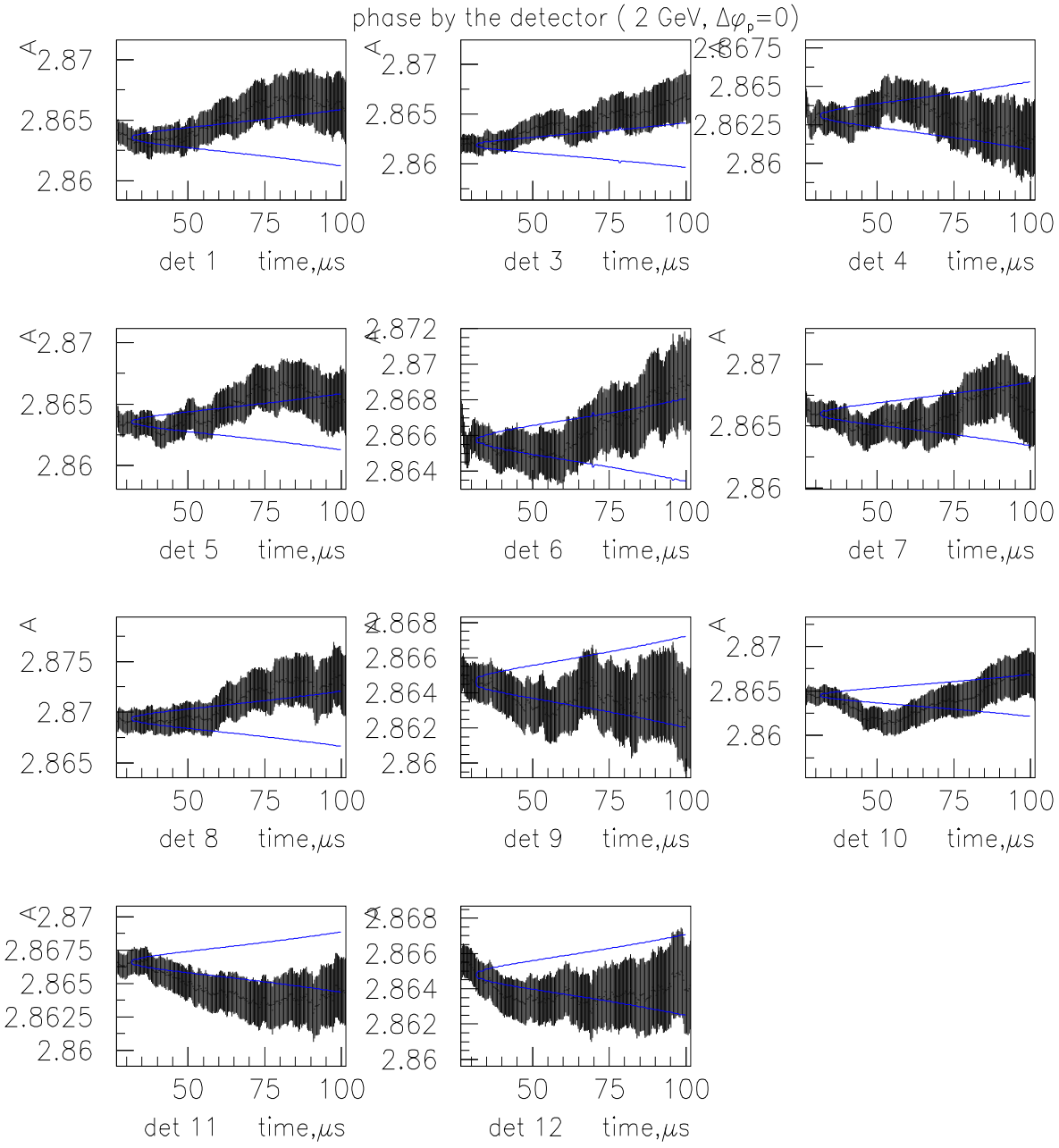

Fig.24a. Fitted g-2 phase (in rad) as a function of fit start time for detectors 1-12, cut 2 GeV. "Kawall bounds" are shown with respect to the start time of 32 μs. A typo: y-axis shows ϕ in radians (not A).

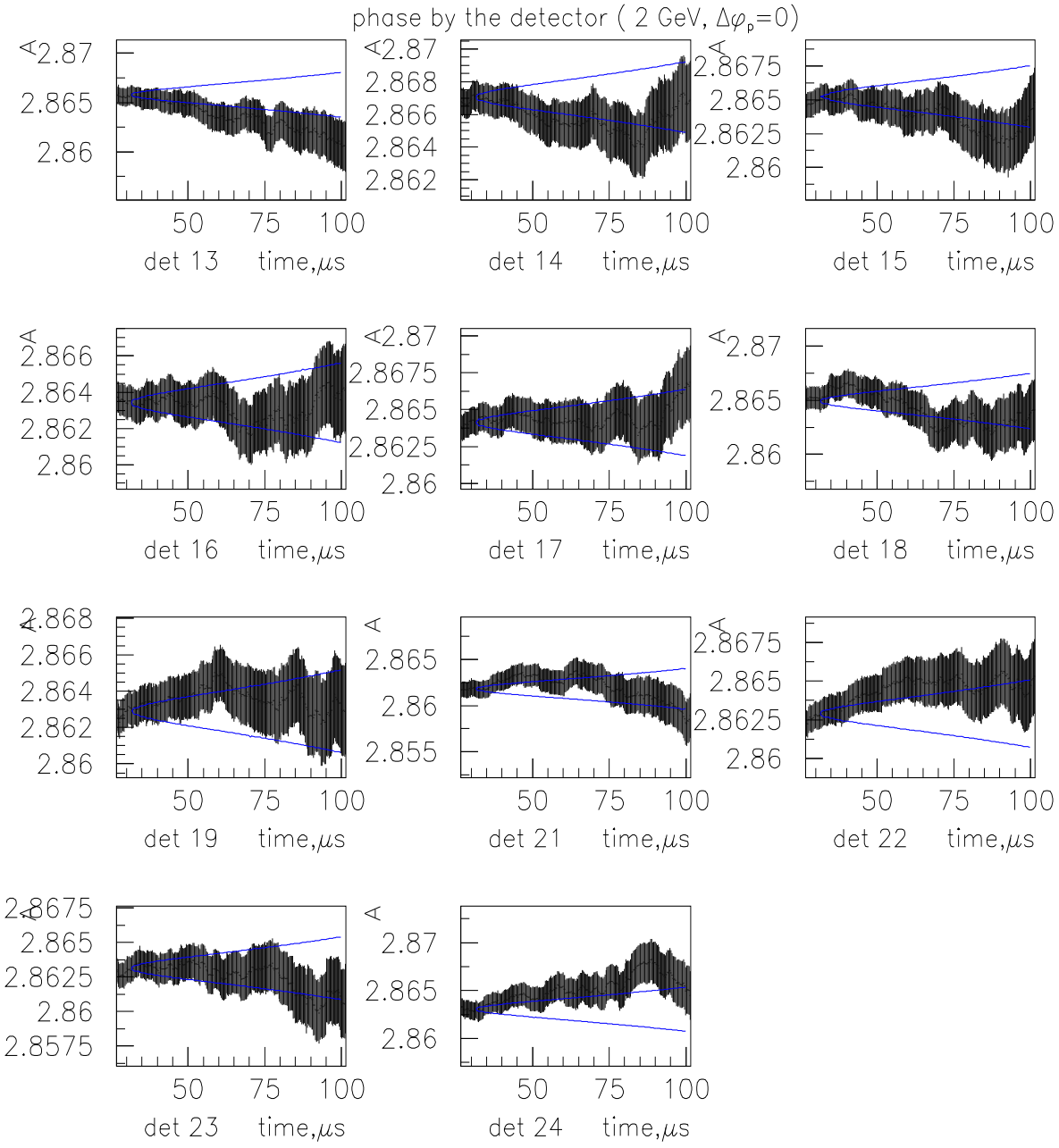

Fig.24b. Fitted g-2 phase (in rad) as a function of fit start time for detectors 13-24, cut 2 GeV. "Kawall bounds" are shown with respect to the start time of 32 μs. A typo: y-axis shows ϕ in radians (not A).

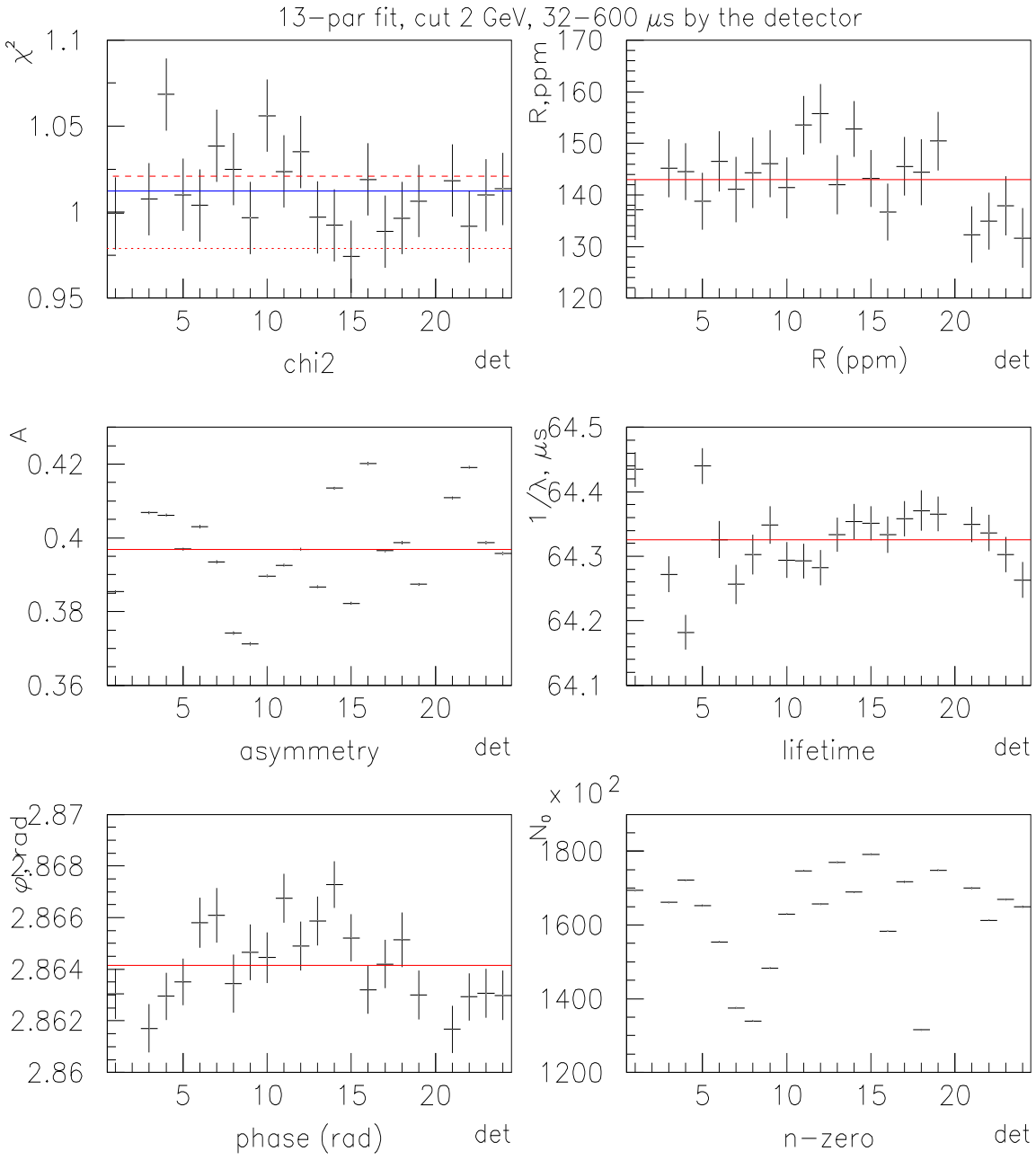

Fig.25a. Values of fit parameters (average over 10 random seeds) by the detector for a fit starting at 32 μs (cut 2 GeV, $\Delta\phi_p = 0$): (top left to bottom right): χ^2, R (ppm), A, $1/\lambda$ (μs), ϕ (rad) and N_0 vs detector number. For comparison, the values of some parameters for the case of detectors added together are shown with horizontal lines.

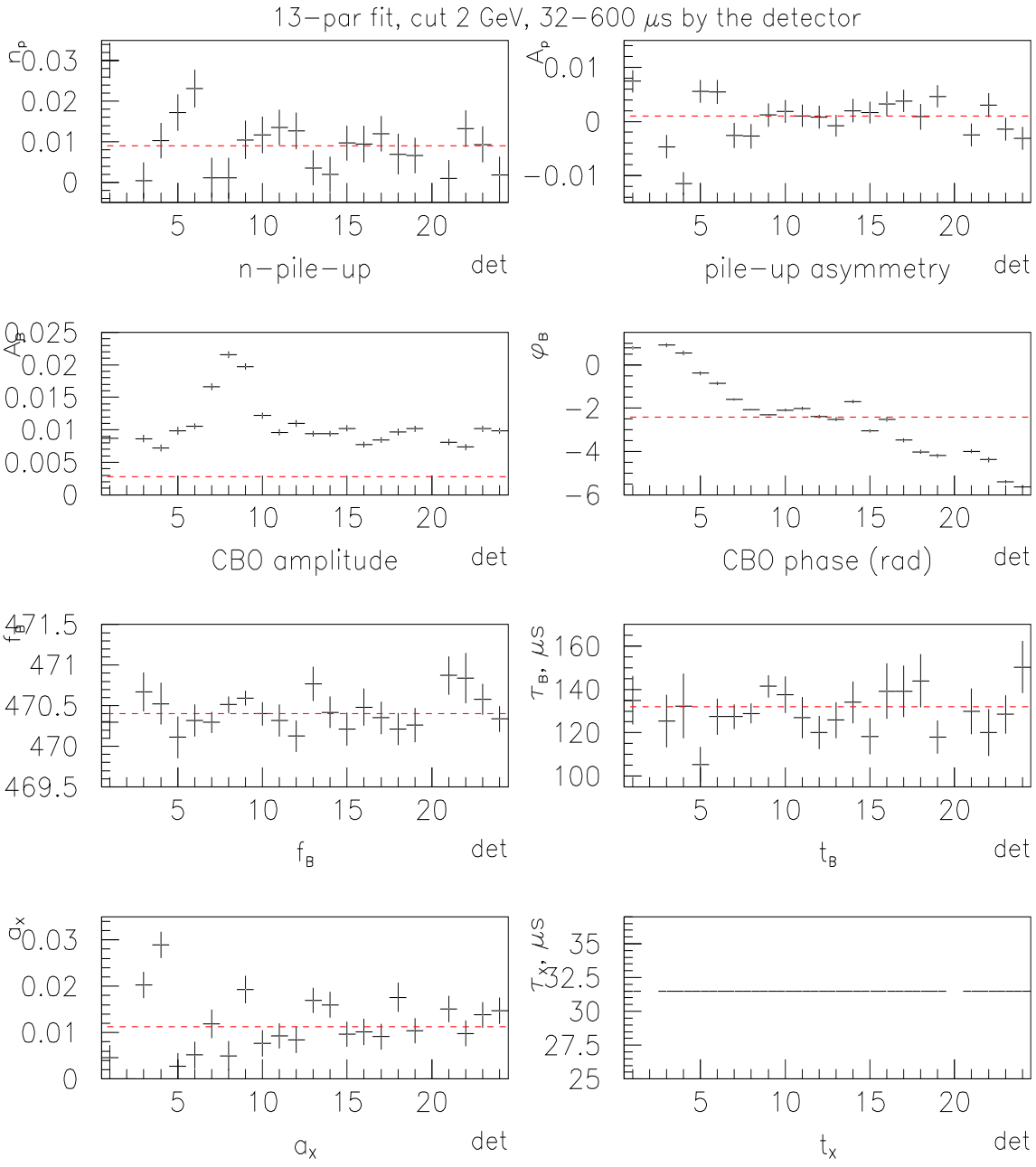

Fig.25b. Values of fit parameters by the detector for a fit starting at 32 μs (cut 2 GeV): (top left to bottom right): n_p, A_p, A_B, ϕ_B (rad), f_B (kHz), τ_B (μs), a_X and τ_X (μs, fixed) vs detector number. For comparison, the values of some parameters for the case of detectors added together are shown with horizontal lines.

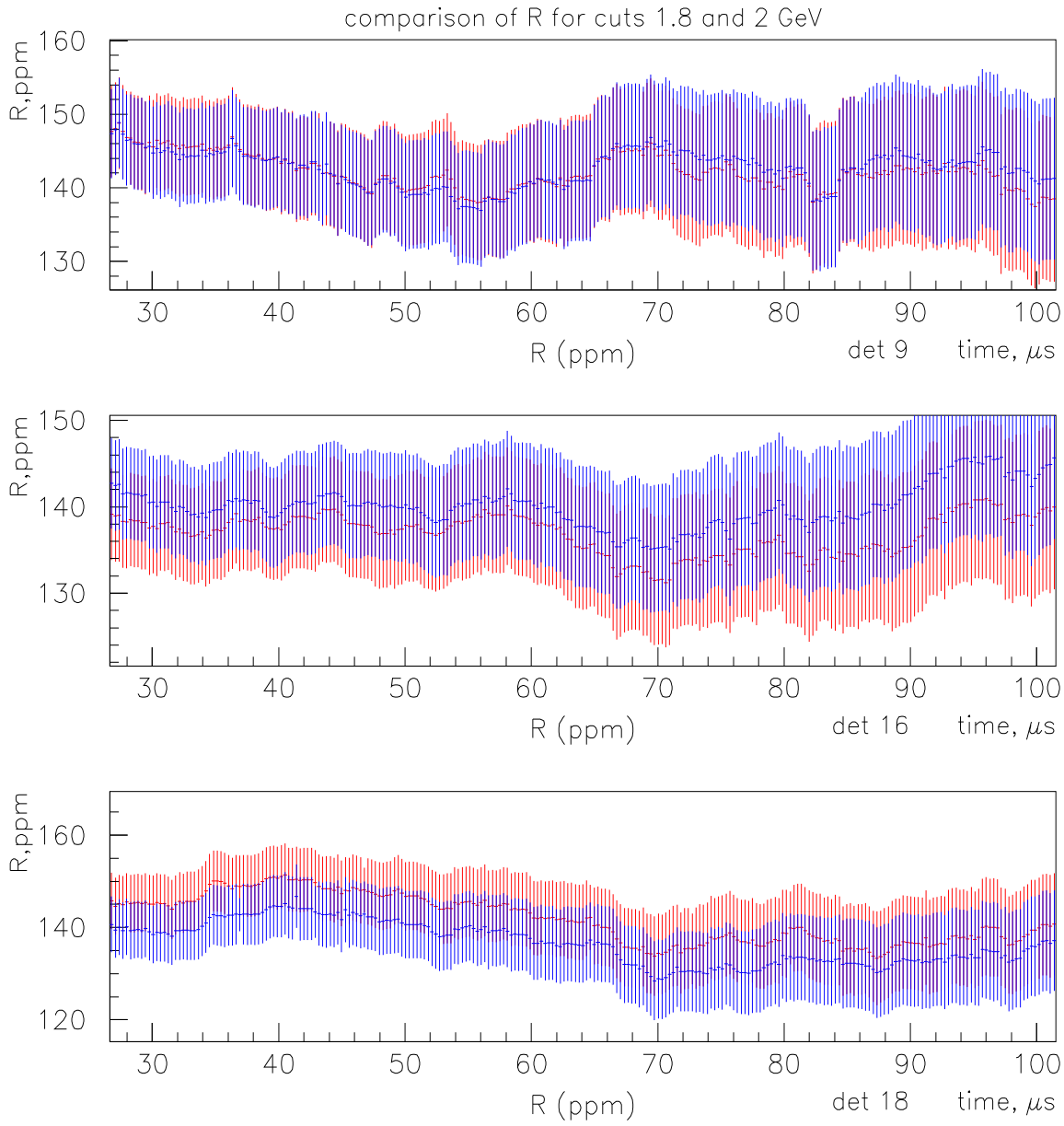

Fig.26. A difference in R values between cuts 1.8 and 2 GeV was observed in some detectors (as well as for the data from all detectors added together), the pile-up phase $\Delta\phi_p$ was fixed at 0 for all detectors. On the plots above: R for the cut 1.8 GeV is shown in blue, for 2 GeV in red. No significant change is seen in detector 9 (top, also dets. 3, 5, 7, 9, 10, 13, 15, 17, 24). Middle: for detector 16, the value of R for the cut 1.8 GeV is lower than for the cut 2 GeV (similar in detectors 1, 6, 8, 11, 22) Bottom: for detector 18, the value of R for the cut 1.8 GeV is higher than for the cut 2 GeV (similar in detectors 4, 12, 14, 19, 21, 23)

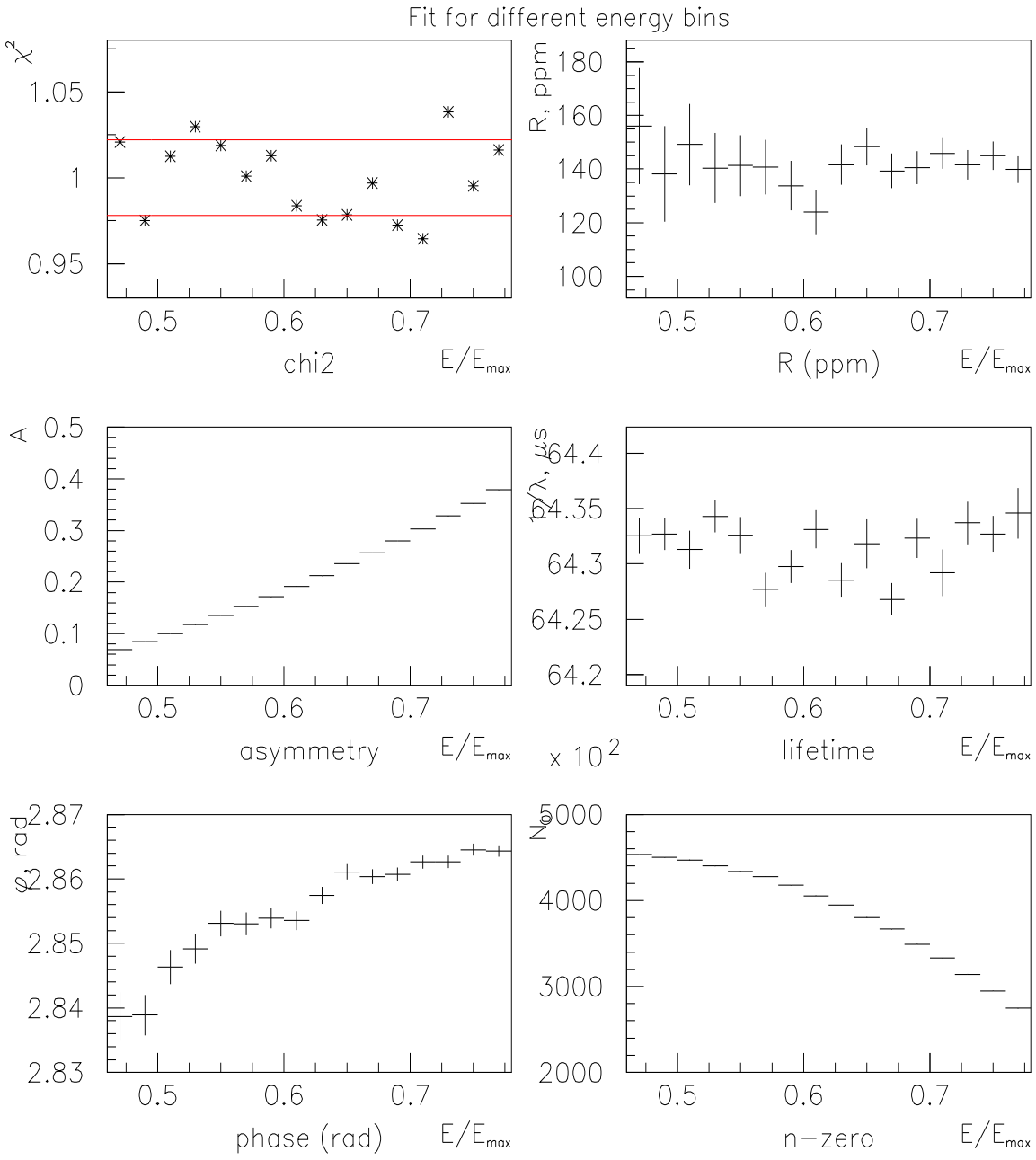

Fig.27a. Fit parameters for selections covering different energy bins: (top left to bottom right): χ^2, A, $1/\lambda$ (μs), R (ppm), ϕ (rad), N_0 vs positron energy (normalized to 3.1 GeV).

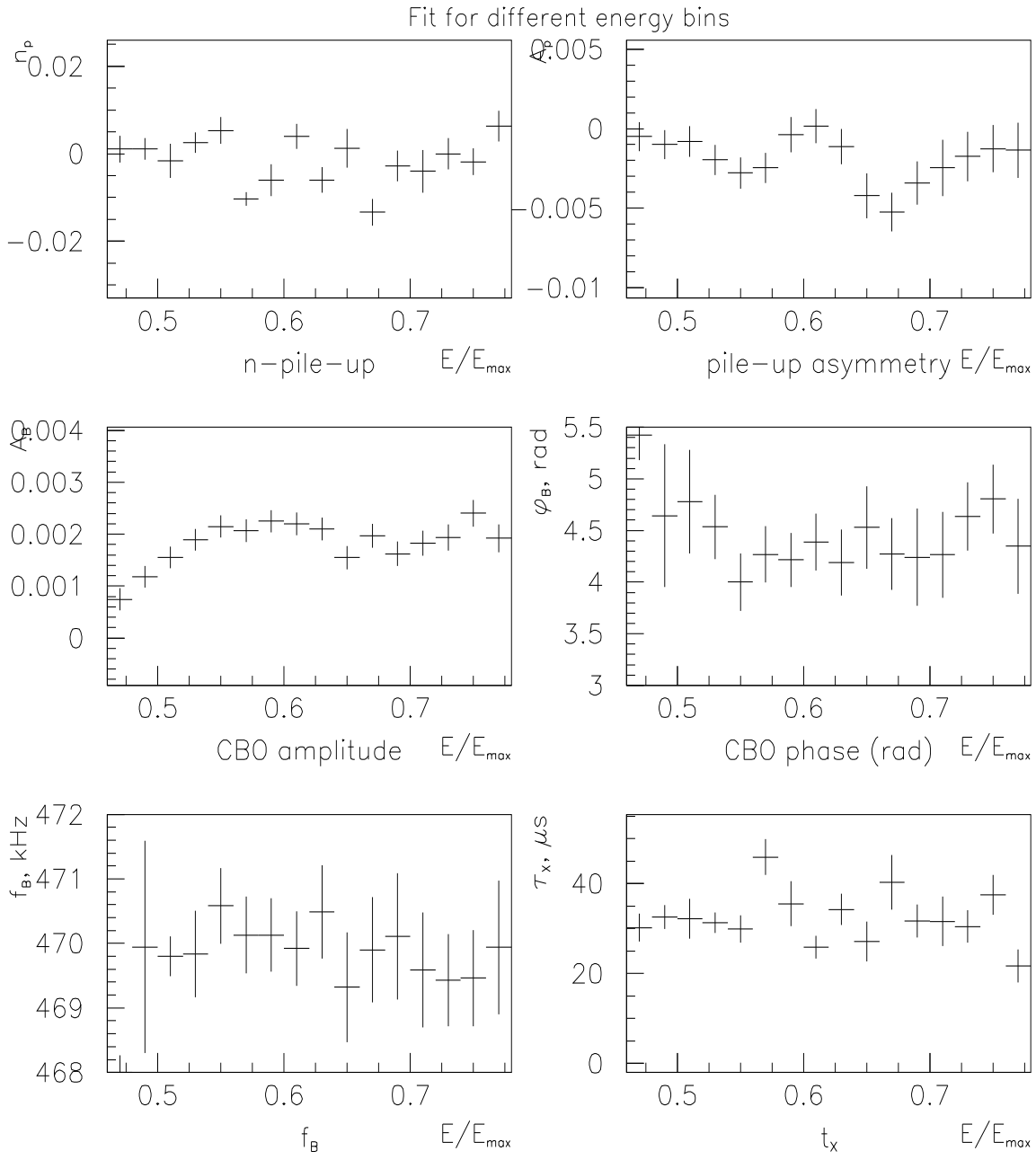

Fig.27b. Fit parameters for selections covering different energy bins (continued): (top left to bottom right): n_p, A_p, A_B, ϕ_B (rad), f_B (kHz) and τ_X vs positron energy (normalized to 3.1 GeV).

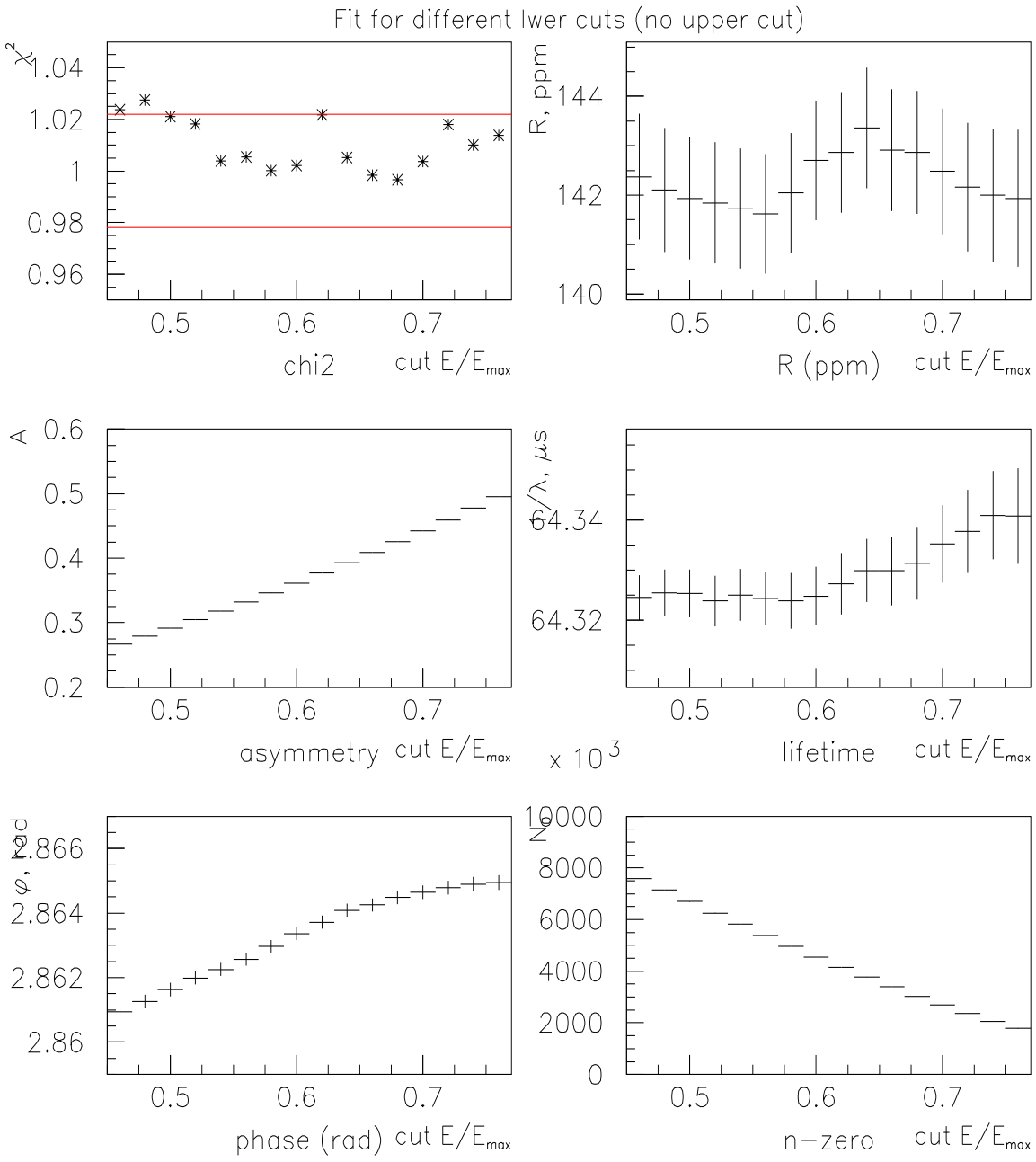

Fig.28a. Fit parameters for selections with different lower cuts: (top left to bottom right): χ^2, A, $1/\lambda$ (μs), R (ppm), ϕ (rad), N_0 vs lower cut value (normalized to 3.1 GeV).

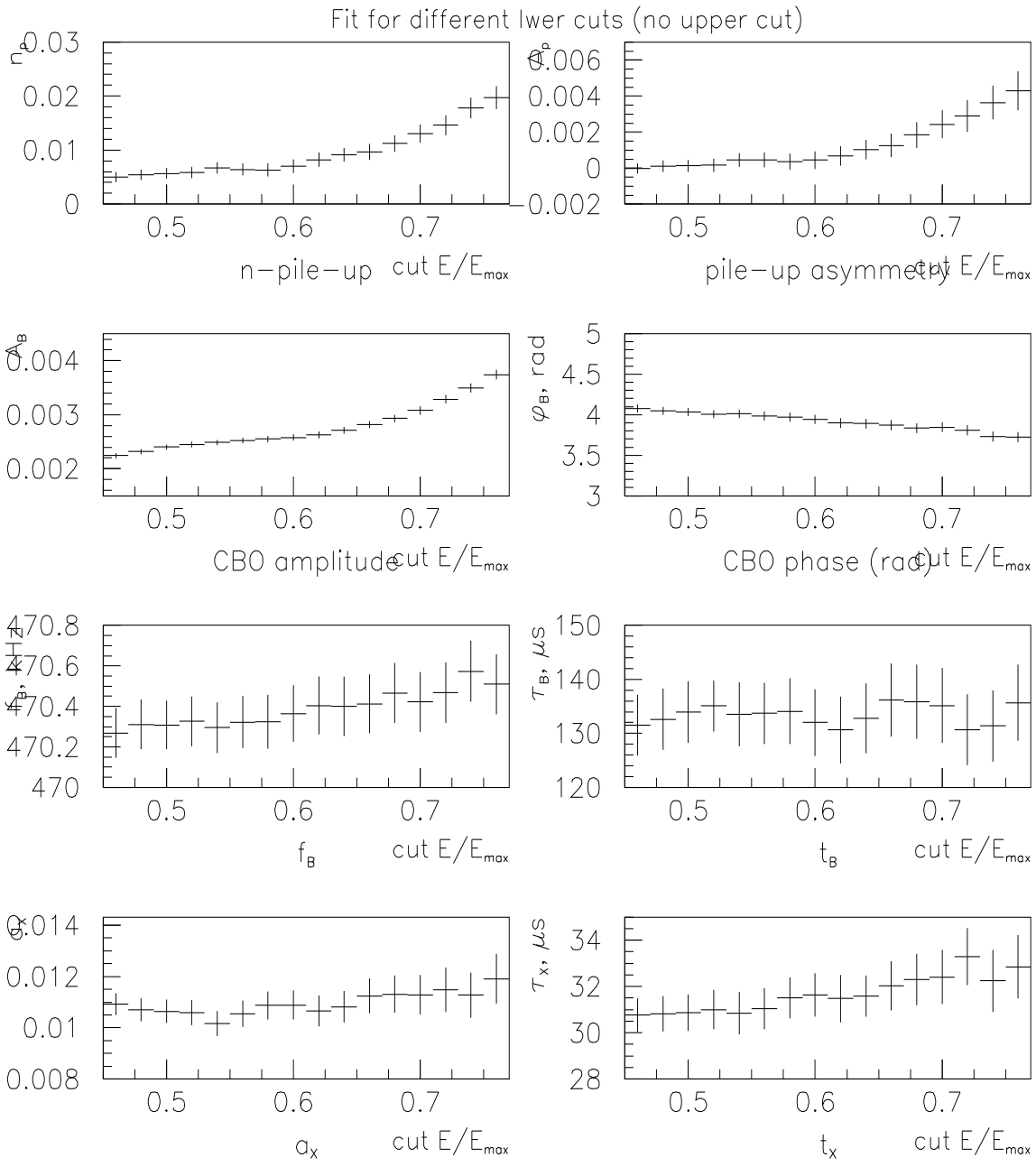

Fig.28b. Fit parameters for selections with different lower cuts (continued): (top left to bottom right): n_p, A_p, A_B, $|phi_B$ (rad), f_B (kHz), τ_B (μs), a_X and τ_X (μs) vs lower cut value (normalized to 3.1 GeV).

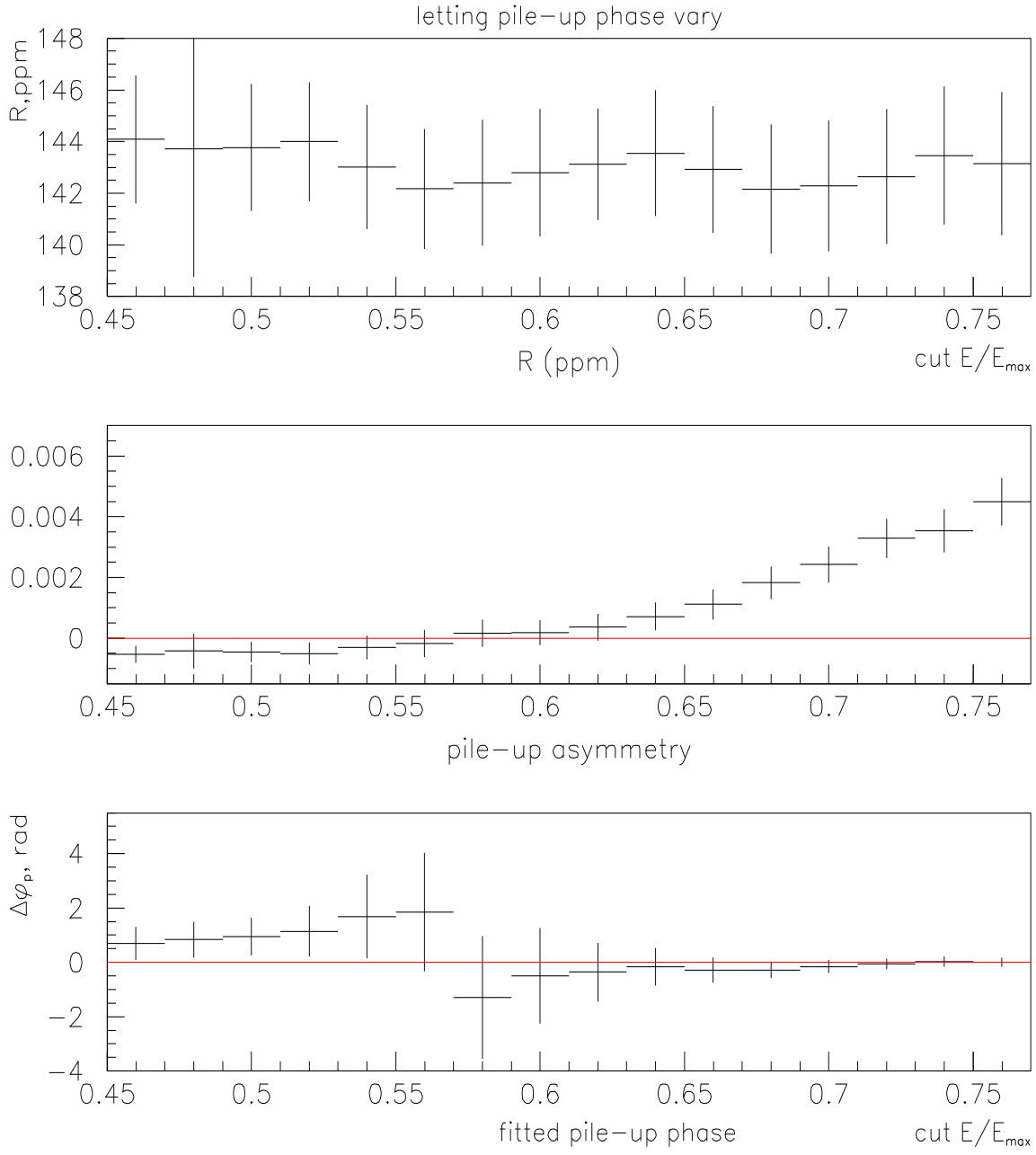

Fig.29. Fit results for different lower cuts: pile-up phase $\Delta\phi_p$ is a free parameter. Pile-up asymmetry is crossing zero for a threshold of around 0.57·E_{max}, slightly lower than 1.8 GeV. The pile-up phase is singular, and its uncertainty is big for that region. Things look a bit better for the cut 2 GeV ($\simeq 0.64 \cdot E_{max}$).

4.5 "Detectors Combined" Revisited (Trying to Find a Correct Pile-up Phase $\Delta\phi_p$)

The results of fitting to the data selections with different energy thresholds, with and without fixing the pile-up phase, shows that the value of R is very sensitive to the choice of $\Delta\phi_p$. This phase shift between the (g-2) and pile-up wiggles may differ from 0 significantly, when pile-up asymmetry is small. Unfortunately, this is exactly the case for the cuts we looked at: 1.8 and 2 GeV. As can be seen in Figs. 13b, 14b, the fitted values of pile-up asymmetry for both of these cuts differ from 0 by less than one standard deviation for most of the fit start times. Obviously, one needs a better estimate of $\Delta\phi_p$ to get more reliable results.

Obtaining an estimate of $\Delta\phi_p$ from the fit by making it a free parameter is not a trivial task. Since pile-up asymmetry for the 1.8 and 2-GeV cuts is very small the fit results are only stable for early fit start times and the fit errors on pile-up phase are very large (Figs.30b,c). On the other hand, a larger asymmetry observed for the cut 1.8-3.1 GeV (see Fig. 15b) allows for a stable fit (Fig.30a). The average fitted phase for that cut was found to be $\Delta\phi_p = 97 \pm 38$ mrad, with the spread of the phase distribution much smaller than the fit errors ($\simeq$150 mrad for the fit starting at 32 μs). (Jumping ahead a bit, this value may seem too large: compare to $\Delta\phi_p = 13 \pm 4$ mrad for the cut 2-3.1 GeV from pile-up subtraction, but since there is no better way to determine $\Delta\phi_p$ for cuts lower than 2 GeV I will use this estimate.)

For the cut 2 GeV and higher, it is possible to obtain estimates of the pile-up phase by applying pile-up subtraction (PUS) and fitting to the pile-up spectrum directly. I used the subtraction method developed by Yannis and Cenap [10] (with a dead time of 2.9 ns, and the offset time of 10 ns). Pile-up spectra were fitted to the function given by Eqn.7 (Only N_{0p}, λ_p, A_p and $\Delta\phi_p$ were free parameters, the rest were fixed at the values obtained by fitting to the pile-up subtracted spectra).

$$N(t) \; = \; N_{0p} \cdot e^{-\lambda_p t}(1 + A_p \cdot \cos(\omega_a t + \phi + \Delta\phi_p)) \cdot f_{fr}(t) \cdot f_{CBO}(t) \cdot f_X(t) \qquad (7)$$

The results of fit to the pile-up parameters for different energy thresholds are shown in Figs.31a,b (with and without an upper cut of 3.1 GeV). For the cut 2 GeV, I found $\Delta\phi_p = -68 \pm 31$ (Using the same method on a slightly different data set, Cenap finds $\Delta\phi_p = -59 \pm 35$ [2]). The pile-up asymmetry for this cut was $A_p \simeq 0.061 \pm 0.002$ (in the notation of Eqn.7, with the pile-up fraction n_p taken out of the brackets). A corresponding number from the fit with Eqn.2 would be $A_p(norm) = A_p/n_p \simeq 0.057 \pm .089$ (at 40 μs), therefore the estimate from pile-up subtraction may be applied to the original (without PUS) data set as a test value of $\Delta\phi_p$. There is no good estimate for the cut 1.8 GeV, but judging by Figs.29,30b, $\Delta\phi_p$ may be significantly larger than for the cut 2 GeV.

If the pile-up phase $\Delta\phi_p$ is fixed at values other than 0 for different cuts, it is possible to reconcile the results. On Fig.33, the results for R are compared between the three discussed cuts, with $\Delta\phi_p$(2 GeV)$= -68 \pm 31$ mrad (PUS), $\Delta\phi_p$(1.8 GeV)$= -500$ mrad (a guess) and $\Delta\phi_p$(1.8-3.1 GeV)$= 100$ mrad (another guess based on Fig.30a). Compared to Fig.17, where all three phases were fixed at 0, the agreement is much better, especially

between the cuts 2 and 1.8-3.1 GeV. It seems, for the cut 1.8 GeV $\Delta\phi_p$ may not be fixed effectively, due to a large uncertainty, but even for a very rough guess of the phase, the results from this cut differ from the other by less than $\frac{1}{2}\sigma$.

To illustrate just how sensitive the fit result for R may be to the choice of the pile-up phase, $\Delta\phi_p$ was fixed at both a "close" value of 100 mrad (a guess from the fit with $\Delta\phi_p$ as a free parameter, Fig.30a) and a "wrong" value of -100 mrad. This resulted in a shift in R of as much as 2σ for early start times (Fig.32).

Comparing figures 17 and 33, one can notice a better agreement between the 1.8 and 1.8-3.1 GeV cuts, when $\Delta\phi_p$ is fixed at 0, despite a big difference in the values of pile-up asymmetry. Fitting with A_p fixed at 0 (Fig.34) shows, that if $\Delta\phi_p$ is fixed at 0 as well, the presence of the pile-up asymmetry term in the fitting function mostly serves improving the χ^2, and the change in R caused by dropping that term altogether is much smaller than the effect caused by a wrong choice of $\Delta\phi_p$ (as in Fig.32). If the pile-up phase is held the same as the (g-2) phase, the term including A_p is taking care of the extra pulses at the peaks and in the valleys of the g-2 wiggle, but apparently does not distort the wiggle itself. If the pile-up phase assumed to be different, the wiggle becomes distorted (or should we say corrected?), which causes a shift in the fit values of R.

4.6 Some Studies With Pile-Up Subtracted Spectra

Pile-up subtracted spectra for different cuts were fitted to a full 17- parameter function (with the pile-up part present). The results confirmed the expectation: after the subtraction was applied, pile-up parameters were consistent with 0 (Figs.35a,b) for fit start times after 30-35 μs. On the average (for different fit start times), the value of non-wiggling pile-up fraction dropped by 94 %, after the procedure was applied. For the pile-up subtracted spectra, whether or not the pile-up parameters were kept in the fitting function, it did not have a significant effect on R (Fig.36).

The agreement was very good between the values of pile-up fraction and asymmetry obtained by fitting to the data and the pile-up spectrum from PUS (Table 7).

Table 7. Comparison of pile-up parameter values for the fit to the pile-up spectrum from PUS and the original data set. Eqns. 7 and 3 were used correspondingly, therefore A_p for the pile-up subtracted data set should be compared to A_p/n_p for the no-PUS case.

Cut, GeV	Pile-up Spectrum from PUS		No Pile-up Subtraction	
	n_p,$\times 10^{-2}$	A_p,$\times 10^{-2}$	n_p, $\times 10^{-2}$	A_p/n_p,$\times 10^{-2}$
2	0.78 ± 0.002	6.1 ± 0.2	0.81 ± 0.16	5.7 ± 8.9
2.1	1.03	12.6 ± 0.2	1.01 ± 0.18	10.8 ± 8.3
2.2	1.37	18.5 ± 0.2	1.30 ± 0.20	14.6 ± 7.8
2.3	1.81	23.0 ± 0.1	1.73 ± 0.22	17.5 ± 7.5
2.4	2.40	27.3 ± 0.1	2.05 ± 0.26	19.0 ± 7.2

The results for R from fitting to different cuts between 2 and 2.4 GeV seed are given in Fig.37 (pile-up subtracted spectra) and Fig.38 (no PUS, but the pile-up phase is taken from the subtraction studies). The results averaged over 10 random seeds for both regular

and pile-up subtracted data sets are given in Tables 8,9.

Table 8. The results for R are compared for different energy cuts at different start times. Averaged over 10 random seeds, **no pile-up subtraction**, $\Delta\phi_p = 0$. *The acceptable deviation of the* χ^2 *from 1 is 0.02295 at 32* μ*s, 0.024 at 80* μ*s.*

cut,	32 μs		40 μs		50 μs	
GeV	R	χ^2	R	χ^2	R	χ^2
2.0	143.00 ± 1.24	1.012	142.59 ± 1.31	1.009	142.67 ± 1.43	1.008
2.1	142.74 ± 1.26	1.018	142.14 ± 1.34	1.014	142.27 ± 1.46	1.014
2.2	142.87 ± 1.30	1.028	141.89 ± 1.38	1.025	142.26 ± 1.50	1.025
2.3	142.31 ± 1.36	1.022	141.91 ± 1.45	1.018	142.44 ± 1.57	1.020
2.4	142.18 ± 1.45	1.030	141.74 ± 1.54	1.030	142.30 ± 1.67	1.031
cut,	60 μs		70 μs		80 μs	
GeV	R	χ^2	R	χ^2	R	χ^2
2.0	142.86 ± 1.54	1.009	143.30 ± 1.67	1.009	143.42 ± 1.81	1.008
2.1	141.85 ± 1.57	1.015	142.06 ± 1.70	1.015	142.15 ± 1.84	1.014
2.2	141.96 ± 1.62	1.025	142.40 ± 1.76	1.024	142.93 ± 1.90	1.024
2.3	142.19 ± 1.69	1.020	142.75 ± 1.84	1.017	143.64 ± 1.99	1.016
2.4	141.78 ± 1.79	1.027	142.76 ± 1.95	1.026	143.85 ± 2.11	1.025

Table 9. The results for R are compared for different energy cuts at different start times. Averaged over 10 random seeds, **for pile-up subtracted data sets**.

cut,	32 μs		40 μs		50 μs	
GeV	R	χ^2	R	χ^2	R	χ^2
2.0	143.23 ± 1.24	1.014	142.68 ± 1.31	1.011	142.78 ± 1.43	1.010
2.1	142.92 ± 1.26	1.020	142.24 ± 1.34	1.016	142.43 ± 1.46	1.015
2.2	143.04 ± 1.30	1.028	142.04 ± 1.38	1.025	142.34 ± 1.50	1.027
2.3	142.45 ± 1.36	1.025	142.21 ± 1.44	1.024	142.54 ± 1.57	1.024
2.4	142.25 ± 1.45	1.036	141.87 ± 1.54	1.036	142.39 ± 1.67	1.037
cut,	60 μs		70 μs		80 μs	
GeV	R	χ^2	R	χ^2	R	χ^2
2.0	143.01 ± 1.54	1.012	143.34 ± 1.67	1.011	143.44 ± 1.81	1.010
2.1	141.95 ± 1.57	1.019	142.12 ± 1.70	1.016	142.16 ± 1.84	1.016
2.2	142.03 ± 1.61	1.029	142.48 ± 1.76	1.027	142.95 ± 1.90	1.029
2.3	142.26 ± 1.69	1.026	142.79 ± 1.84	1.021	143.61 ± 1.99	1.021
2.4	141.83 ± 1.80	1.035	142.87 ± 1.95	1.031	143.82 ± 2.11	1.032

From a simulation, I estimated an acceptable difference between the cuts 2 and 2.1 GeV to be of the order of $0.4{\cdot}\sigma$ (this can be a good approximation for any two "adjacent" cuts, with a threshold difference of 100 MeV), $0.54{\cdot}\sigma$ between the cuts 2 and 2.2 GeV, $0.67{\cdot}\sigma$ between 2 and 2.3, and $0.8{\cdot}\sigma$ between 2 and 2.4 GeV. Similar result can be obtained by using Sergei's formula for the variation of R between two sets of data, one of which is a

complete subset of the other [11]:

$$\sigma^2 \;=\; \sigma^2_{R_1} \cdot \left(1 + \frac{\sigma^2_{R_2}}{\sigma^2_{R_1}} - 2\frac{A_1}{A_2}\cos(\phi_1 - \phi_2)\right) \tag{8}$$

where "2" is a subset of "1", σ_{R_1}, A_1, ϕ_1 are the error on R, asymmetry and phase for the set-1 etc. Kawall's formula is a special case of (8), with $A_1 = A_2$, and $\phi_1 = \phi_2$. Based on these estimates, Yannis has demonstrated that the variation in R between different cuts is a statistical effect [12].

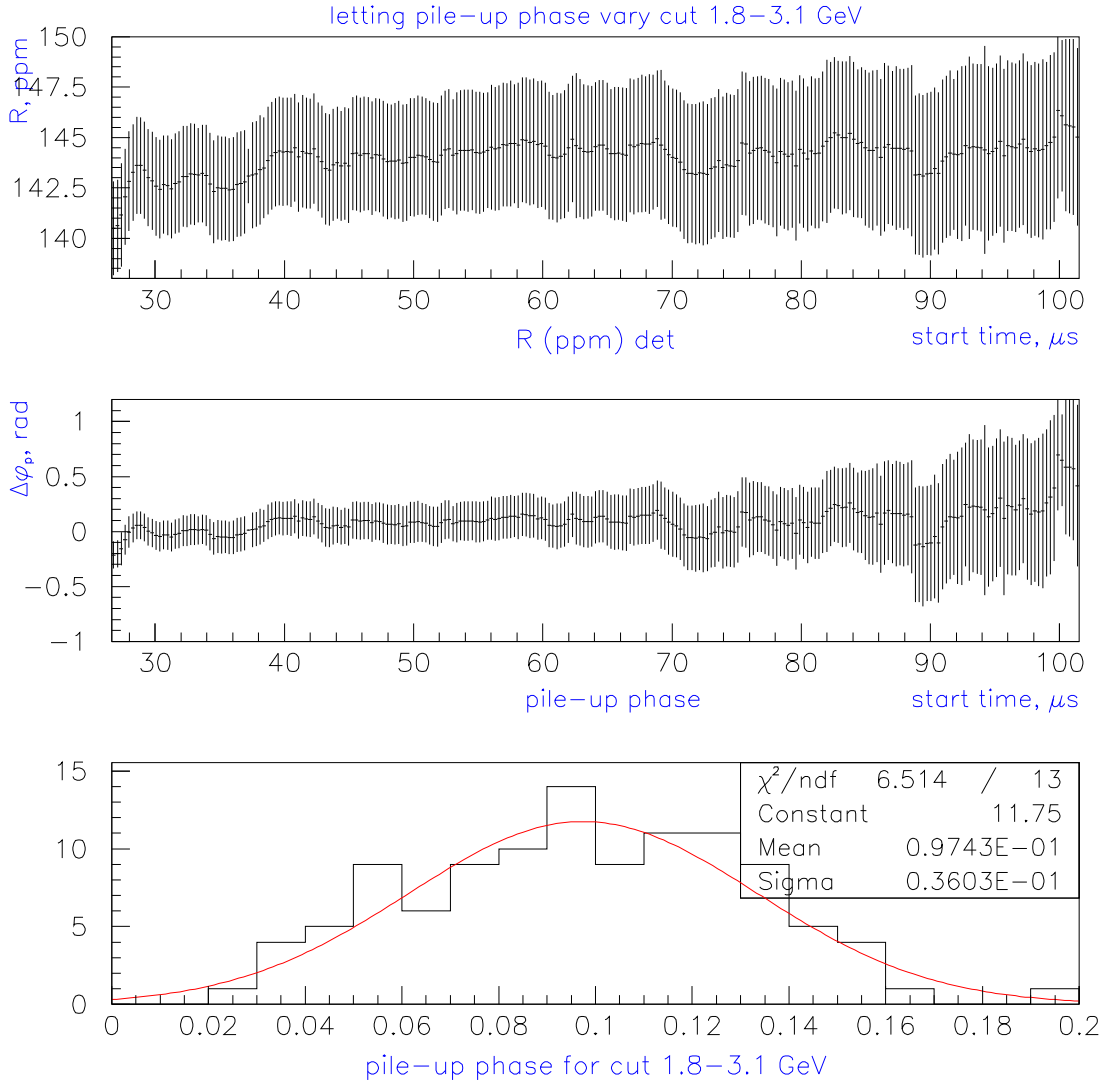

Fig.30a. Fit with the pile-up phase $\Delta\phi_p$ as a free parameter gives stable results for the cut 1.8-3.1 GeV. Top: R vs fit start time. Middle: pile-up phase vs fit start time. Bottom: the distribution of the pile-up phase fitted value for the cut 1.8-3.1 GeV.

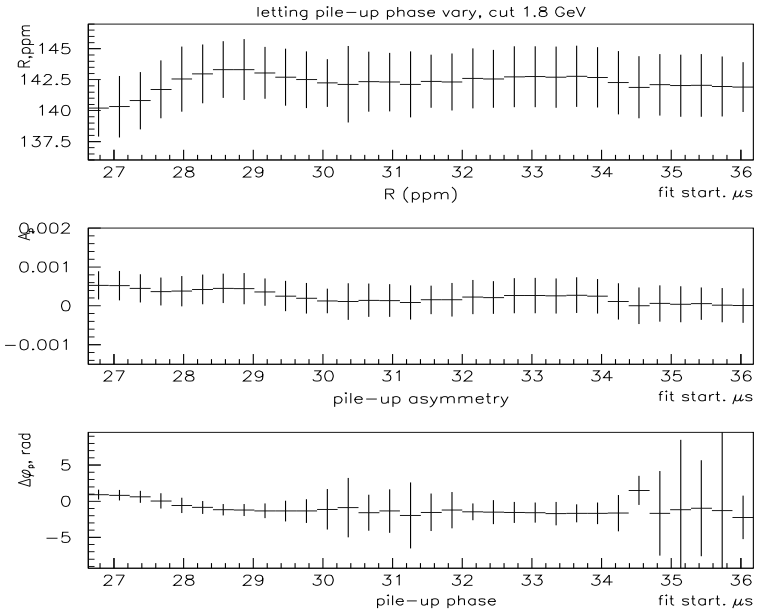

Fig.30b. Fit with the pile-up phase $\Delta\phi_p$ as a free parameter for the cut 1.8 GeV. Top: R vs fit start time. Middle: pile-up asymmetry vs fit start time. Bottom: pile-up phase vs fit start time: mostly consistent with 0, but the errors are very large.

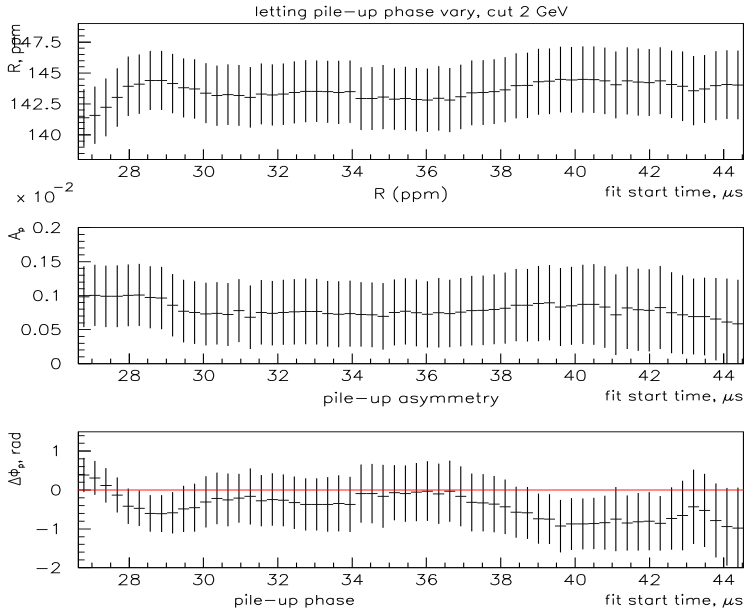

Fig.30c. Fit with the pile-up phase $\Delta\phi_p$ as a free parameter for the cut 2 GeV. Top: R vs fit start time. Middle: pile-up asymmetry vs fit start time. Bottom: pile-up phase vs fit start time: mostly consistent with 0 within errors.

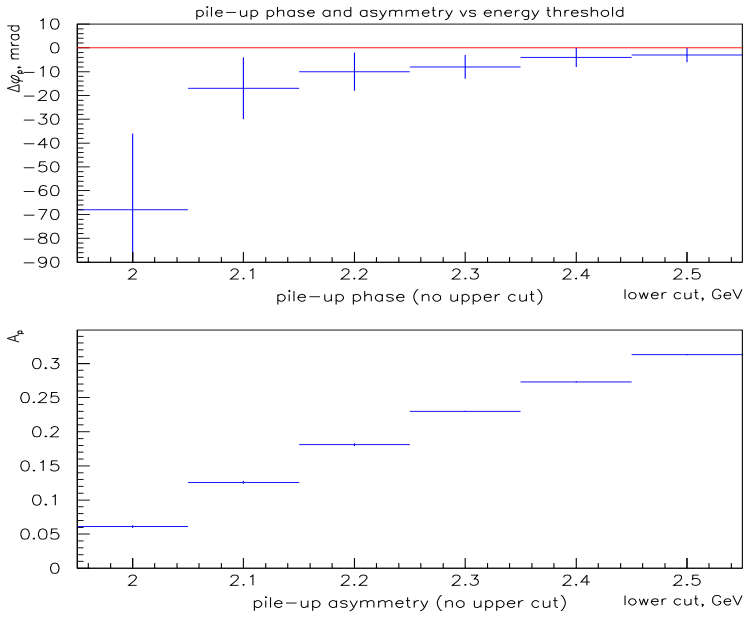

Fig.31a. Fitted pile-up parameters (from pile-up subtraction) vs lower energy threshold, without an upper energy threshold. The values of asymmetry are given in the notation of Eqn.7, and should be multiplied by corresponding pile-up fractions to be compared to A_p from the multiparameter function (Eqn.2) used for the full data set.

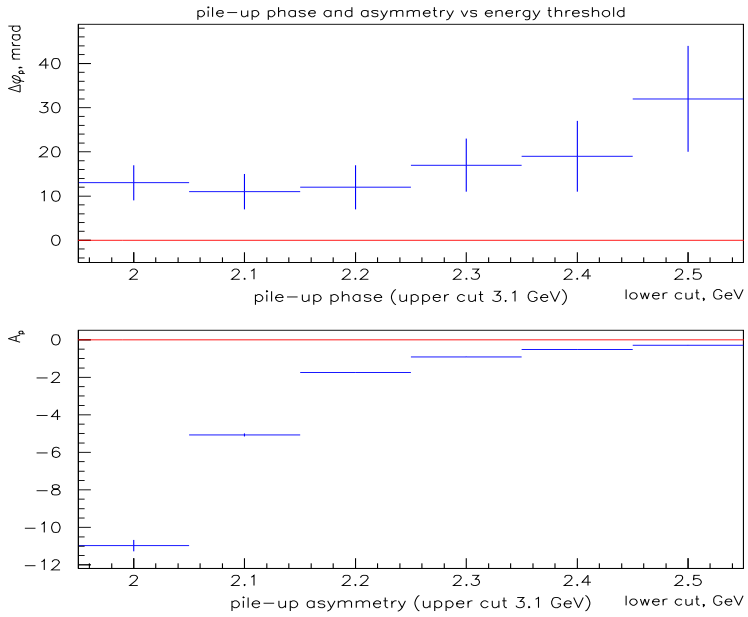

Fig.31b. Fitted pile-up parameters (from pile-up subtraction) vs lower energy threshold, with an upper energy threshold at 3.1 GeV. The values of pile-up asymmetry are large and negative, since pile-up in this case is dominated by the negative fraction ("hidden" pulses) and the non-wiggling part of pile-up is small (approximately as many pulses lost as gained)

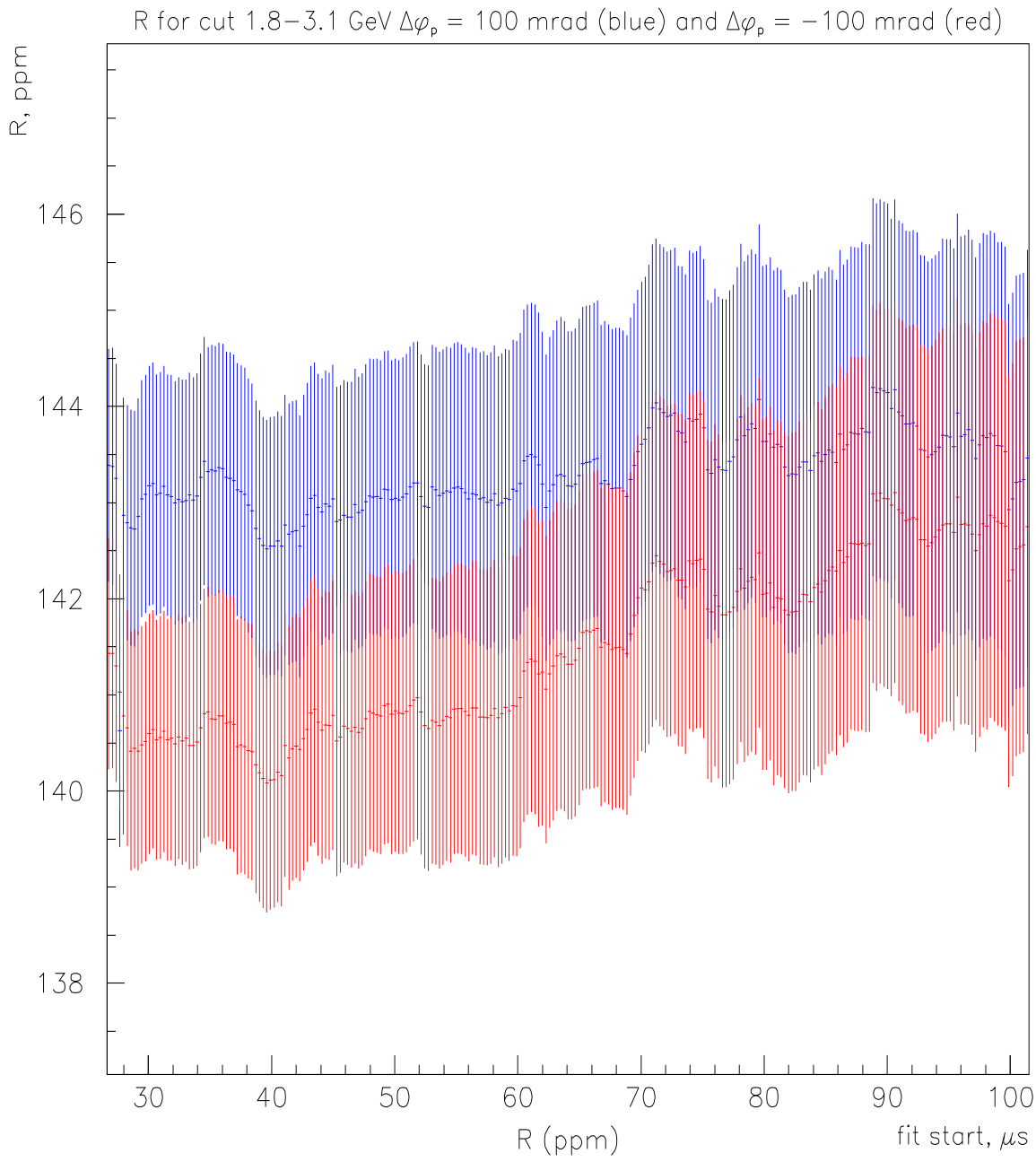

Fig.32. For the same data selection (cut 1.8-3.1 GeV), a change in the fixed value of $\Delta\phi_p$ of as little as 200 mrad (from 100 to -100 mrad) results in a difference of 2σ in the values of R at early times. This difference due to a wrong choice of pile-up phase is decreasing with time. Also, the result with $\Delta\phi_p = 100$mrad (blue), which we believe is closer to the truth is much more stable early to late time.

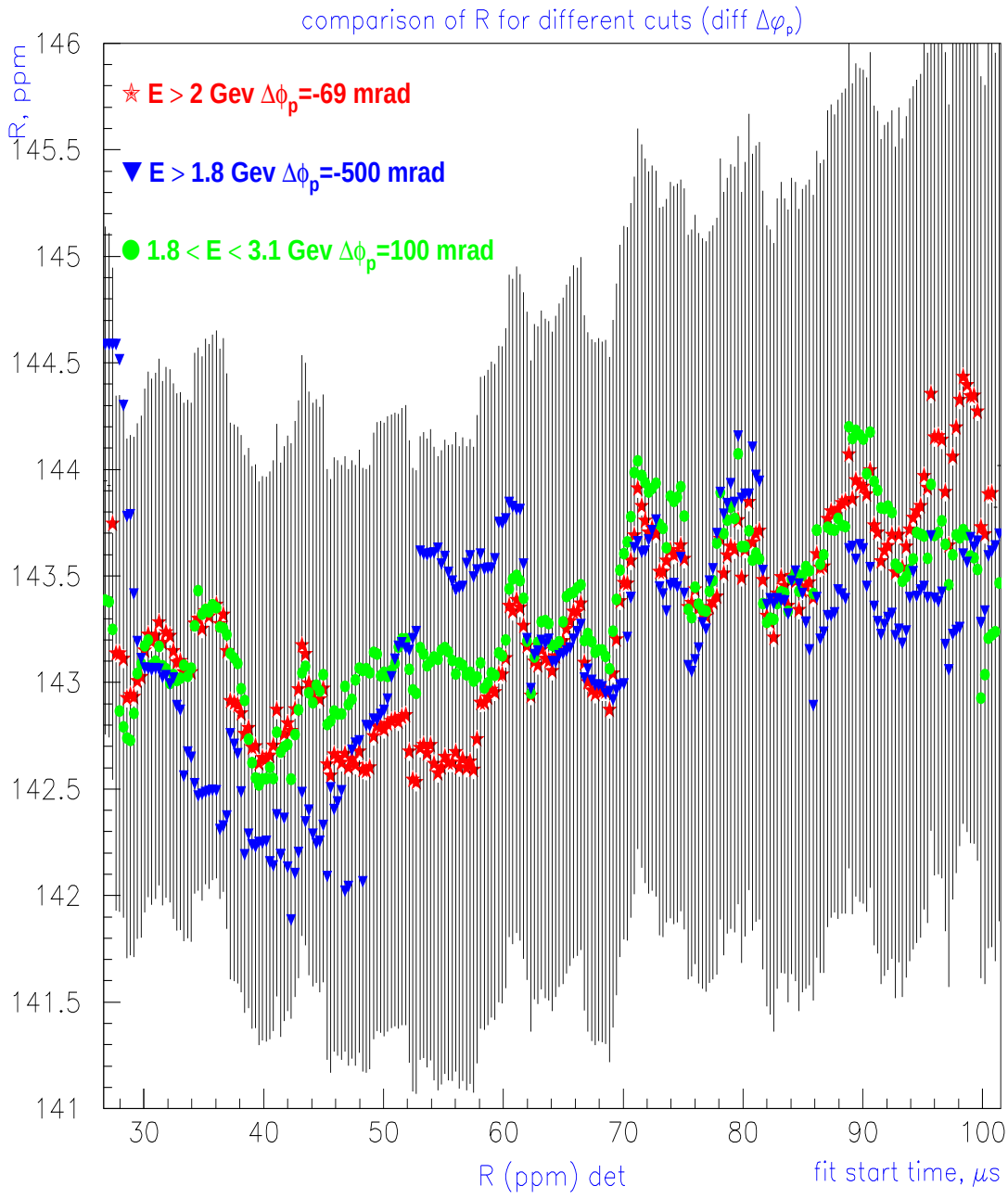

Fig.33. Comparison of fitted values of R for different cuts **with $\Delta\phi_p$ fixed at different values for each cut**. *The errors are given for the results from the cut 2 GeV only.*

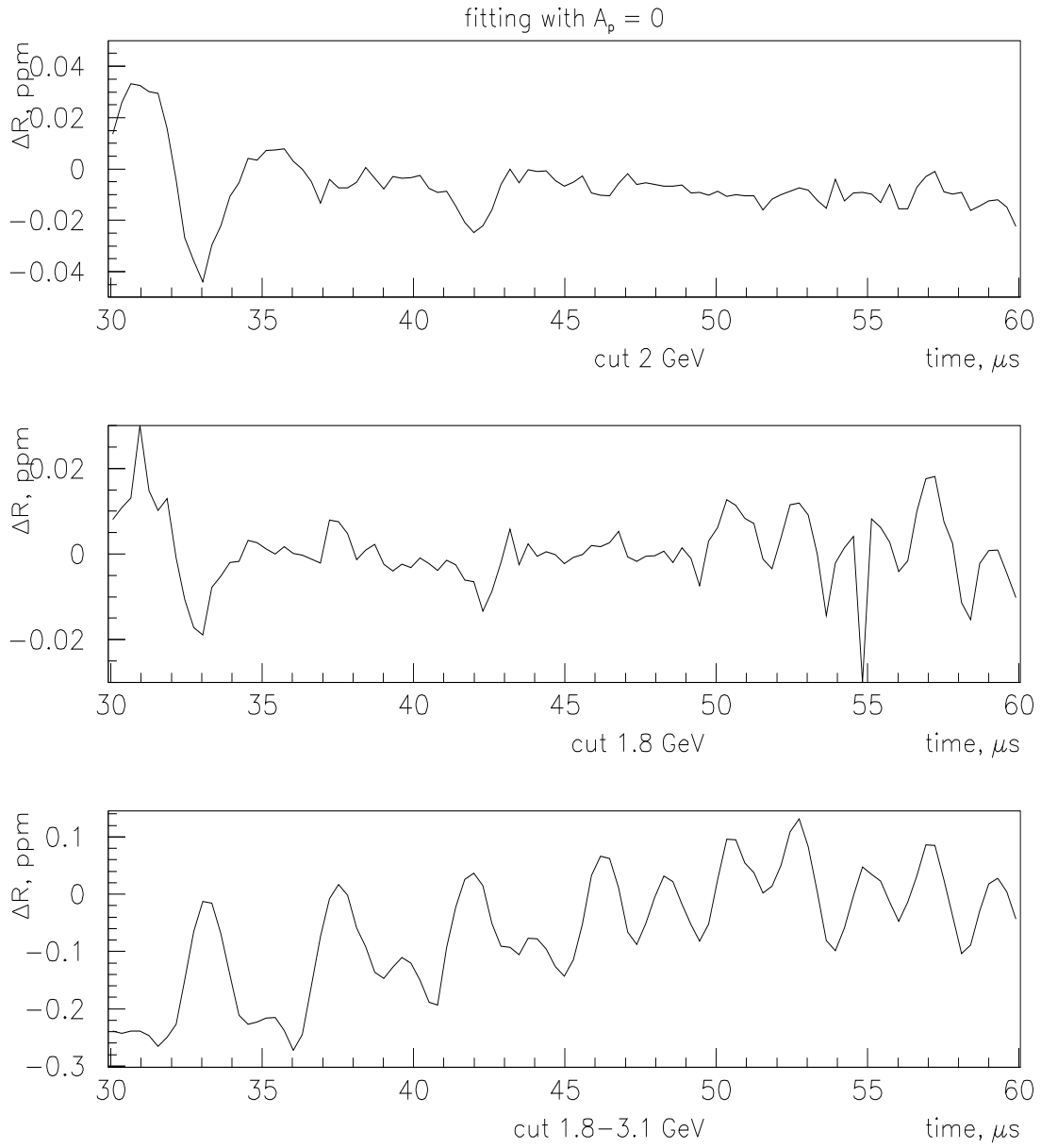

Fig.34. Difference in the fitted values of R for different cuts **with A_p fixed at 0, i.e. pile-up wiggle is not fitted to** *and with A_p as a free parameter. The pile-up phase was fixed at 0 as well. For the cuts 1.8 and 2 GeV, A_p is within one standard deviation from zero, and dropping it from the fit function does not result in a significant change in R (unlike changing $\Delta\phi_p$), and the χ^2 is only about 0.1% worse. For the cut 1.8-3.1 GeV, dropping A_p results in a significant phase pulling, which is still much smaller than the effect from changing $\Delta\phi_p$), in this case the χ^2 is 0.3% worse, but still acceptable.*

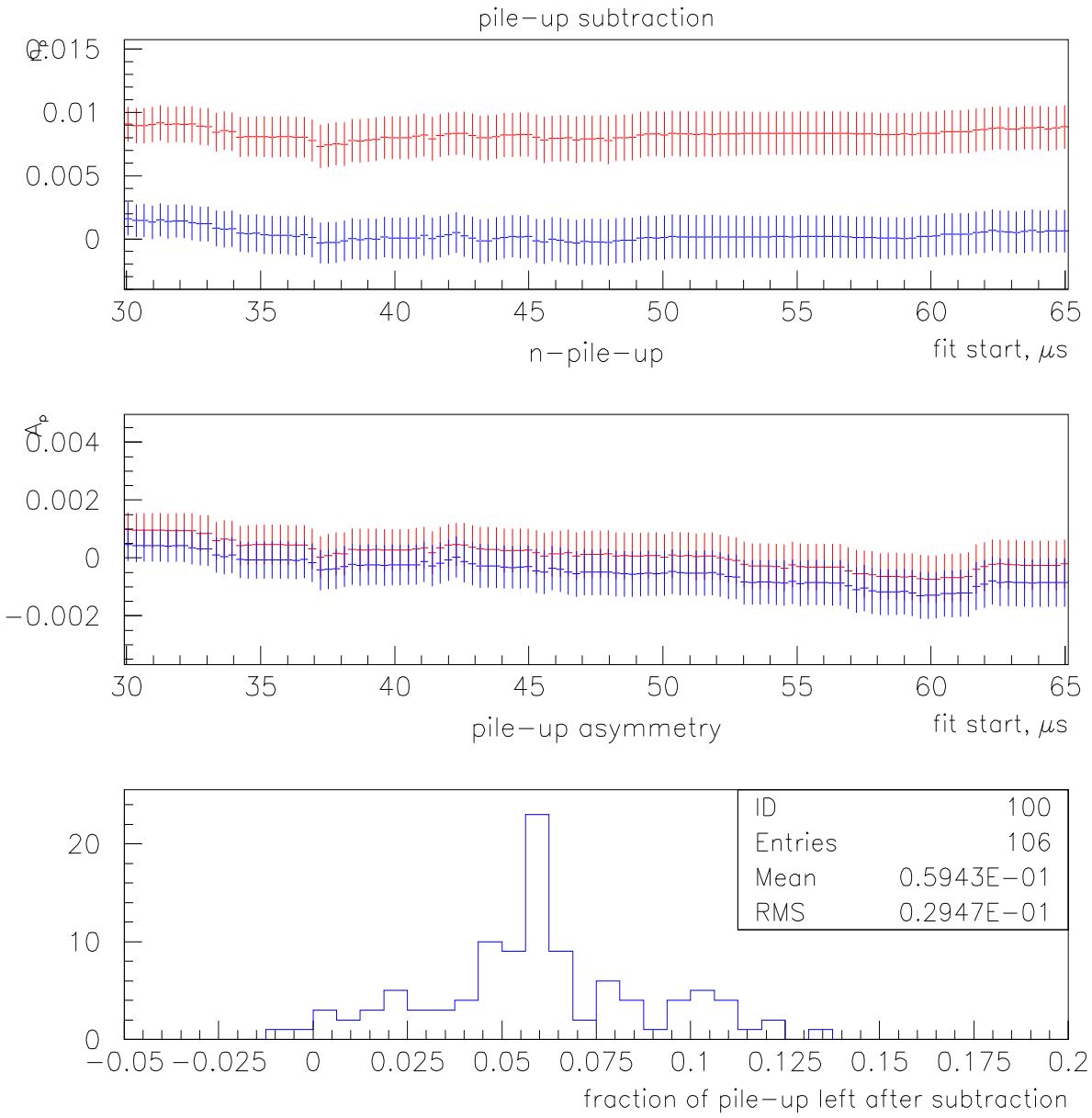

Fig.35a. The effect of pile-up subtraction on the cut 2 GeV. Both the "subtracted" and the original data sets were fitted to a 16-par function, including the pile-up parameters. The results from the data set to which no subtraction was applied are plotted in red, the results from the pile-up subtracted set are in blue. Top: the fraction of pile-up pulses is significantly lower for the "subtracted" data set. Middle: the pile-up asymmetry is small (mostly consistent with 0) in both cases. Bottom: ratio of pile-up fractions for the "subtracted" and the original data set; about 6% of pile-up pulses are still present after the subtraction was applied (agrees with Cenap's estimate of PUS efficiency).

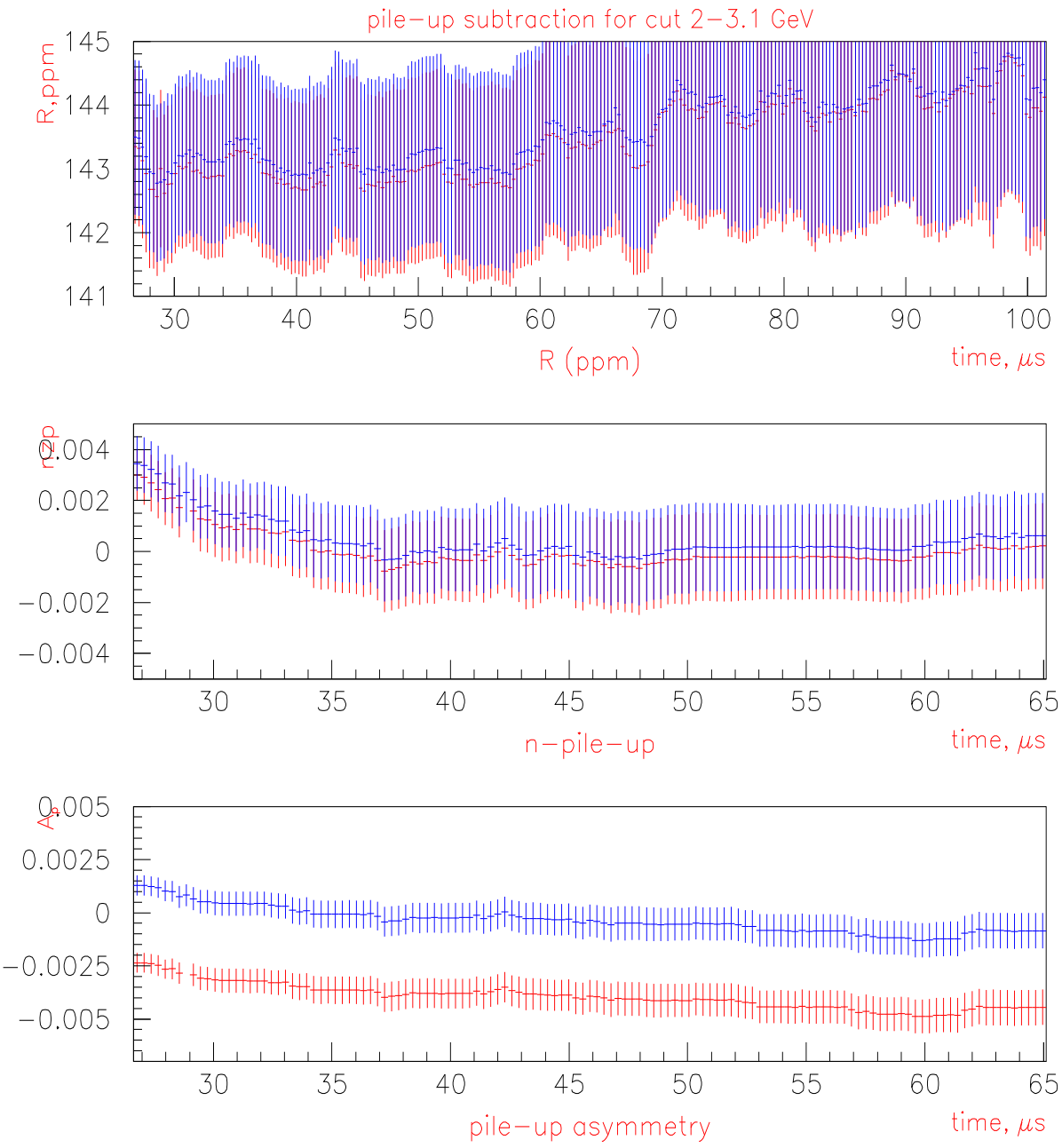

Fig.35b. The effect of pile-up subtraction on the cut 2-3.1 GeV. The results from the data set to which no subtraction was applied are plotted in red, the results from the pile-up subtracted set are in blue. Top: The value of R is about 0.3 ppm higher for the pile-up subtracted data at early times. Middle: the non-wiggling fraction of pile-up is small in both cases. Bottom: the pile-up wiggle is removed after the subtraction was applied.

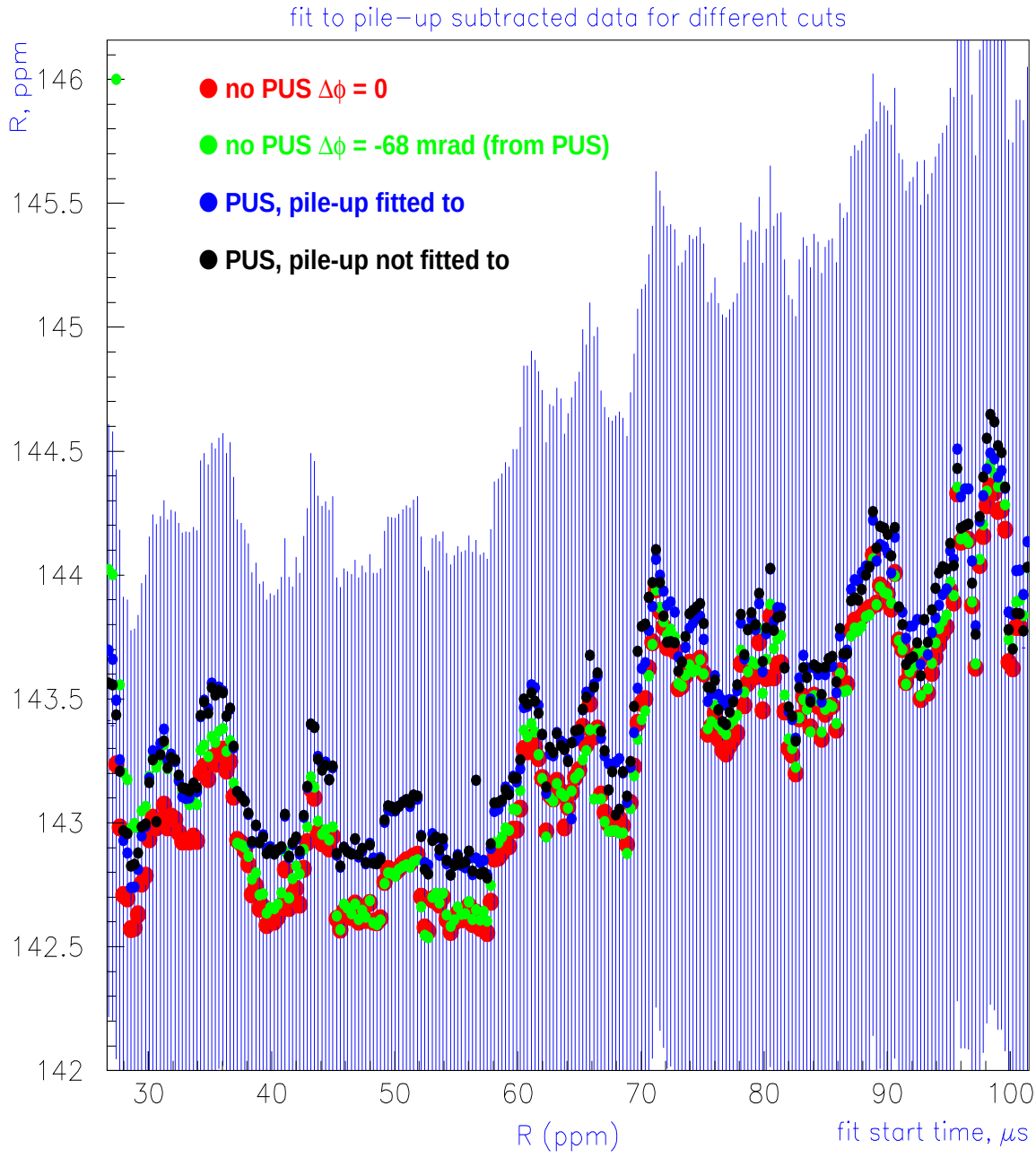

Fig.36. The results are compared for the cut 2 GeV, with and without PUS. Red: the original data set, $\Delta\phi = 0$. Green: same with the $\Delta\phi$ from PUS studies. Blue: pile-up subtracted data set fitted to a full function (with pile-up parameters included). Black: same, but with pile-up parameters dropped. The difference between the latter two (black and blue) is negligible. Taking the pile-up phase from PUS studies brings the results from the two data sets close together at early times (30-40 μs), but has a rather small effect at later times.

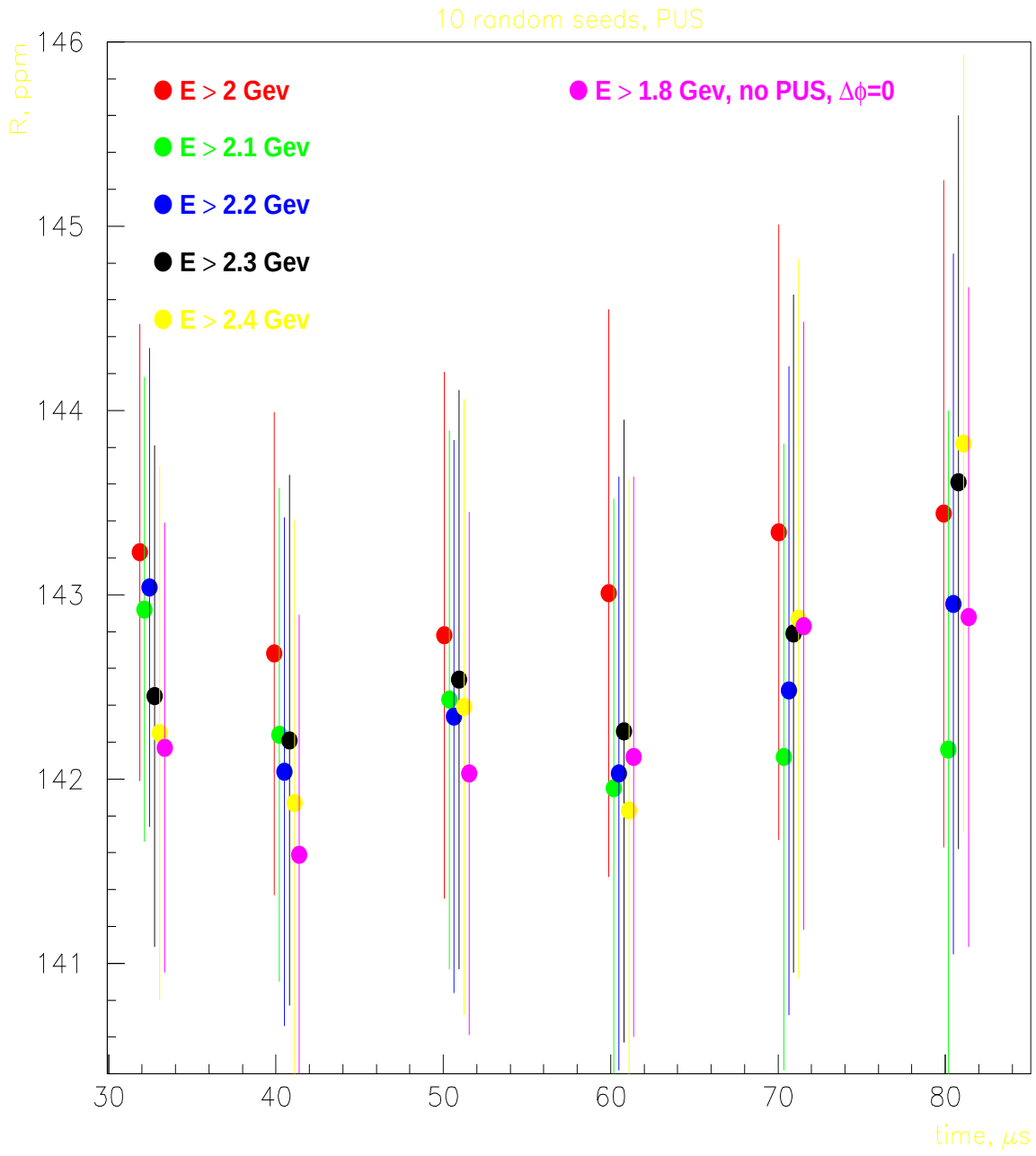

Fig.37. Results for R at 32, 40, 50 etc. μs, from pile-up subtracted data with different energy thresholds. (averaged 10 random seed). The result for the cut 1.8 GeV (no PUS) is shown as well for comparison.

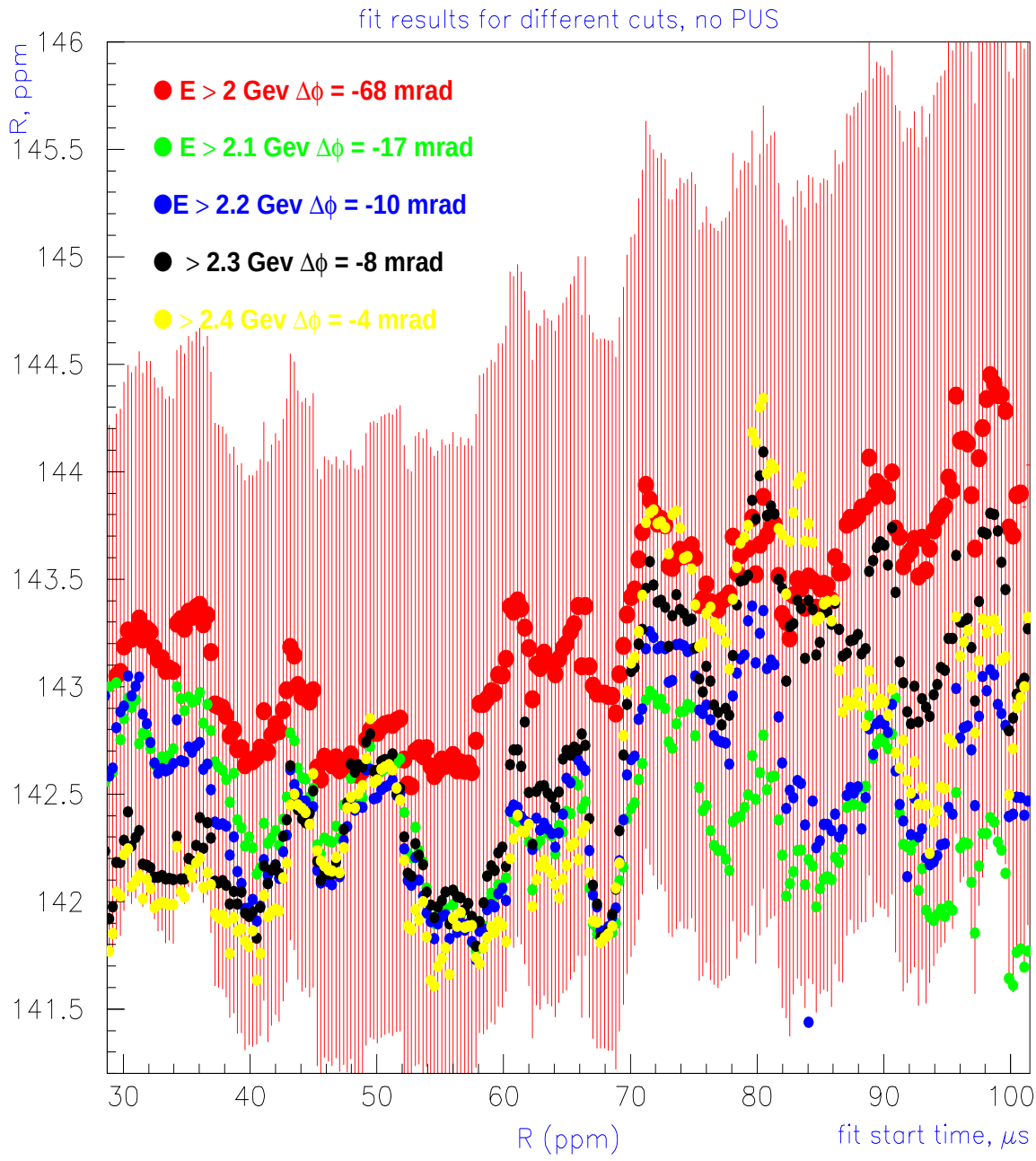

Fig.38. For different energy thresholds: no pile-up subtraction, but pile-up phase is fixed at the values from PUS studies. (One random seed).

4.7 More on the Muon-Loss Correction

As has been mentioned in Section 3, two forms of the muon-loss correction were used (Eqns.6 and 6a). The gaussian form was used for most of the fits in this analysis, since it gave more stable and consistent results. As a comparison of fits to pile-up subtracted and regular data sets shows (Fig.39a), the values of the muon loss parameters change within one standard deviation after PUS is applied.

On the other hand, if an exponential form is used, the results differ significantly for both the muon and muon-loss lifetimes, as much as 2-3 standard deviations in the latter case (Fig.39b). Comparing the results when no PUS applied, it is easy to see, why the τ_X changes so much (Fig.39c): both the pile-up fraction and asymmetry are underestimated (as Table 7 shows, the gaussian correction in its turn gets pile-up parameters right), meaning that a significant number of pile-up pulses (with a lifetime close to 32 μs) are fitted as "muon losses", which causes the loss lifetime to increase. Therefore, the exponential form of muon losses can only be used along with pile-up subtraction, in which case $\tau_X(exp) = 22.1 \pm .9\mu$s (at 32 μs).

The estimates of the muon losses based on fit results for the cuts 1.8 and 2 GeV ("gaussian", no PUS) demonstrate a good agreement with the results from fitting 2-GeV pile-up subtracted data with an exponential muon loss correction (Table 10).

Table 10. The size of the "muon loss" correction (in %) at different times after the injection (estimated using fitted a_X and τ_X values), with and without pile-up subtraction.

Fit Start Time, μs	Muon Losses for the Cut 1.8 GeV (gaussian form), in %				
	32 μs	40 μs	50 μs	60 μs	70 μs
32	0.66 ± 0.04	0.50 ± 0.03	0.31 ± 0.02	0.18 ± 0.01	0.09 ± 0.01
40		0.51 ± 0.05	0.33 ± 0.03	0.19 ± 0.02	0.10 ± 0.01
50			0.32 ± 0.09	0.19 ± 0.06	0.10 ± 0.04
60				0.19 ± 0.03	0.10 ± 0.02
70					0.07 ± 0.03
	Muon Losses for the Cut 2 GeV (gaussian form), in %				
32	0.68 ± 0.05	0.51 ± 0.04	0.33 ± 0.03	0.19 ± 0.02	0.10 ± 0.01
40		0.54 ± 0.06	0.36 ± 0.05	0.22 ± 0.03	0.12 ± 0.02
50			0.36 ± 0.11	0.21 ± 0.08	0.11 ± 0.05
60				0.21 ± 0.04	0.12 ± 0.02
70					0.08 ± 0.04

Fit Start Time, μs	Muon Losses for the Cut 2.0 GeV (PUS, gaussian form), in %				
	32 μs	40 μs	50 μs	60 μs	70 μs
32	0.72 ± 0.04	0.54 ± 0.04	0.34 ± 0.03	0.19 ± 0.02	0.10 ± 0.01

Fit Start Time, μs	Muon Losses for the Cut 2.0 GeV (PUS, exponential form), in %				
	32 μs	40 μs	50 μs	60 μs	70 μs
32	0.79 ± 0.09	0.55 ± 0.07	0.35 ± 0.05	0.22 ± 0.04	0.14 ± 0.03

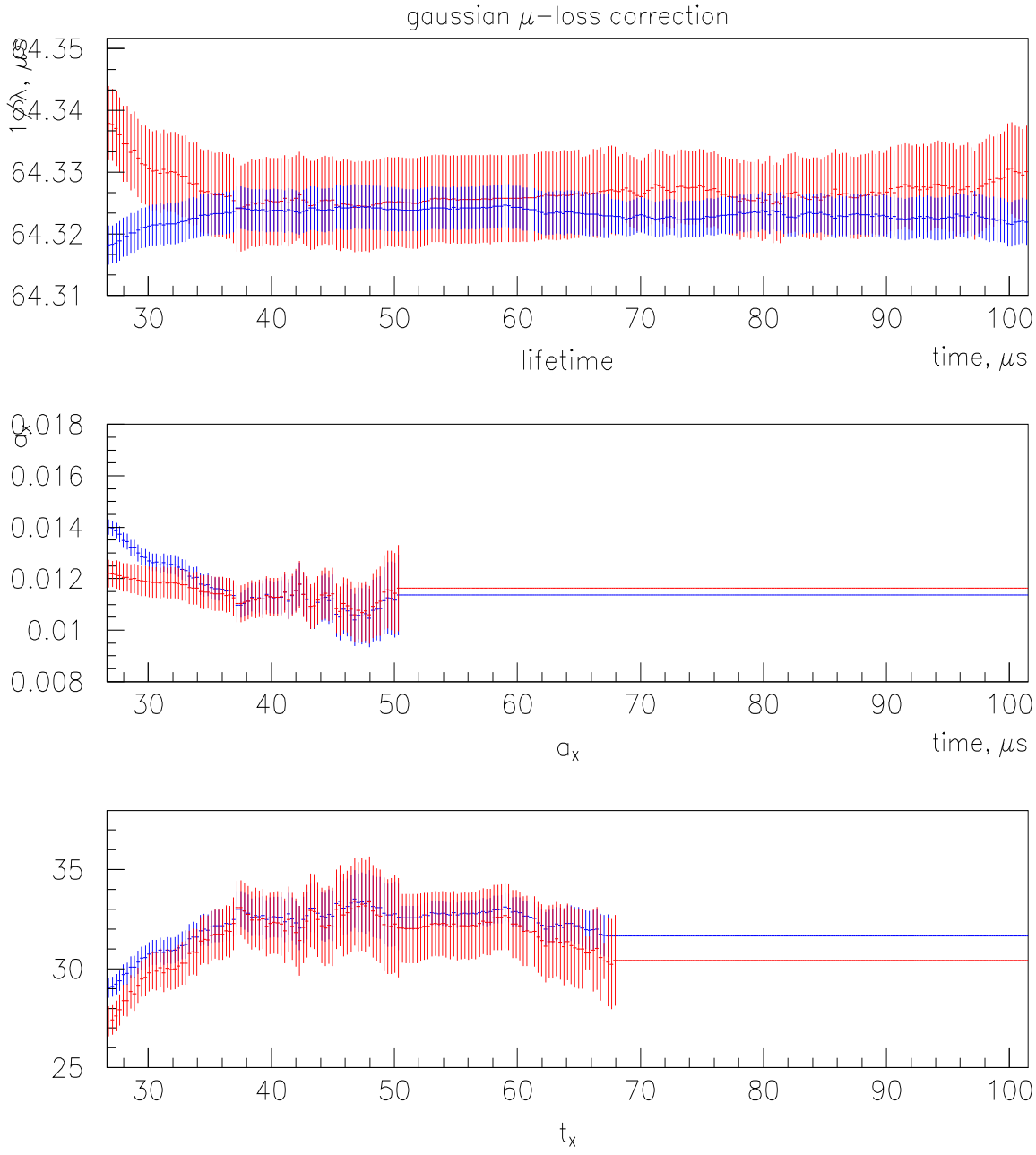

Fig.39a. For the cut 2 GeV, the muon lifetime, and the muon-loss amplitude and lifetime are shown for pile-up-subtracted (in blue) and regular (in red) data sets, when a **gaussian** *correction was used. The results agree within one standard deviation for the fit start times after 30 μs.*

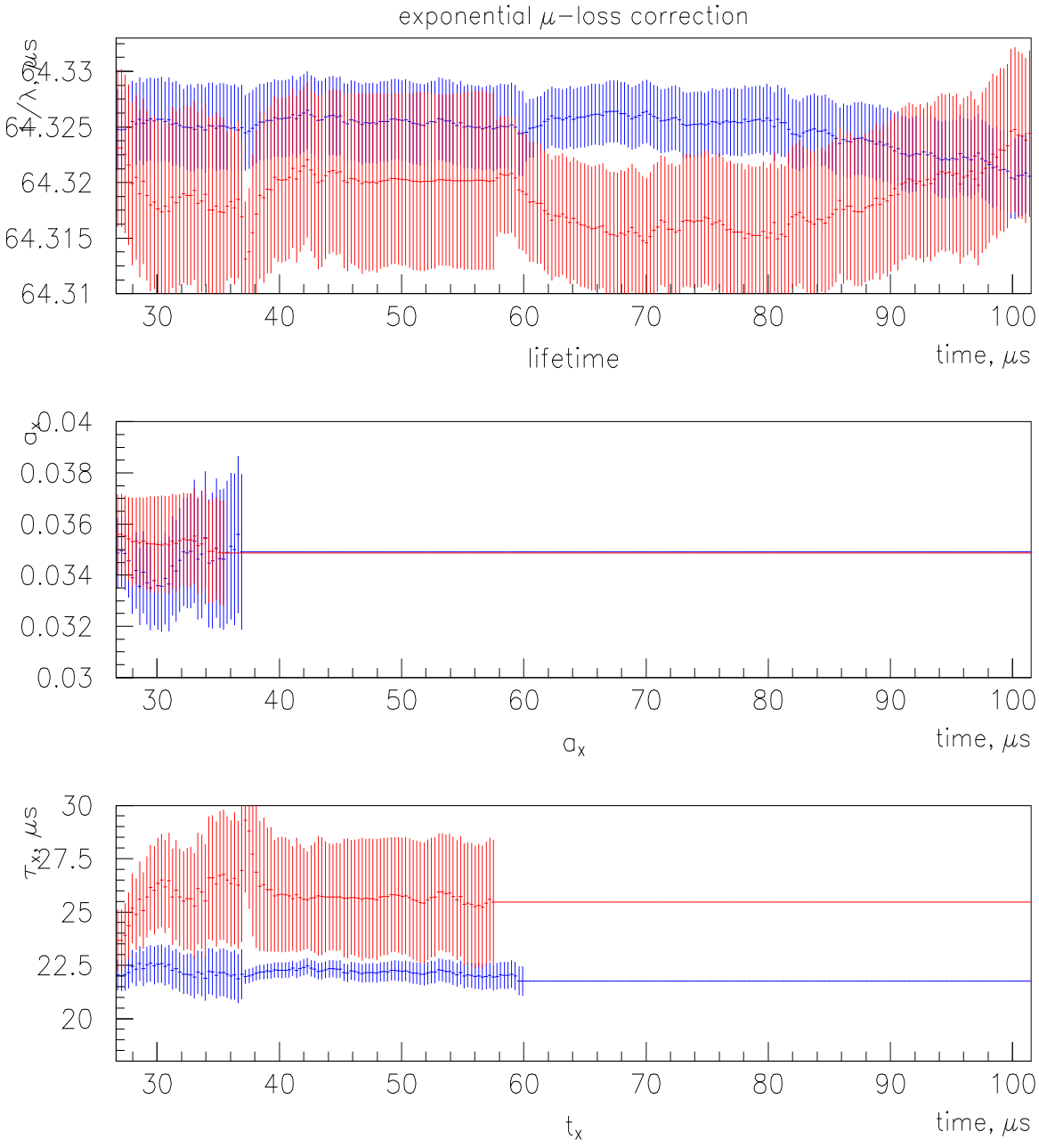

Fig.39b. For the cut 2 GeV, the muon lifetime, and the muon-loss amplitude and lifetime are shown for pile-up-subtracted (in blue) and regular (in red) data sets, when an **exponential** *correction was used. In this case, both the muon and muon-loss lifetimes differ by more than a standard deviation. Much larger errors on red curves show that there is a significant correlation between the muon-loss and pile-up parameters in this case.*

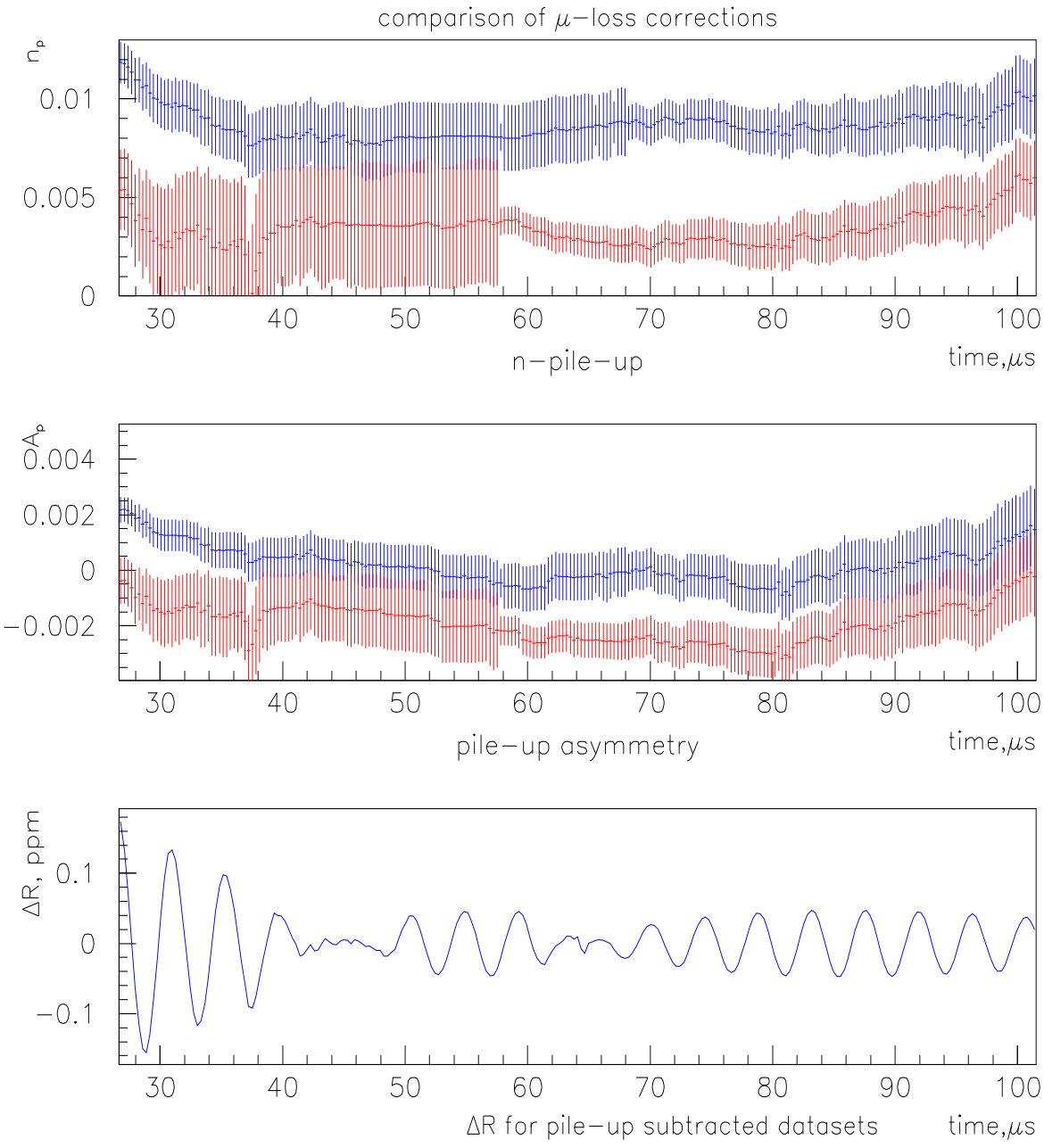

Fig.39c. If no PUS used, the exponential form of muon losses cuts into the pile-up fraction and asymmetry, causing the increase in the fitted lifetime. Top and middle: pile-up parameters are shown in red for the exponential form of the muon-loss correction, and in blue for the gaussian form (the "gaussian" number agree well with the result of directly fitting to subtracted pile-up spectrum). On the bottom plot, the difference in the fitted values of R is plotted for **pile-up subtracted data sets**, *between fits with a gaussian and exponential muon-loss corrections.*

An approximate muon-loss spectrum can be obtained e.g. from the studies of 3-fold FSD coincidences. For the 1999 data, Rob finds

$$f_X(t) \;=\; 1 + a_X \cdot (e^{-\frac{t}{\tau_1}} + 0.68363 \cdot e^{-\frac{t}{\tau_2}}) \qquad (9)$$

with $\tau_1 = (17.9 \pm 0.1)\mu$s and $\tau_2 = (55.0 \pm 0.1)\mu$s (only the fit erros are given for the lifetimes) [9]. If this shape is fixed in the fit, the value of muon lifetime becomes closer to the one expected from special relativity, while the fit results for R do not change at zero-crossings (Fig. 40).

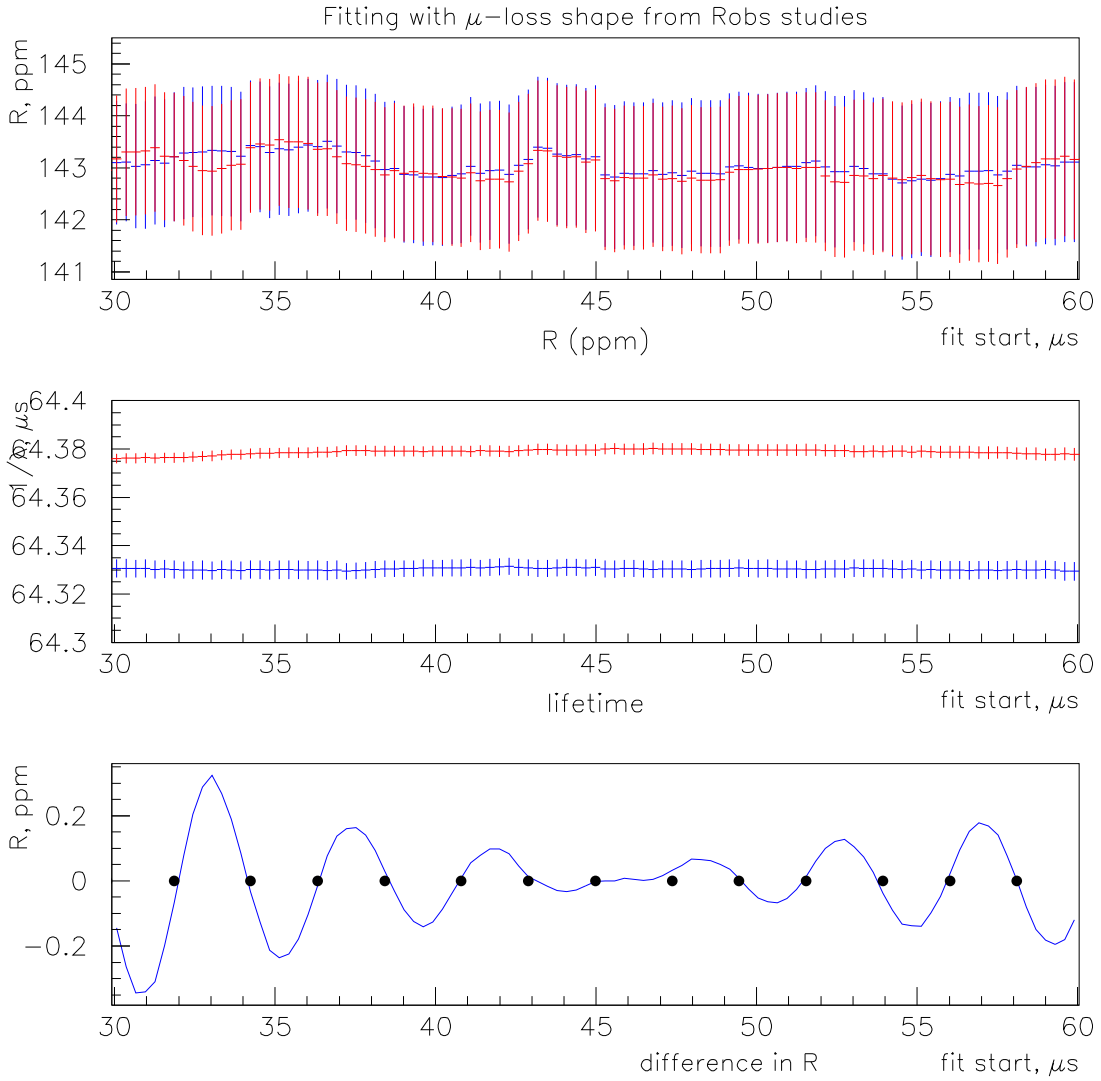

Fig.40. For this study the shape of the muon-loss function was taken from Rob's studies with 3-fold FSD coincidences. The results are compared for the pile-up subtracted data set with the cut 2 GeV, with μ-losses fixed (red) and described by an exponential function with free parameters a_X and τ_X (blue). Fixing parameters leads to a phase pulling, which is minimal at zero-crossings (black dots). The muon lifetime (middle plot) is close to 64.38 μs if the fixed μ-loss shape is used.

4.8 Different Run Periods Compared

For this study, the data from 12 different run periods were fitted separately. The values of the fit parameters averaged for 12 data sets turned out the same as for the data together. The variation in the g-2 phase was greater than $5{\cdot}\sigma$ due to differences in the beam tuning throughout the run (Fig.41a). This shift in the phase was seen by all detectors (Fig.41b).

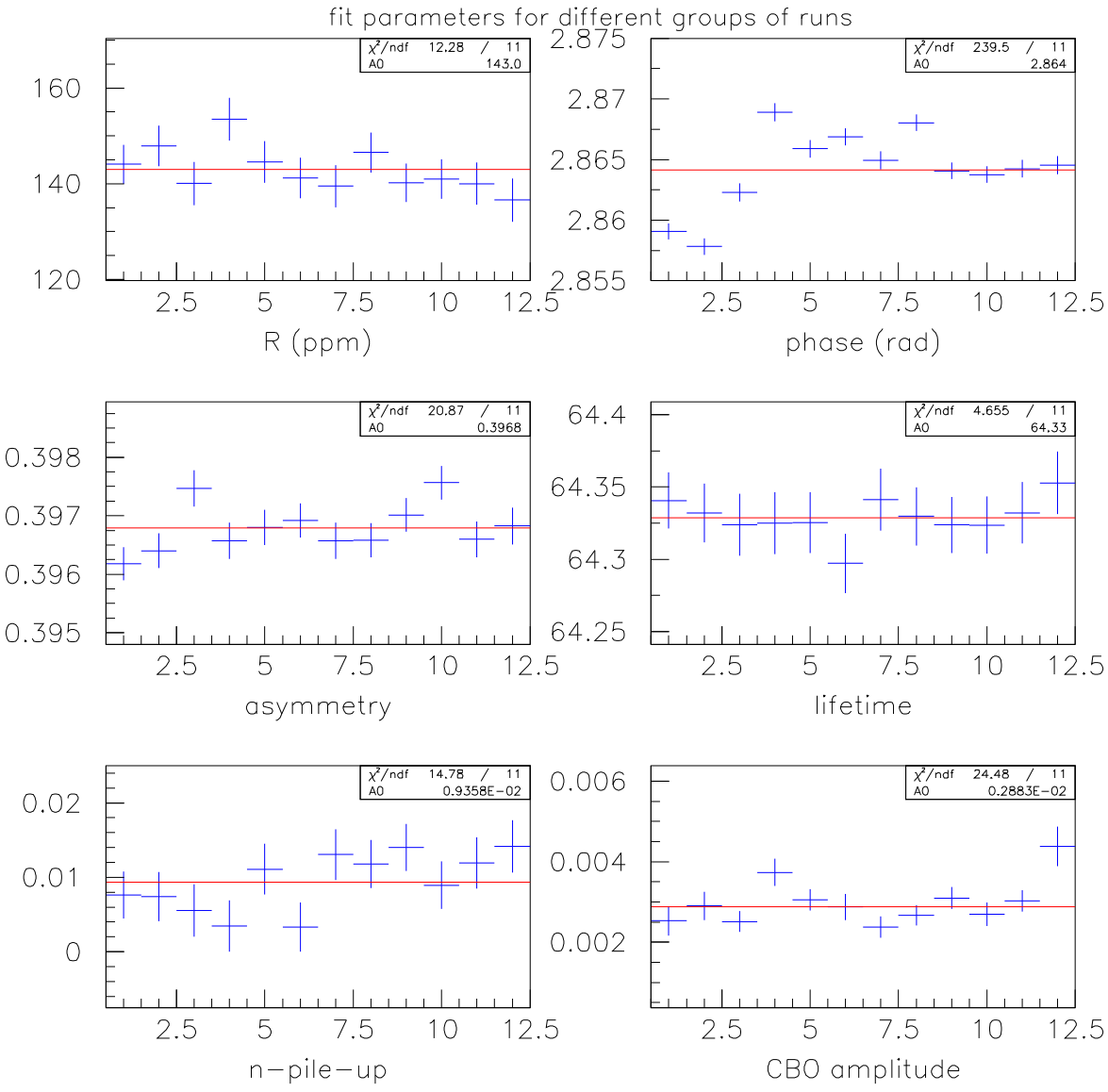

Fig.41a. Some fit parameters shown for 12 run periods (cut 2 GeV). The data were divided into 12 groups and fitted separately. X-axis: runs 3813-3903 (1), 3904-3990 (2), 3993-4089 (3), 4090-4193 (4), 4194-4285 (5), 4286-4389 (6), 4390-4532 (7), 4533-4639 (8), 4640-4756 (9), 4757-4855 (10), 4857-4980 (11), 4981-5093 (12). One random seed only, $\Delta\phi = 0$.

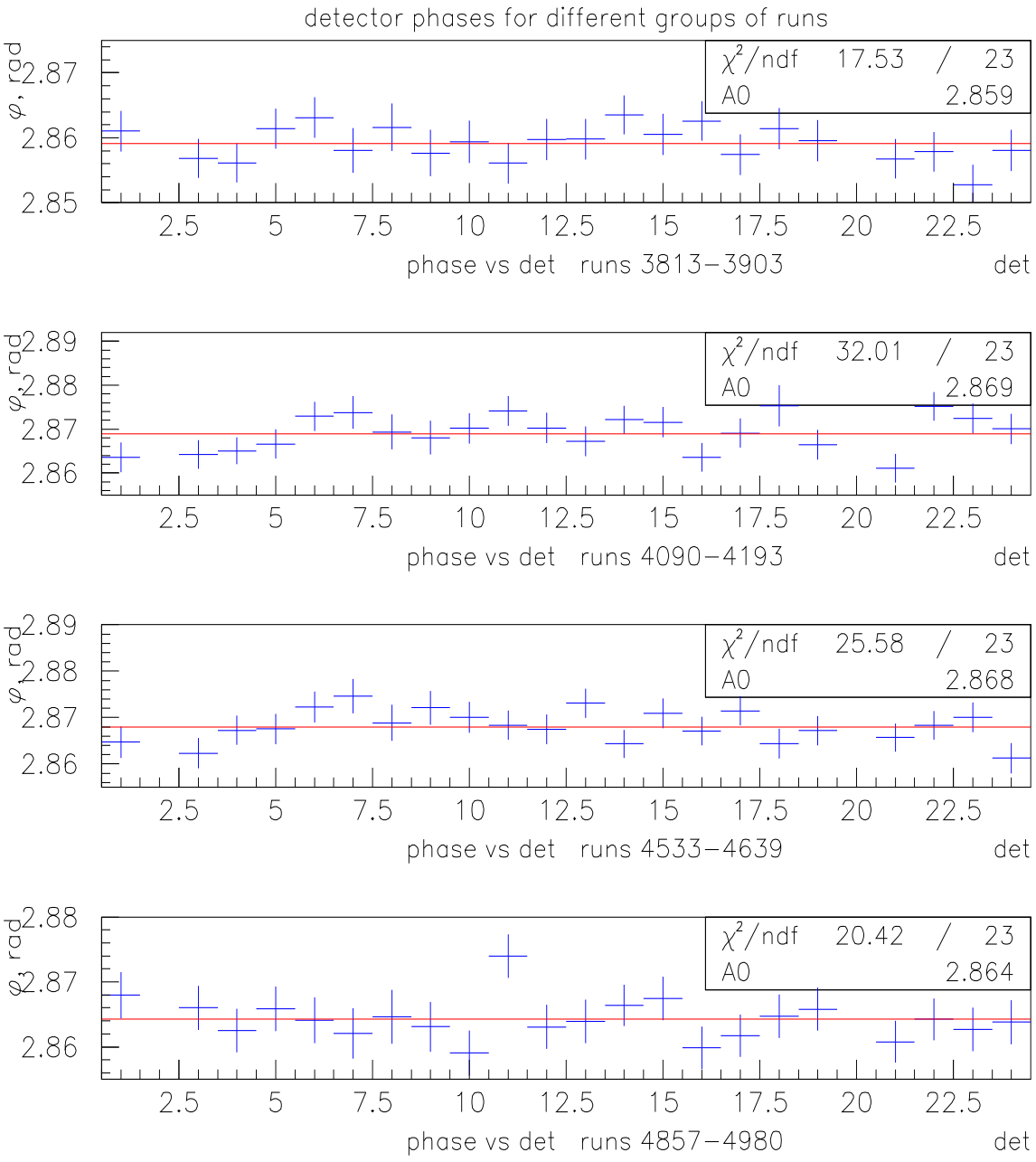

Fig.41b. Phase by the detector for some run periods. The shift in phase is seen by all detectors.

5 Systematic Errors

5.1 Errors from Fixing Fit Parameters.

As may be obvious from the previous section, the main systematic uncertainty in R came from fixing the difference between g-2 precession phase and the phase of pile-up. There is a strong correlation between $\Delta\phi_p$ and R, and letting the former vary as a free parameter leads to a two-fold increase in the statistical error on R [6].

The sensitivity of R to the pile-up phase was estimated by fixing $\Delta\phi_p$ at different values between -3 and 3 rad (with respect to the g-2 precession phase). This was done for 1.8, 1.8-3.1 and 2-GeV cuts at different fit start times (Figs.42a,b). The results are given in Table 11. The 1.8-3.1 GeV selection has a greater pile-up asymmetry, therefore the value of R is much more sensitive to the choice of pile-up phase.

Table 11. Error in R from fixing the pile-up phase (no PUS).

Fit start	ΔR, (ppm / 100 mrad)		
time, μs	cut 1.8 GeV	cut 2.0 GeV	cut 1.8-3.1 GeV
32	< 0.25	< 0.4	< 1.4
40	< 0.2	< 0.12	< 1.4
50	< 0.17	< 0.1	< 1.3
60	< 0.33	< 0.18	< 1.3
70	< 0.1	< 0.1	< 1.2
80	< 0.22	< 0.14	< 1.0
error	???	$\pm$ 31 mrad	?? ($\pm$ 40 mrad)†

† An "optimistic" estimate from Fig.30a.

The sensitivity of R to the choice of the pile-up phase was found to mostly depend on the size of pile-up wiggle asymmetry. It did not depend significantly on whether or not the start time was chosen at a "zero-crossing".

The 2-GeV cut, for which the phase is known quite well, gives the smallest systematic error due to the choice of $\Delta\phi_p$ (if the PUS estimate is used): approximately **0.12 ppm** at 32 μs. For the 1.8-GeV cut, the uncertainty is too big; and for the 1.8-3.1 GeV cut, the sensitivity is too big (no reliable estimate of $\Delta\phi_p$ either).

For the "pile-up subtracted" spectra, as established by Yannis in a simulation, the uncertainty in $\Delta\phi_p$ of 50 mrad leads to a 0.1 ppm error on R.

To investigate the result of fixing τ_B, ω_B (f_B), a_X and τ_X, I compared the fitted values of R obtained by two different methods: regular fit described in section 3 in which the mentioned parameters were fixed for late start times; and a fit, in which all 4 parameters were fixed for all fit start times. The sensitivity of R to these parameters was found to be of the order of **40 ppb** on the average, regardless of fit start time and whether or not the fit started at a "zero-crossing" (Fig.43).

Changing the values of the parameters describing pile-up inflation due to fast-rotation re-

sulted in a weak phase pulling with an amplitude of about 10 ppb (at 30 μs) for the values of a_p and τ_p increased or decreased by two standard deviations (with respect to the central values found in pile-up studies described in Appendix A). The value of R was almost unaffected for fits started at "zero-crossings" of g-2 precession (Fig.44).

5.2 Binning and Randomization Errors

The error due to binning was investigated by fitting histograms containing the same data, but having different bin widths. For this study, 10 histograms with bin widths between 148.8 and 149.7 ns (0.1-ns step) were fitted with the function (2). Only one random seed was used in randomizing the injection time. The results of this study are shown on Fig.46. The error due to binning was found to increase significantly for later fit start times: from 0.08 ppm at 32 μs to 0.16 ppb at 60 μs.

Yuri Orlov has shown in [14] that binning may create undesirable resonances in the data, some of which may be dangerously close to ω_a. He recommended a bin width of $\Delta t = T_{fr} \cdot (\frac{2l+1}{4})$, where T_{fr} is the cyclotron period, and l is an integer. For $l = 2$ ($\Delta t = 1.25 T_{fr}$), the difference in the values of R with respect to the "traditional" binning ($\Delta t = 149.185$ ns, used for all other histograms in this analysis) was found to be less than 0.1 ppm for all start times (Fig.47), consistent with the result of the above-mentioned study for 10 different bin width close to T_{fr}. Given this I will put an uncertainty due to binning at **0.08 ppm** (at 32 μs).

If the fill start time randomization is done, the dependence of R on the start time of binning becomes smaller than 0.1 ppm (Fig.48). On the average, the results with and without fill start time randomization in this study differed by less than 50 ppb (for one random seed only).

Another estimate of the error due to randomization of the start time of spills, can be made from the spread of R values for selections with different random seeds: **less than 40 ppb**.

5.3 Errors Due to Changes in the Energy Scale .

An estimate of the effect of the energy-scale change was done by comparing the values of fit parameters from fits to ESC-corrected and uncorrected data. It was found that even a significant change in ESC (0.3-0.7% in detectors 1,4) has little effect on the fitted value of R at the "zero-crossings" (Fig.49). For ESC under 0.1% (estimate for the 1999 data set), the systematic error on R is less than $0.1 \cdot \sigma$ (**less than 10 ppb at the "zero crossings"** for the full 1999 data set), whereas the effect is much greater for the lifetime, pile-up and muon loss parameters. A similar result has been obtained by artificially changing the energy scale for a "good" detector.

The average ESC correction can be useful, even if the effect is different for different calorimeter quadrants as shown for detector 1 (Figs.20,50).

5.4 Flashlets.

The AGS Flashlets can be seen in the Fourier transform spectrum of the fit residuals (Fig. 51): the peaks are present both at the AGS frequency, 371 kHz (corresponding to the AGS period of 2.694 μs) and 2.228 MHz (6 times AGS frequency, flashlets from 6 AGS

bunches). The peak at 371 kHz appears because the flashlets are not distributed over the AGS bunches evenly: most of them come in the first bunch [15,16] (the effect aka "The head of the snake spits the venom" [17]). The flashlet contamination can therefore be approximated as a sum of two spectra:

$$f_{FL}(t) = N_1(t) \cdot \sum_{i>0} \delta(t - \frac{i}{371kHz}) + N_2(t) \cdot \sum_{i>0} \delta(t - \frac{i}{2.228MHz}) \qquad (10)$$

where i is a positive integer, and $N_1(t)$, $N_2(t)$ are functions describing flashlet distribution time-dependence (I used the parabolic envelope form similar to the one proposed by Long in his note [18] to describe these functions)

$$N_1(t) = 6 \cdot N_2(t) = N_{flashlets} \cdot \frac{11.409 - 1.6947 \cdot 10^{-3} \cdot t - 5.3516 \cdot 10^{-4} \cdot t^2}{398.982294} \qquad (11)$$

To estimate the effect of flashlet presence in the data on the fitted value of R, flashlet spectra were generated for "best" (flashlets are distributed evenly over AGS bunches, f = 2.228 MHz, $N_1(t) \equiv 0$) and "worst" (all flashlets come from the same bunch, f = 371 kHz, $N_2(t) \equiv 0$) cases of contamination (100 and 126-ppm level in both simulations). The simulation results are shown in Figs.53,54 (for 100-ppm contamination). The uncertainty in R due to the presence of flashlets at the level of 126 ppm was found to be less than **120 ppb** (for the "worst" case).

5.5 Fit Function Inefficiencies.

As shown in Fig.55, not accounting for the CBO and muon loss terms in the fitting function results in a strong phase pulling on R. Only after these terms were included, the fit χ^2 became reasonable and the fit parameters more stable. One can conclude that the function used in this analysis describes the data pretty well, but it would be naive to think that it is ideal.

As was shown in section 3.1 (Fig.10,39c), different forms of fit function can be used to describe the **muon losses**. Both forms help reduce the χ^2, but do not remove the phase pulling on R completely. The difference between the two results can serve as a measure of the efficiency of fitting to the muon losses. As illustrated in Fig.10, this difference is oscillating with the (g-2) frequency and is less than **0.1 ppm** on the average (for the zero-crossings this number is smaller by at least a factor of 10).

A similar comparison between the results obtained by using different forms of the CBO function (i.e. Figs.11,12) gives an estimate of the error due to the inefficiency of **CBO** fitting of the order of **40 ppb** (for the entire data set, Fig.56). A similar study for the detector 8 alone gives an uncertainty of about 0.1 ppm (Fig.57) (The amplitude of the CBO in detector 8 is approximately 8.5 times higher than for the sum of all detectors).

An attempt to study how the background (residuals of the multi-parameter fit) affects fitting CBO showed that this effect is apparently negligibly small: less than 10 ppb (Fig.58).

5.6 Some Other Errors.

Start time of fit estimated from the fluctuation of the fitted R value for different fit start

times within one precession period: **0.18 ppm** (Fig.59). This error summarizes the effect of all "phase-pulling" effects (flashlet, fit function inefficiencies, energy scale change etc.)

End time of fit: setting the end time of fit to different values between 600 and 730 μs resulted in a fluctuation in the fitted value of R of less than 5 ppb for the 1.8-GeV cut, and **less than 10 ppb** for the 2-GeV cut.

Errors due to rounding of the histogram bin boundaries in PAW: less than 10 ppb. (This error is no longer relevant for this analysis, since for the latest results, a double precision was used to describe pulse times and binning).

"Errors from fit errors": using an integrated value of the fit function rather than the function value at a bin center, when calculating uncertainties in the histogram bin values, produces a difference of the order of 15 ppb in R (Fig.60). At the same time, the change in the value of the asymmetry is quite significant: 4-5$\cdot\sigma$ due to the difference in error evaluation at the peaks and in the valleys of the g-2 wiggle. (This error is a part of the uncertainty due to fitting procedure.)

Table 12. A summary of the systematic errors on R. As was decided by the analyzers, for the sum, the errors from CBO, double CBO, vertical waist were added linearly, as were the errors from energy scale, muon loss, pile-up; the resulting errors were then added to the rest in quadratures.

Source	Error (ppm)
Pile-Up	$0.12^{\dagger}$ $(0.11)^{*}$
Flashlets	< 0.12
Energy Scale	<0.1 $(<0.01)^{\ddagger}$
Fast Rotation, Binning	0.08
Lost Muons	<0.1 $(<0.01)^{\ddagger}$
CBO	0.04
Randomization	0.04
Fixing Parameters	$<0.04^{\flat}$
Double CBO [2]	0.03
Vertical Waist [2]	0.02
Sum	<0.36 $(<0.22)^{\ddagger}$

† For the cut 2 GeV, fit start time 32 μs, using the estimate of $\Delta\phi_p$ from pile-up subtraction

* For pile-up subtracted data (quoted from [2]); includes errors due to the uncertainty in pile-up phase and subtraction inefficiencies.

‡ At a zero crossing (e.g. 32 μs).

$^{\flat}$ For fits starting after 50 μs.

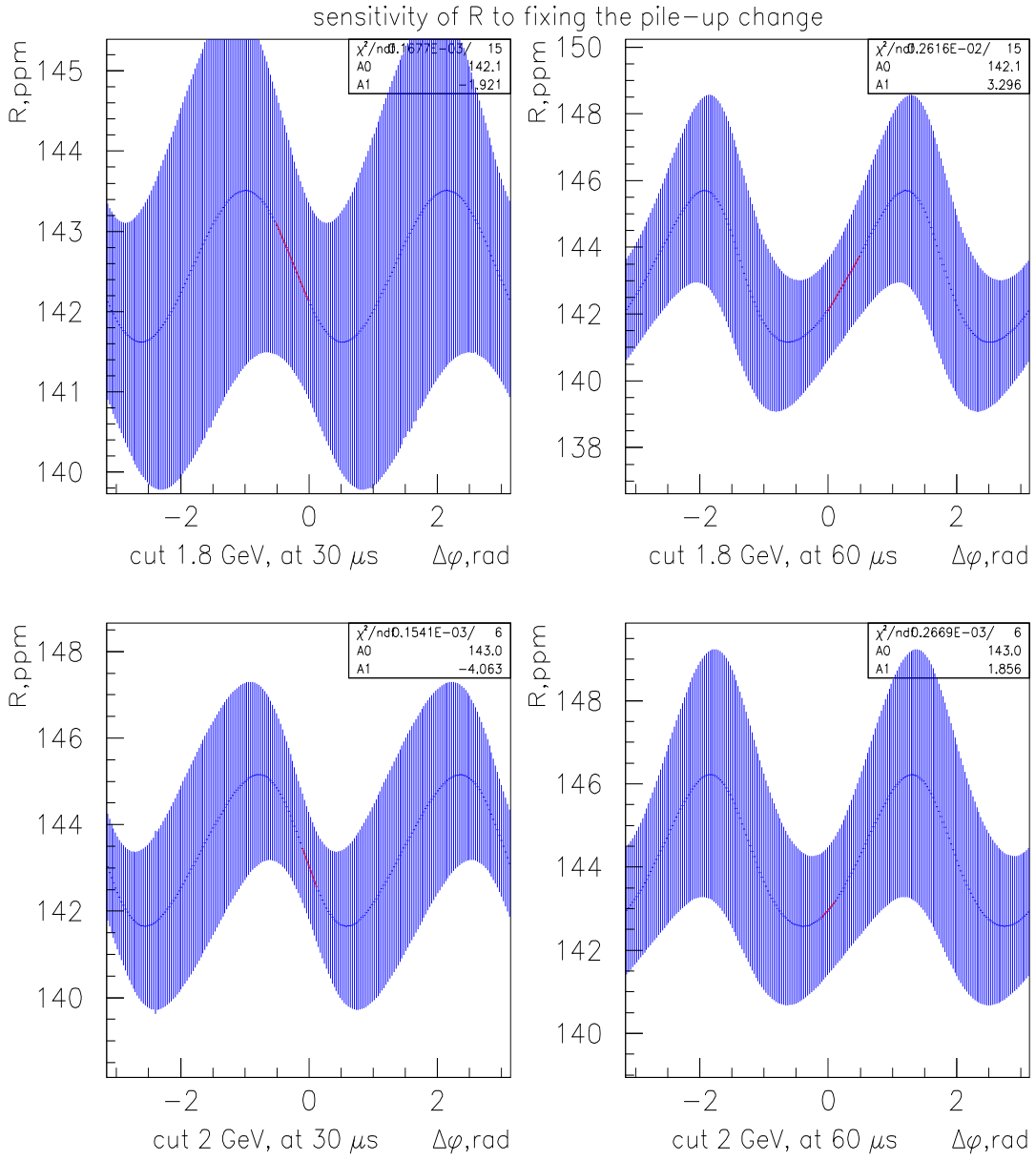

Fig.42a. Change in the fitted value of R caused by changing the difference between the g-2 and pile-up phases (fixed parameter $\Delta\phi_p$) for fit start times 30 and 60 μs, and for cuts 1.8 and 2.0 GeV. The 2.0-GeV cut is more sensitive to the change in pile-up phase, since the pile-up fraction for that cut is higher than for 1.8 GeV.

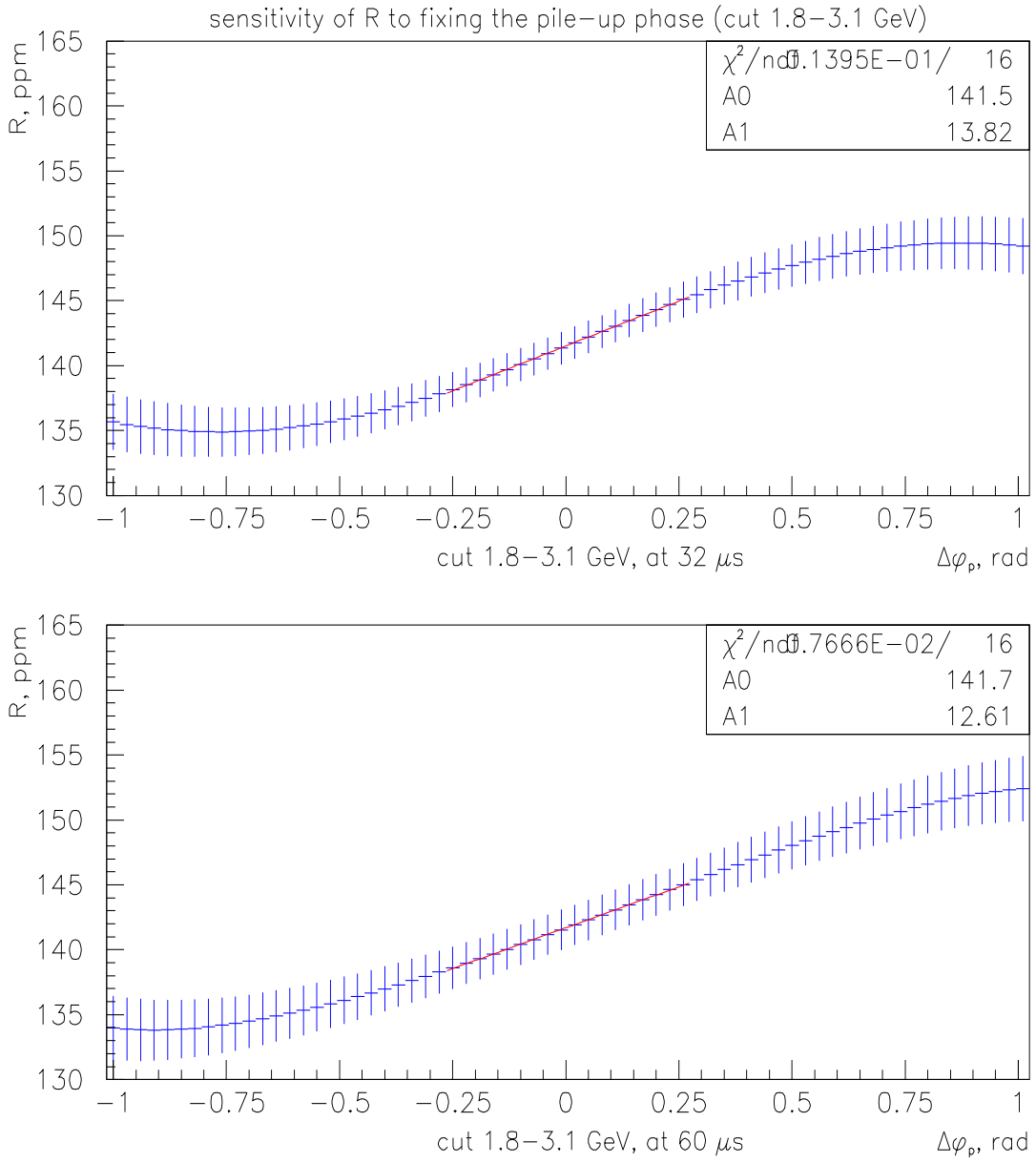

Fig.42b. Change in the fitted value of R caused by changing the difference between the g-2 and pile-up phases (fixed parameter $\Delta\phi_p$) for fit start times 32 and 60 μs (cut 1.8-2 GeV). This cut is more sensitive to the choice of $\Delta\phi_p$, since the pile-up asymmetry is much larger.

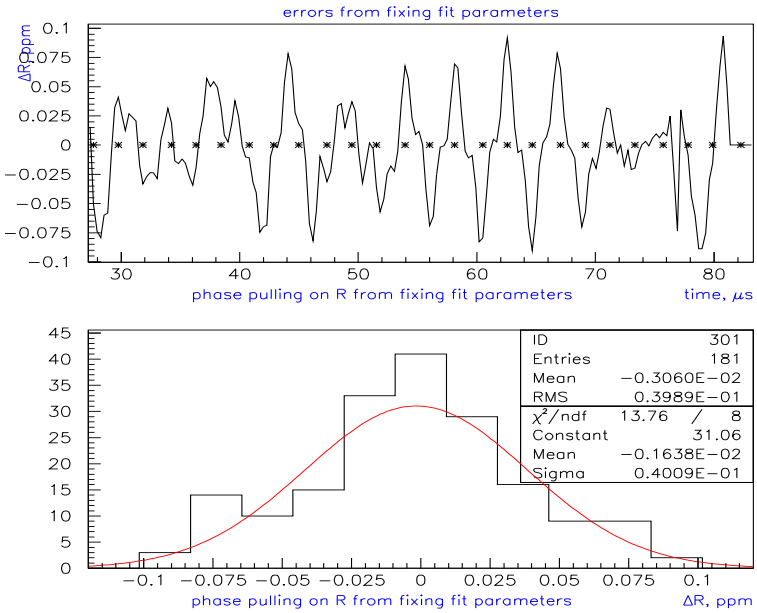

Fig.43. Difference in R values between a fit with τ_B, ω_B (f_B), a_X and τ_X varying as free parameters and a fit with these parameters fixed. Top: as a function of start time (with asterisks at g-2 zero-crossings). Bottom: projection of the top plot to the y-axis.

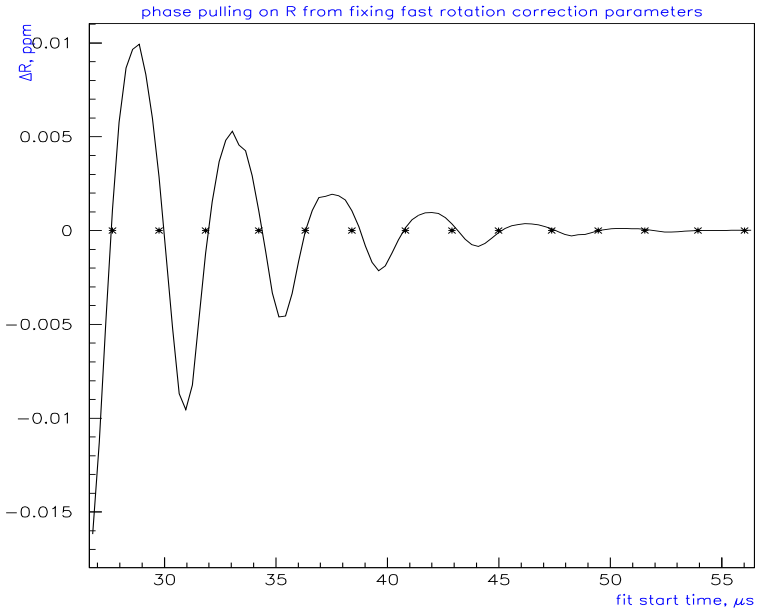

Fig.44. Phase pulling on R from fixing the fast rotation correction parameters at wrong values. Asterisks show g-2 zero-crossings. The effect is generally very small and is minimal at the zero-crossings.

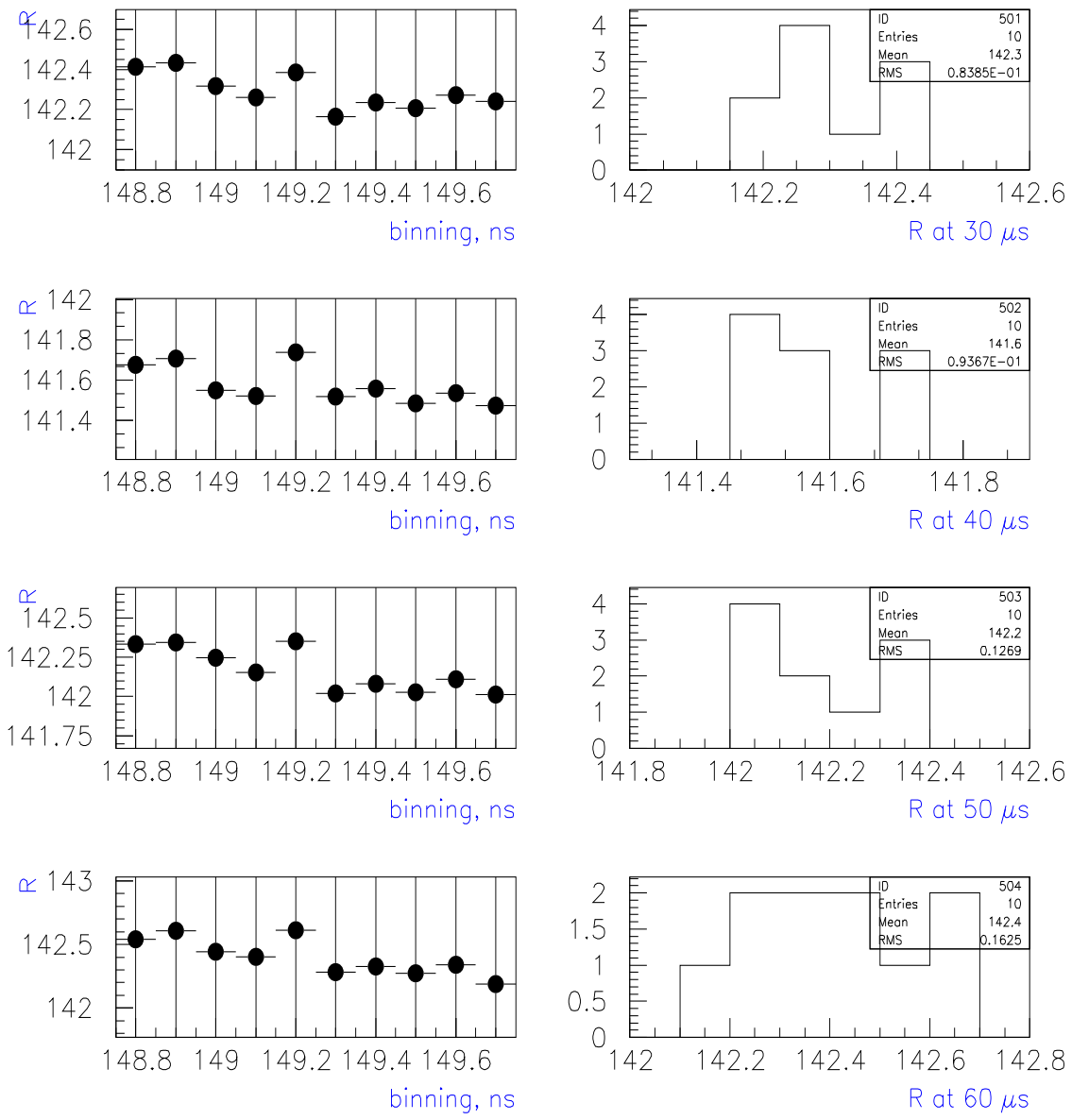

Fig.46. Fitted values of R for 10 different bin sizes between 148.8 and 149.7 ns, for fits starting (top to bottom) at 30, 40, 50 and 60 μs. The same data was used to fill all 10 histograms. The results are given for a single random seed only.

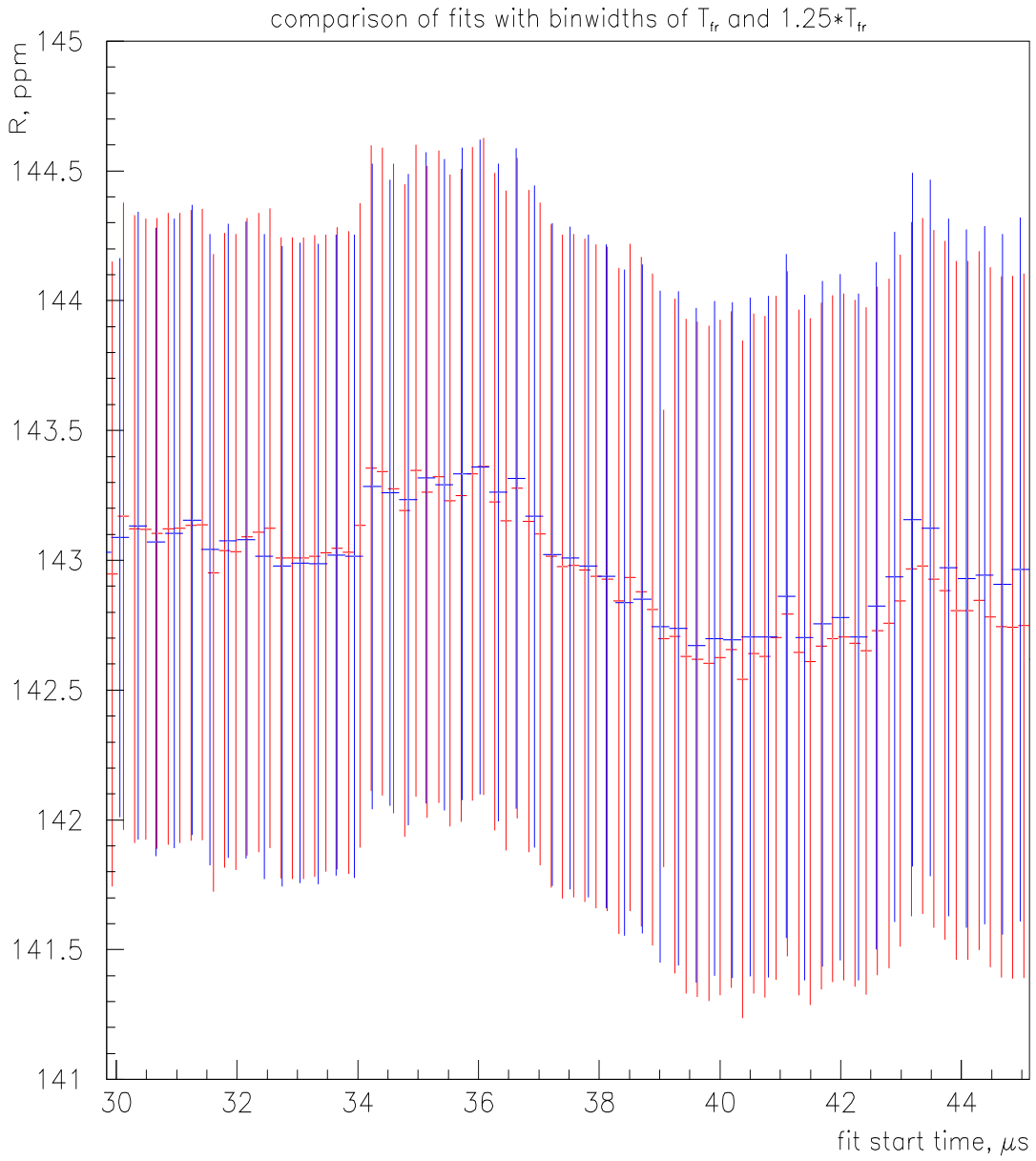

Fig.47. Comparison of the fitted values of R for bin width of 149.185 ns (fast rotation period) and 186.48125 (1.25 times wider, as recommended by Yuri [14]).

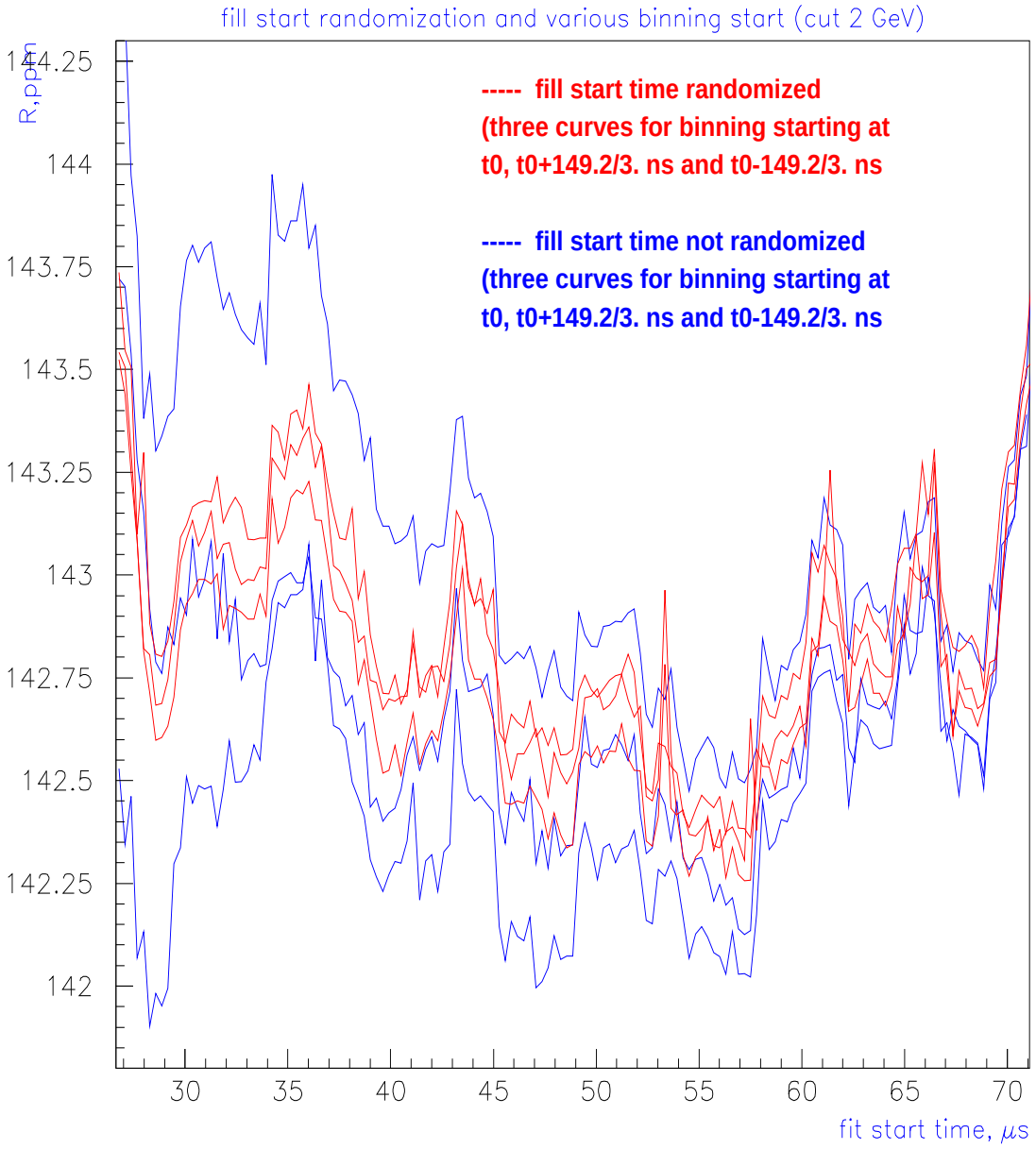

Fig.48. Comparison of fit results for R (cut 2 GeV) for 3 different start times of binning ("natural" at t0, shifted back and forth by 1/3 of the bin width), with (red) and without (blue) fill start time randomization. If the start times of spills are not randomized, there is a systematic shift in R at early times with respect to the results from randomized data. The sign and size of this shift varies with the choice of the binning start time. On the average, the results with and without randomization differ by less than 0.1 ppm. If the data is randomized, the error due to the choice of binning start time is again less than 0.1 ppm

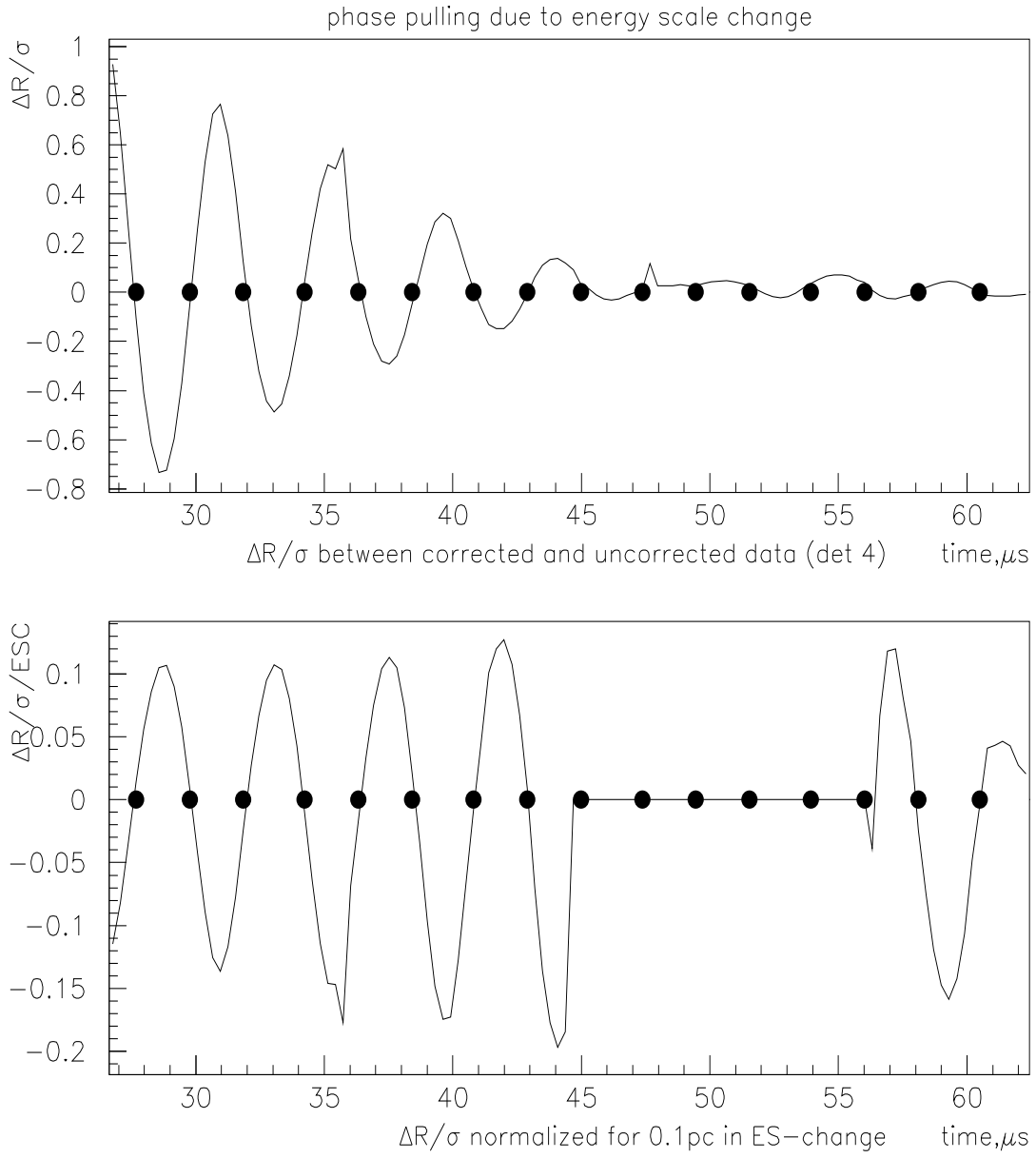

Fig.49. Phase pulling on R due to energy-scale change (e.g. detector 4). Top: shift in the fitted R value (normalized by one standard deviation) between the data uncorrected and corrected for energy scale change vs fit start time; black dots are zero-crossings of g-2 precession: the effect is minimal there. Bottom: Top plot normalized by the size of the ESC effect (approximation of the phase pulling for 0.1% ESC); black dots are zero-crossings of g-2 precession; ESC function for detector 4 crosses zero at 50 μs: $\Delta R/\sigma/ESC$ *is singular there and is not shown on the plot.*

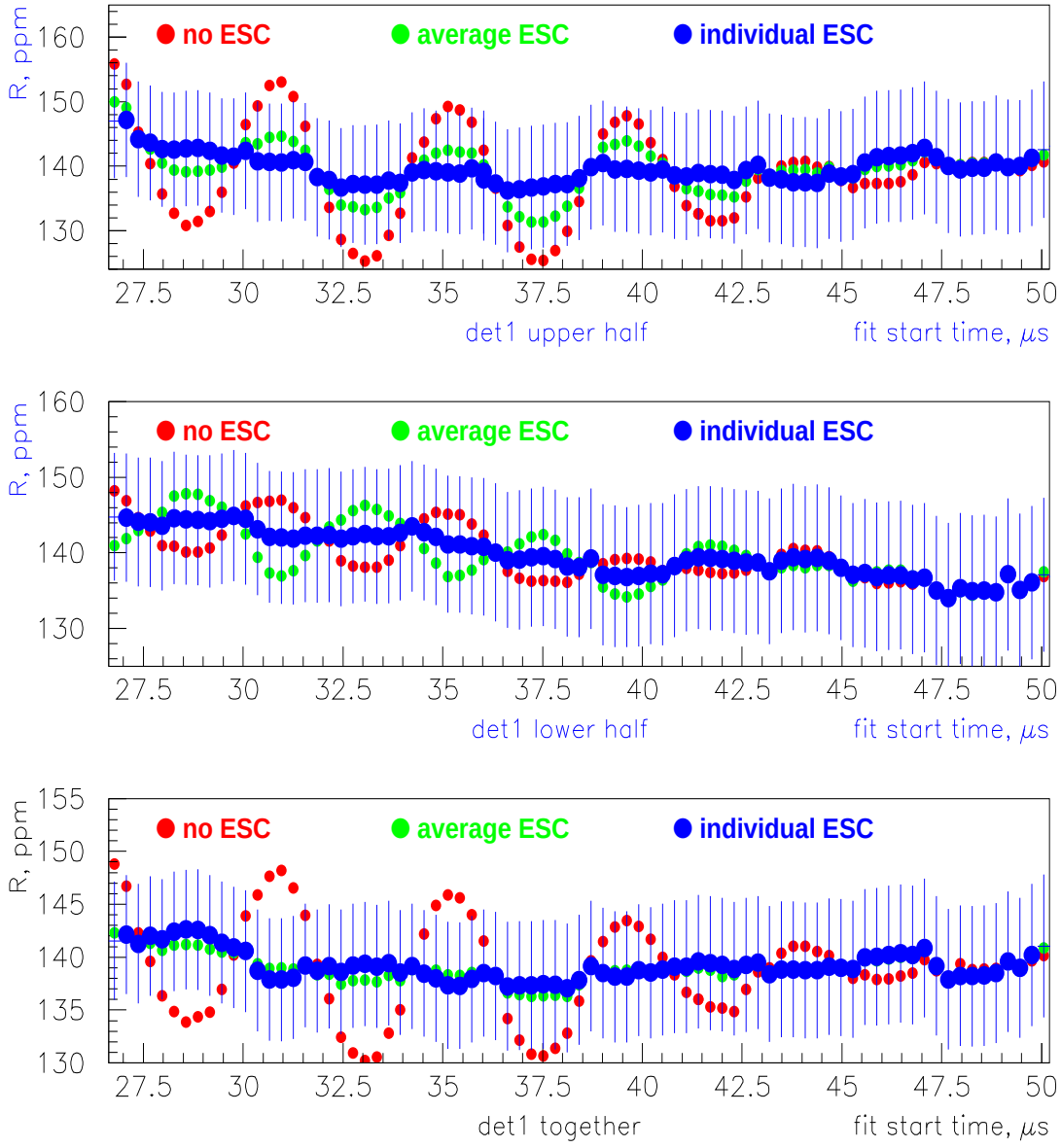

Fig.50. The effect of ESC correction is shown for the upper and lower parts of detector 1, separately and together. Red: no correction was applied, green: "average" correction was applied, blue: both halves were corrected individually. As shown in Fig.7a, the ESC is different for the upper and lower parts of the calorimeter, and while the average correction is not enough for the upper part, the effect is overcompensated for in the lower half. For the entire data from detector 1 (bottom plot), the difference in R was small (less than 0.1·σ) whether an average or a more accurate correction was applied.

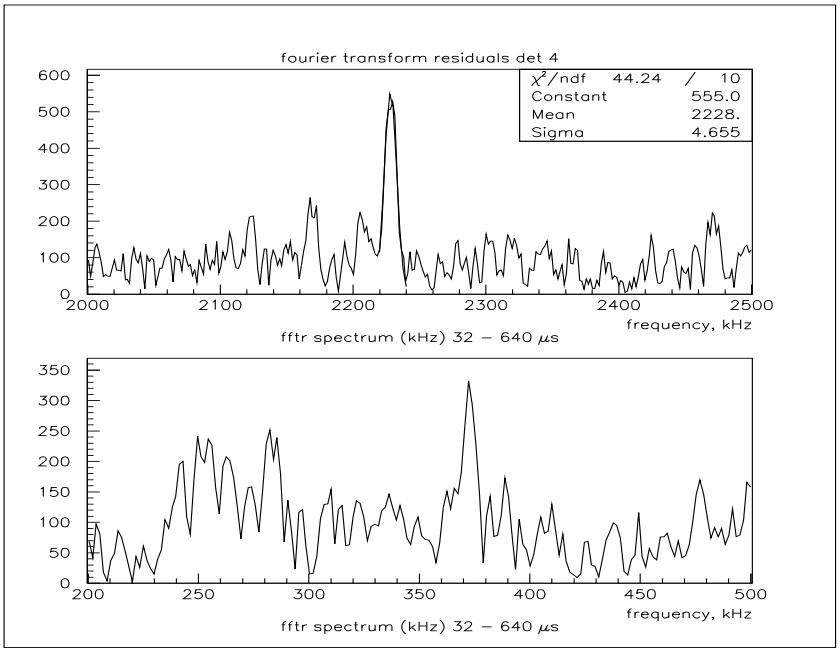

Fig.51. Flashlets can be seen in the Fast Fourier Transform spectrum of the fit residuals (e.g det 4). Two peaks with f = 371 kHz (AGS frequency, bottom plot) and f = 2228 kHz (6 times AGS frequency, top plot) are present.

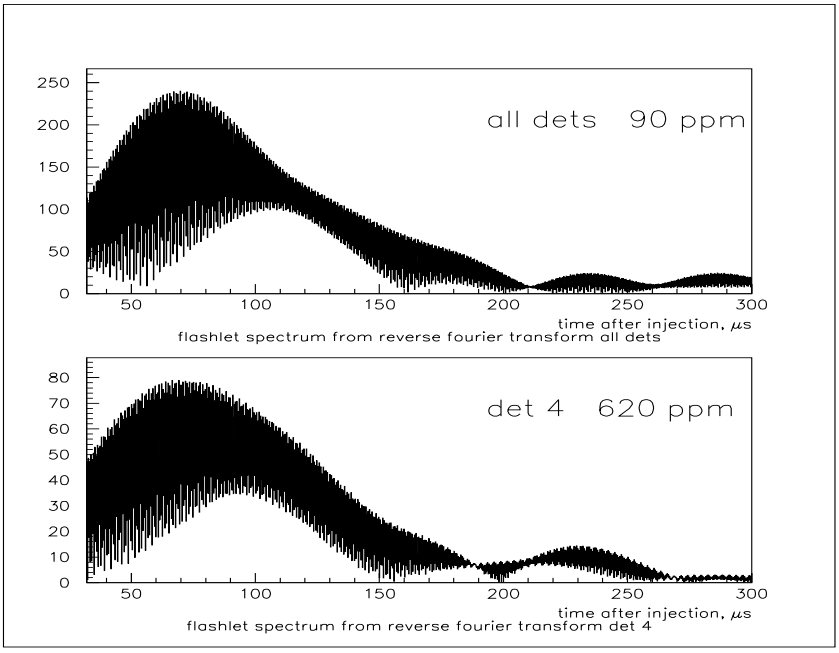

Fig.52. Not a very scientific, but a curious result: an inverse Fourier transform of the flashlet peaks brings an estimate of the flashlet contamination of 90 ppm for the entire data set, and more than 6 times as much in detector 4 (Vladimir and Genna saw the same ratio in the 2000 data [15]). If these spectra are used in a simulation, the results are similar to those shown in Figs.52,53 with $\Delta R < 50$ ppb.

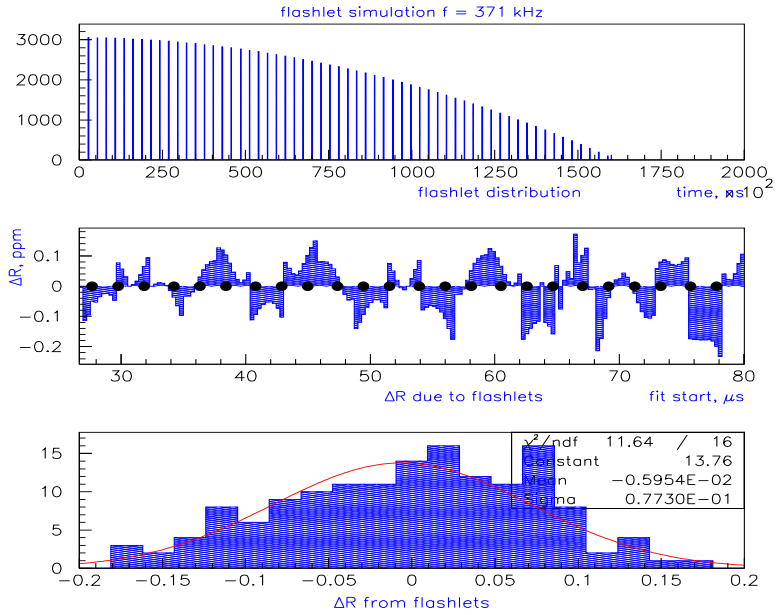

Fig.53. Results of a flashlet simulation ("worst" case, f = 371 kHz (AGS period)). Top: flashlet spectrum generated with the AGS frequency (100 ppm level). Middle: Shift in the fitted R value due to flashlet contamination as a function of fit start time. Bottom: distribution of the bias in R due to 100 ppm flashlet contamination.

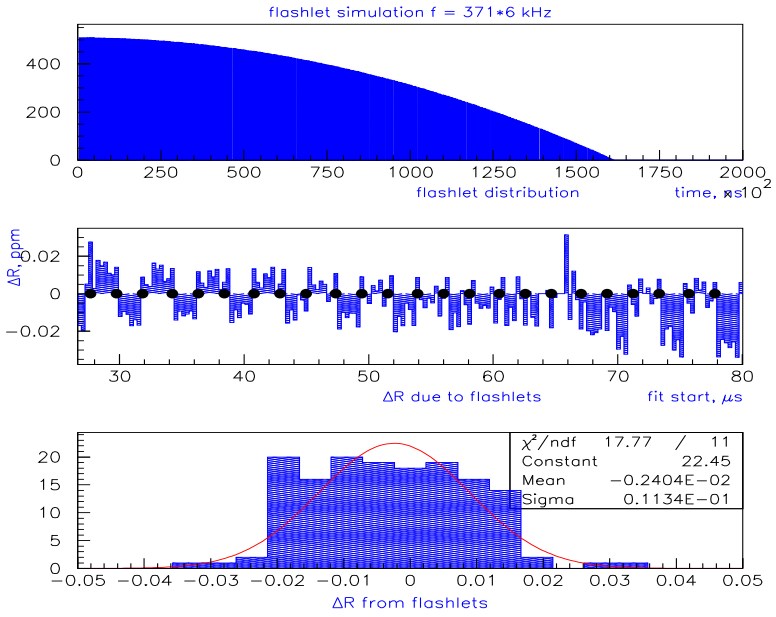

Fig.54. Results of a flashlet simulation ("best" case: flashlets are distributed evenly over bunches. Top: flashlet spectrum generated with 6 times the AGS frequency (100 ppm level). Middle: Shift in the fitted R value due to flashlet contamination as a function of fit start time. Bottom: distribution of the bias in R due to 100 ppm flashlet contamination.

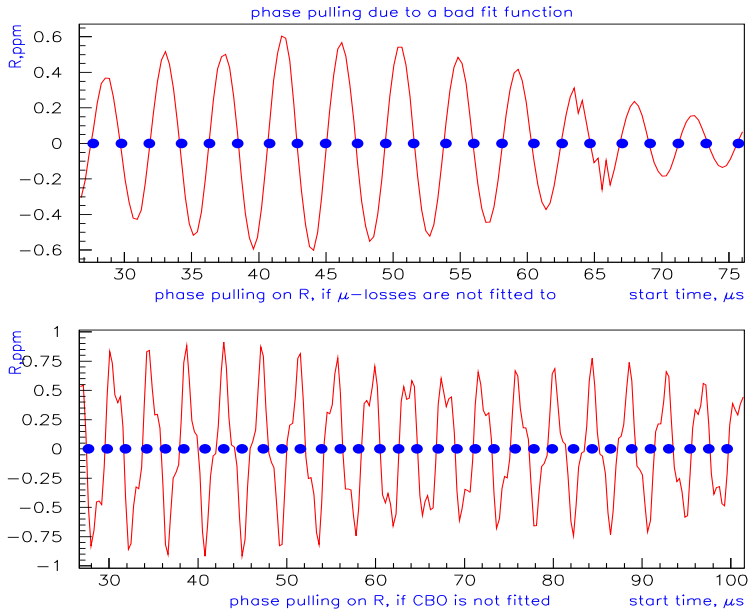

Fig.55. If the CBO and muon loss terms are **not** *included in the fitting function at all, one observes a strong phase pulling. In the case of muon losses, this phase pulling has a period of the (g-2) precession and is negligible at the zero-crossings (blue dots). The phase pulling due to CBO has a more complicated character and is affected by both a_μ and the CBO frequency.*

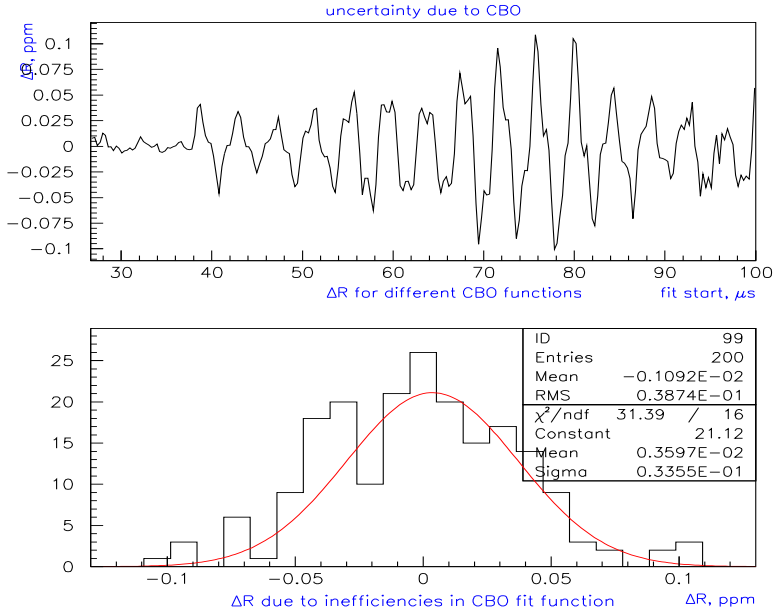

Fig.56. Letting the center of the CBO packet τ_{0B} vary as a free parameter in the fit (see Figs.11,12) changes the value of R. Top: the difference between the R values as a function of the fit start time, between the fits with τ_{0B} fixed and free (cut 2 GeV, all data). Bottom: the distribution of this difference can serve as an estimate of the systematic error due to inefficiencies in fitting to CBO.

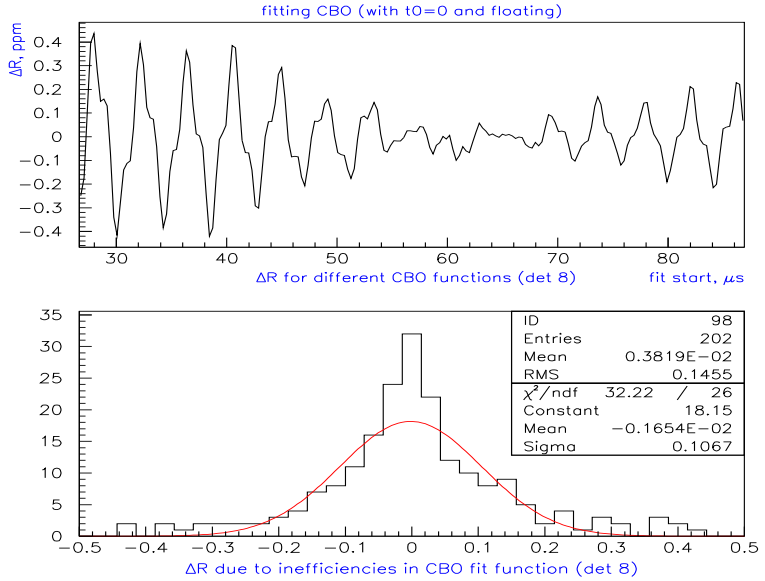

Fig.57. Similar to Fig.49. This study was done separately for detector 8, in which the amplitude of CBO is about 8.5 times higher than when all detectors are added together. Top: the difference between the R values as a function of the fit start time, between the fits with τ_{0B} fixed and free. Bottom: the distribution of this difference.

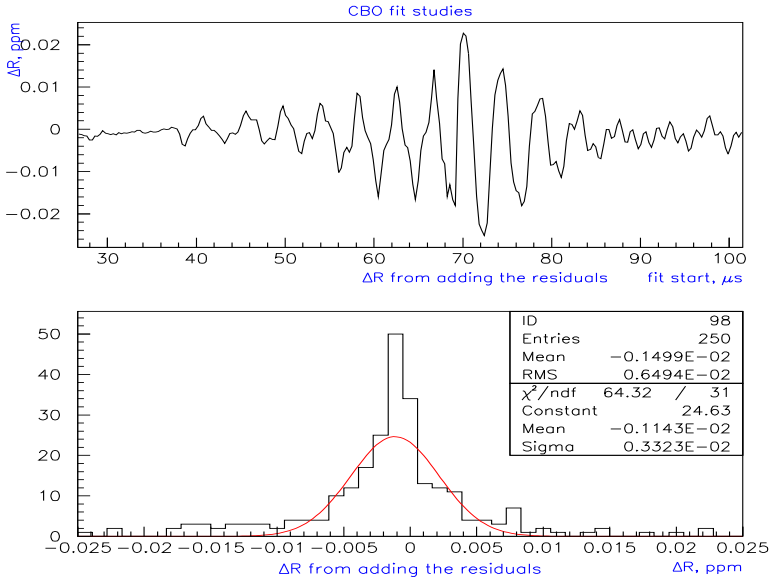

Fig.58. An attempt to see how the background (residuals of the fit with a full multi-parameter function) affects R. On the top plot: the difference in R between fits to two modified data sets; in one, the fit residuals of a full fit function were added to the data set once (effectively doubling the background); in the other, both the residuals and the CBO distribution were added (double CBO amplitude and the background). Bottom: the distribution of this difference is very small, leading to a conclusion that the residuals do not affect fitting to CBO significantly.

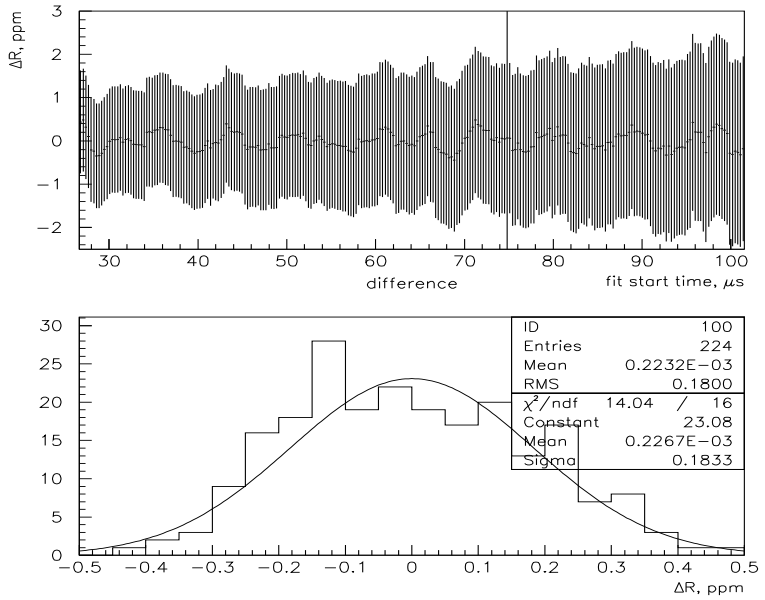

Fig.59. "Phase-pulling" on R (with respect to the average over a g-2 precession period) vs fit start time. The top plot shows the difference between the fitted R and the average R value for 29 adjacent bins (approximately one precession period). Bottom plot shows the distribution of this shift.

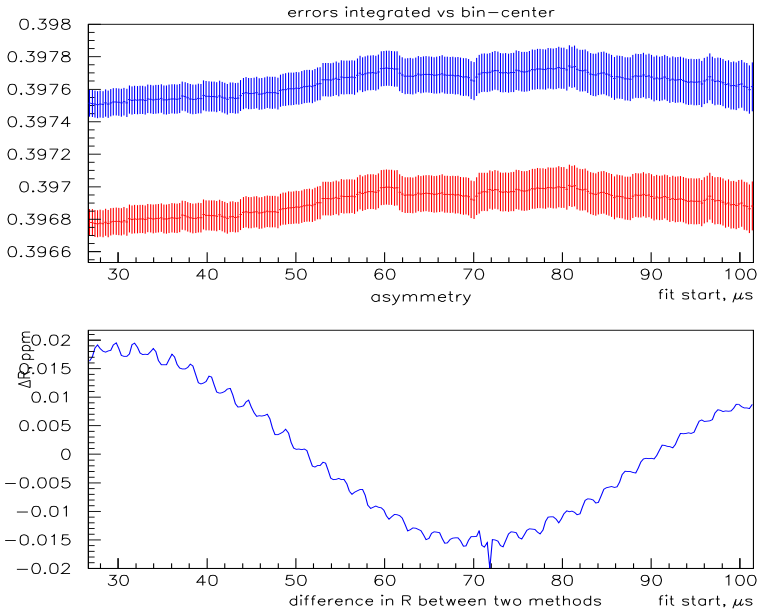

Fig.60. The results for A and R compared with the errors calculated as a square root of the function at the center of a bin (red), and a square root of the integral over the bin (average over 5 points, in blue). Better evaluation of the error gives a significant increase in the asymmetry, the effect on R is minimal. (Cut 2 GeV was used.)

6 Summary and Conclusions

As was discussed in Sections 3 and 4, the 1999 data, for each detector separately and for the sum of all detectors, could be fitted to a function with 13 free parameters (with 5 more parameters fixed in the fit after their values were determined from simulation, trial fits etc.).

If the pile-up phase is fixed at 0 for each of the cuts 1.8, 1.8-3.1 and 2 GeV, the results are self-consistent, and there is a good agreement between the values of R obtained by fitting the detectors separately and then averaging the result, and fitting the summed data from all detectors. But the difference in R values between the cuts turns out to be 0.6 - 1 ppm for different fit start times (Fig.17), greater than the acceptable variation of $0.5 \cdot \sigma$. A more careful choice of the value of pile-up phase helps reconcile the results for different cuts (Fig.33).

For the cut 2 GeV and higher, good estimates of $\Delta\phi_p$ can be obtained using the pile-up subtraction. As shown in Table 13, the discrepancy in the results for R from a full data set and a "pile-up subtracted" data set is well within the systematic error. Averaging the values of R from 22 detectors brings a close result as well (Table 14). Other parameters show a good early-to-late time stability and are not affected significantly by pile-up subtraction.

The results for cuts 2 GeV and higher agree within the acceptable statistical variation, both for the pile-up subtracted data sets and the regular data sets (with the pile-up phase taken from PUS studies) (Figs.37,38).

Based on this, one can say that the 1999 data can be well described by the 17-parameter function given by Eqn.2 or a 12-parameter function, if PUS is used (with 13 and 11 free parameters correspondingly). The main result of this study comes from the fit to the 2-GeV selection with $\Delta\phi_p$ = - 68 mrad (fixed):

R = 143.25 $\pm$ 1.24 $\pm$ 0.22 ppm

Table 13. Summary of fit results for the cut 2.0 GeV. The values of R include an offset. In the case of pile-up subtraction, systematic errors include the PUS related uncertainties as tabulated in [2] (0.13 ppm overall).

Start Time, μs	Cut 2 GeV with pile-up subtraction		Cut 2 GeV no PUS, $\Delta\phi_p = -68 \pm 31$mrad	
	R	χ^2	R	χ^2
32	$143.23 \pm 1.24 \pm 0.21$	1.014	$143.25 \pm 1.24 \pm 0.22$	1.012
40	$142.68 \pm 1.31 \pm 0.21$	1.011	$142.61 \pm 1.32 \pm 0.23$	1.009
50	$142.78 \pm 1.43 \pm 0.21$	1.010	$142.68 \pm 1.43 \pm 0.23$	1.008
60	$143.01 \pm 1.54 \pm 0.21$	1.012	$142.94 \pm 1.54 \pm 0.24$	1.009
70	$143.34 \pm 1.67 \pm 0.21$	1.011	$143.35 \pm 1.67 \pm 0.24$	1.008
80	$143.44 \pm 1.81 \pm 0.21$	1.010	$143.45 \pm 1.81 \pm 0.24$	1.008

Table 14. Fit results for the cut 2.0 GeV averaged over 10 random seeds for 22 detectors (with the pile-up phase fixed at the value from PUS). The values of R include an offset.

Start Time, μs	Cut 2 GeV detector average, $\Delta\phi_p = -68$mrad	
	R	χ^2
32	143.12 ± 1.25	1.012
40	142.62 ± 1.32	1.009
50	142.69 ± 1.43	1.008
60	142.80 ± 1.55	1.006
70	143.28 ± 1.68	1.005
80	143.47 ± 1.82	1.005

Acknowledgments

I would like to thank everyone in the g-2 collaboration who participated in running the experiment, data analysis and discussion. My special thanks go to my thesis advisor Jim Miller for valuable suggestions and comments on this note. I very much appreciate comments and corrections from Cenap Özben, Jörg Pretz, Ernst Sichtermann, Bill Morse, Yannis Semertzidis, Yuri Orlov and Rob Carey.

Appendix A: Studies of Energy-Scale Changes (ESC) and Pile-up using `g2off` data

Time-dependent changes in the average of the energy distribution (AED) were investigated for different detectors at different times following the beam injection. For each slice of time equal to the g-2 precession period (approximately 4365.4 ns), energy distribution histograms were created for all 22 detectors used in the analysis. Since the energy calibration changed from run to run for some detectors, pulse amplitudes were normalized to the end-point values (maximal positron energy) in every run. The average energy was then calculated for each detector with lower cut-off at 60, 70, 80, 90 and 100% of the maximal positron energy (3.1 GeV).

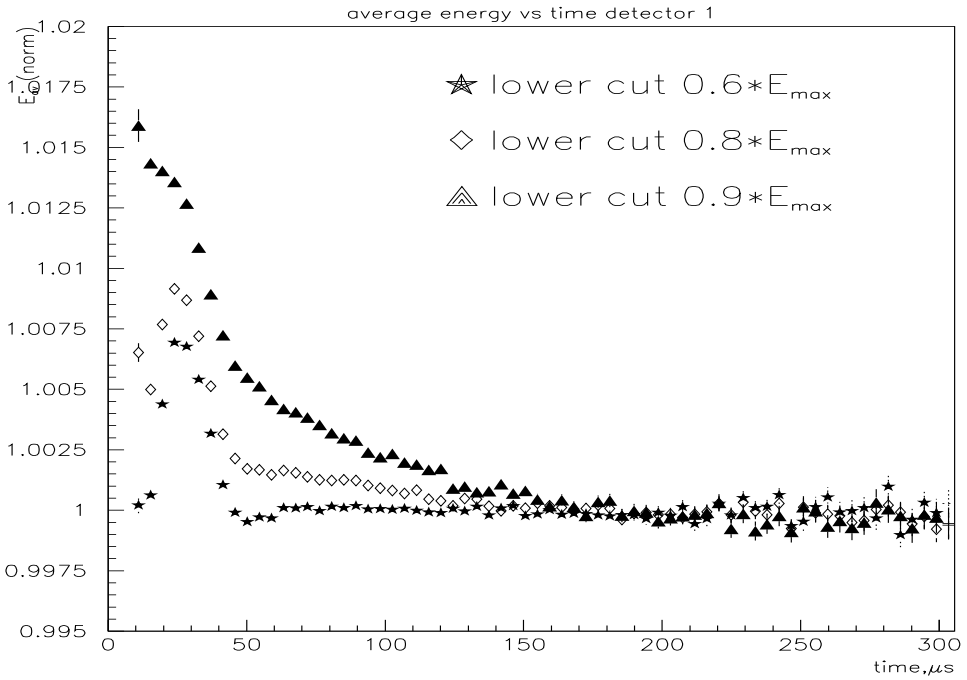

Fig.A1. Change in the average positron energy (normalized to the late time average) seen by detector 1 for different lower cuts

As illustrated by Fig.A1, the relative size of contributions to the average energy coming from pile-up and ESC varies for different lower cuts. Detector 1 shows a manifest Özben effect wiggle at early times for cuts 0.6 and $0.8 \cdot E_{max}$, but pile-up contribution is growing for higher cuts, as the fraction of pile-up pulses is increasing (see Appendix B, Fig.B4). For cut $0.9 \cdot E_{max}$, the change in the average energy is mainly contributed to by pile-up.

The average energy at higher cuts is also less sensitive to the ESC. The estimate of this sensitivity was obtained applying artificial "gain" to the real data pulses, while holding the cut-off threshold the same for different cuts. As shown on Fig.A2, at a lower cut of $0.6 \cdot E_{max}$, the AED sees only approximately 48.7% of the real scale change. This num-

ber is going down for higher cuts: 42.2% for a 0.7·E_{max} cut, 34.6% for 0.8, 24.5% for 0.9, and only 2% for $E_{cut} = E_{max}$. (If there's no lower cut, i.e all pulses are taken into account, the change in the average energy would be the same as the change in the energy scale.)

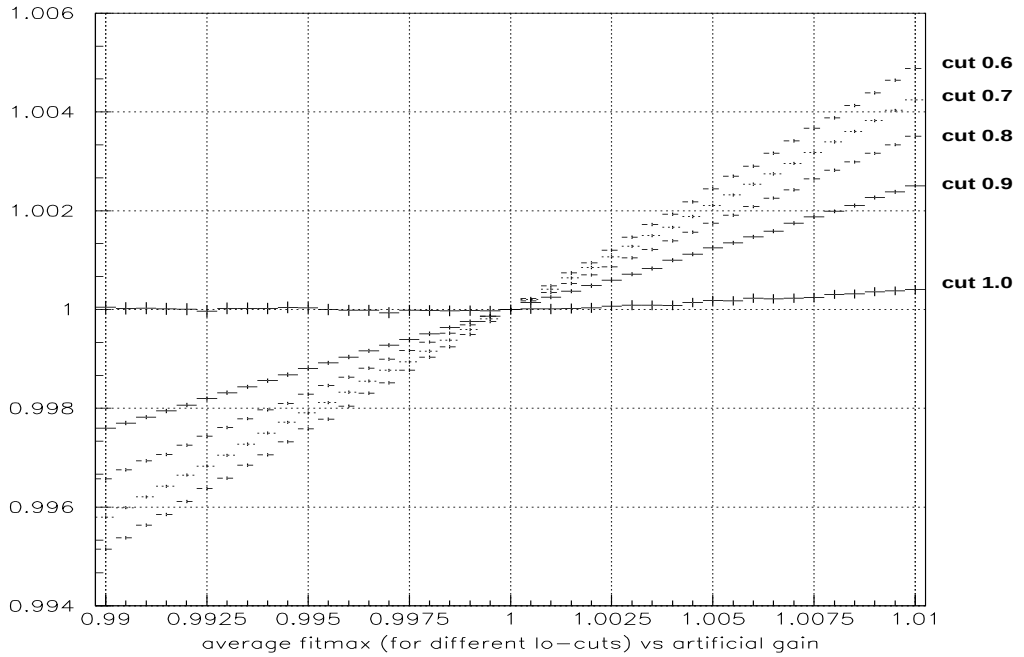

Fig.A2. Correlation between the change in the average energy (normalized) and artificial gain (simulation using real data) for different lower cuts.

Assume a simple model of the AED change with the time:

$$\langle E(t)\rangle = \big(\langle E_{true}\rangle + n_p \cdot \langle E_p\rangle \cdot f_{pu}(t)\big) \cdot \big(1 + a \cdot f_e(t)\big) \qquad (A1)$$

where the "true average" $\langle E_{true}\rangle$ is determined from the late time data (after 200 μs), n_p is pile-up fraction, $\langle E_p\rangle$ is the average energy of pile-up contribution, $f_{pu}(t) = e^{-\lambda t} \cdot f_{fr}(t)$ describes the decrease in the relative number of pile-up pulses with respect to the total number with time and includes a fast rotation correction, a is a sensitivity of a certain cut to the energy scale determined from simulation mentioned above, and $f_e(t)$ is a function describing the ESC.

Parameter $A_p(E_{cut}) = n_p(E_{cut}) \cdot \frac{\langle E_p(E_{cut})\rangle}{\langle E_{true}(E_{cut})\rangle}$ is independent of the time, but obviously varies for different cuts. And the equation (A1) can be rewritten as:

$$\langle E_{norm}(t)\rangle = \frac{\langle E(t)\rangle}{\langle E_{true}\rangle} = \big(1 + A_p \cdot f_{pu}(t)\big) \cdot \big(1 + a \cdot f_e(t)\big) \qquad (A2)$$

As it is known, that the energy scale changes are negligible after 50 μs in most detectors, one can neglect the term $(1 + a \cdot f_e)$ when describing AED change at late times. It is

therefore caused by pile-up contribution alone. With the assumption that pile-up time behaviour is cut-independent, the relative strength of pile-up contribution:

$$B(E_1, E_2) \quad = \quad \frac{A(E_1)}{A(E_2)} \quad = \quad \frac{\langle E_{norm}(E_1)\rangle - 1}{\langle E_{norm}(E_2)\rangle - 1} \qquad (A3)$$

turns out to be independent of time (Fig.A3).

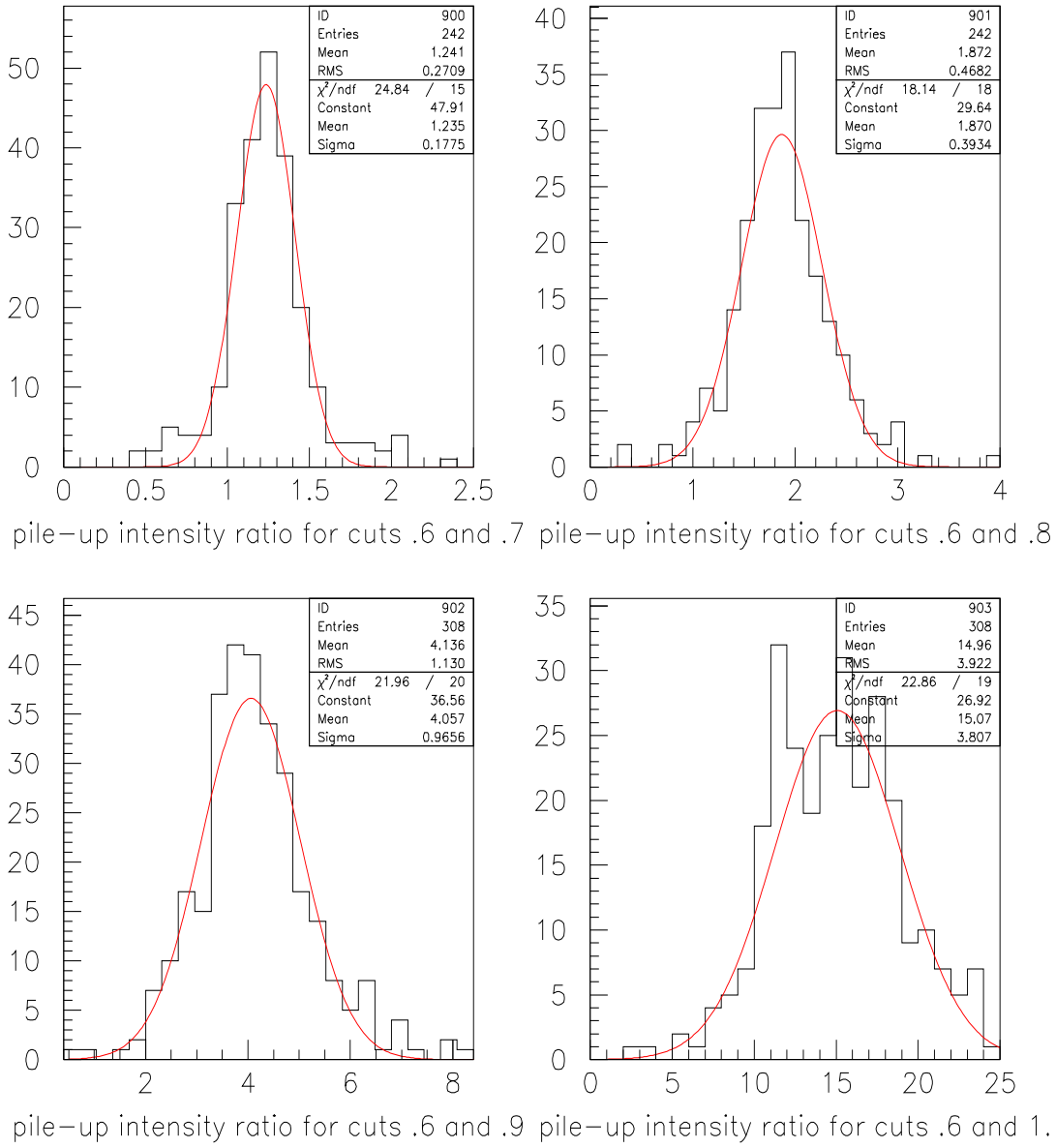

Fig.A3.Relative strength of pile-up contribution to AEC for different combinations of cuts is independent of time and obeys gaussian distribution.

If $B(E_1, E_2)$ is known, A_p can be eliminated from a pair of equations (A2) describing the results for two different cuts for the same detector. Neglecting the small term

$A_p \cdot f_{pu}(t) \cdot a \cdot f_e$ (which is estimated to be smaller than 0.03% for all detectors at the time of the injection and dies off quickly) one obtains a function describing the energy scale change alone:

$$f_e(t) \simeq \frac{\langle E_{norm}(E_2,t)\rangle \cdot B(E_1,E_2) - \langle E_{norm}(E_1,t)\rangle - (B(E_1,E_2)-1)}{a(E_2)\cdot B(E_1,E_2) - a(E_1)} \qquad (A4)$$

Since due to the difference in energy spectra and other conditions, different detectors see different levels of pile-up (Figs.A4,A6), $B(E_1,E_2)$ is not necessarily the same for all of the detectors, but it is possible to divide the detectors in three different groups and calculate an average B for each of these groups. Most detectors fall into the "high-pile-up" category: 3 - 5, 10, 11, 14 - 17, 21 and 22. The "medium" group consists of detectors 1, 6, 9, 12, 13, 18 and 23. And the detectors with the lowest level of pile-up are 7-9, 19, 24. The variation in pile-up levels is most probably caused by differences in the shape of energy spectra for different detectors.

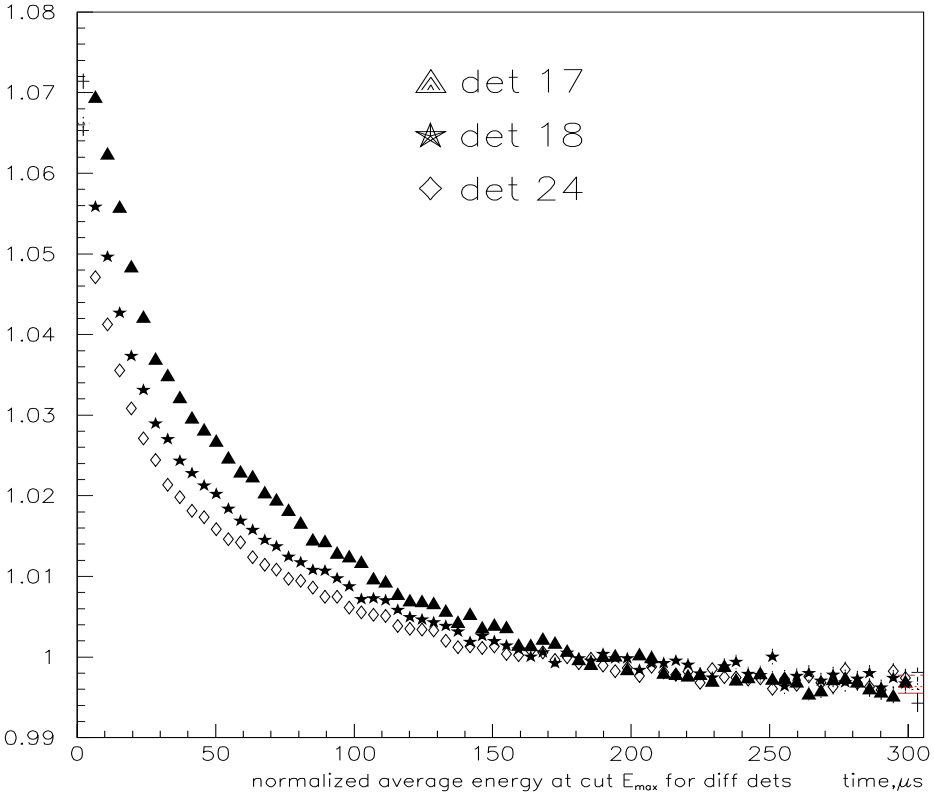

Fig.A4. Average energy for cut E_{max} for different detectors. Changes in the AED at this cut are due almost entirely to pile-up alone.

Formula (A4) was used to determine ESC for different detectors and different combinations of cuts. The results obtained using different combination of cuts for the same detectors show a good agreement (Fig.A5). The combination of cuts 0.8 and 0.6 of the

maximal energy produces the lowest statistical error, and was used to obtain ESC time dependence for individual detectors (see Figs.6a,b in the main section). ESC was fitted to a function of the form

$$f_e(t) = g \cdot e^{-\frac{t}{\tau_g}} + a_g e^{-\frac{1}{2}(\frac{t-t_0}{\sigma})^2} \quad (A5)$$

The gaussian term was used only in fits to detectors 1 and 4, to account for a noticeable "Özben-effect" wiggle, the other detectors were fitted to a 2-parameter exponential part of eq. A5. Fit results and estimates of ESC at 30 μs are given in Table 1 (main section).

The results of these studies agree very well with those found by Long (similar studies of average energy) and Cenap (pile-up subtraction).

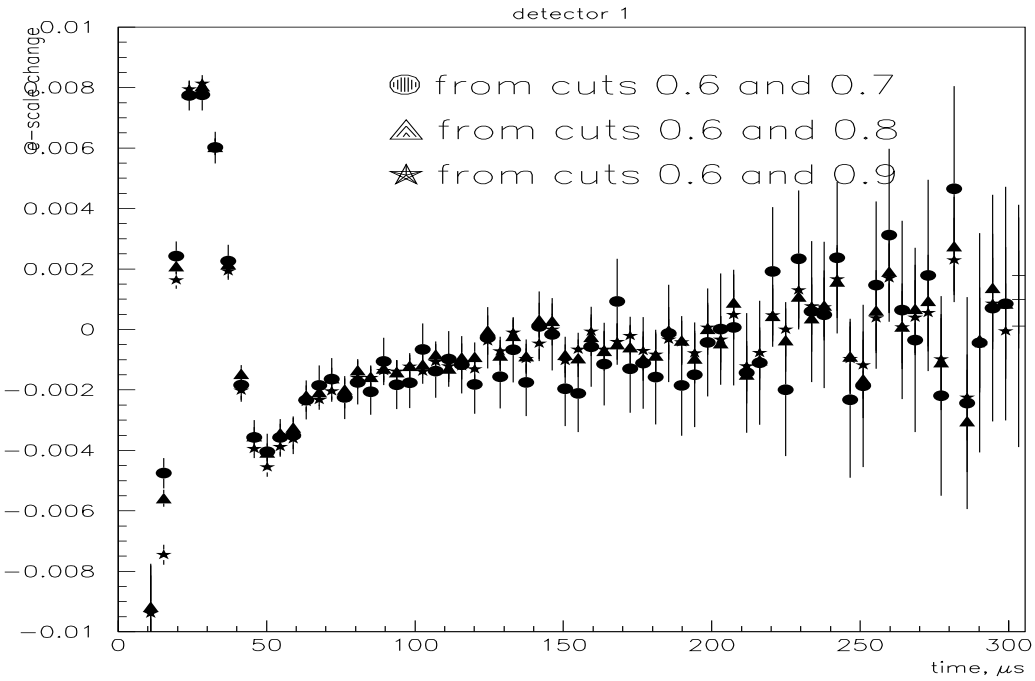

Fig.A5. Energy scale change as a function of time for detector 1: comparison of results obtained using 3 different combinations of lower energy cuts show an excellent agreement.

If the energy scale change contribution to the average energy is known for each detector, pile-up contribution can be estimated by simply dividing the total change in the average energy by $1 + a \cdot f_e(t)$ (see Eq.A2). This was done for all detectors and the resulting histograms were fitted to a 3 parameter function

$$f_p(t) = A_p \cdot (1 + a_p e^{-\frac{1}{2}(\frac{t}{\tau_p})^2}) \cdot e^{-\frac{t}{\lambda}} \quad (A6)$$

where λ is dilated muon life time (was fixed at 64.38 μs), A_p is a term describing pile-up contribution to the average energy (proportional but not identical to the (g-2)-fit parameter n_p), a_p, and τ_p are parameters describing the fast rotation inflation of pile-up.

Pile-up fitting gave consistent results for detectors 8 through 24, which are gated on before the short-lived fast rotation correction dies out (Fig.A6). This gave an independent estimate of the fast rotation correction to pile-up (Fig.A7).

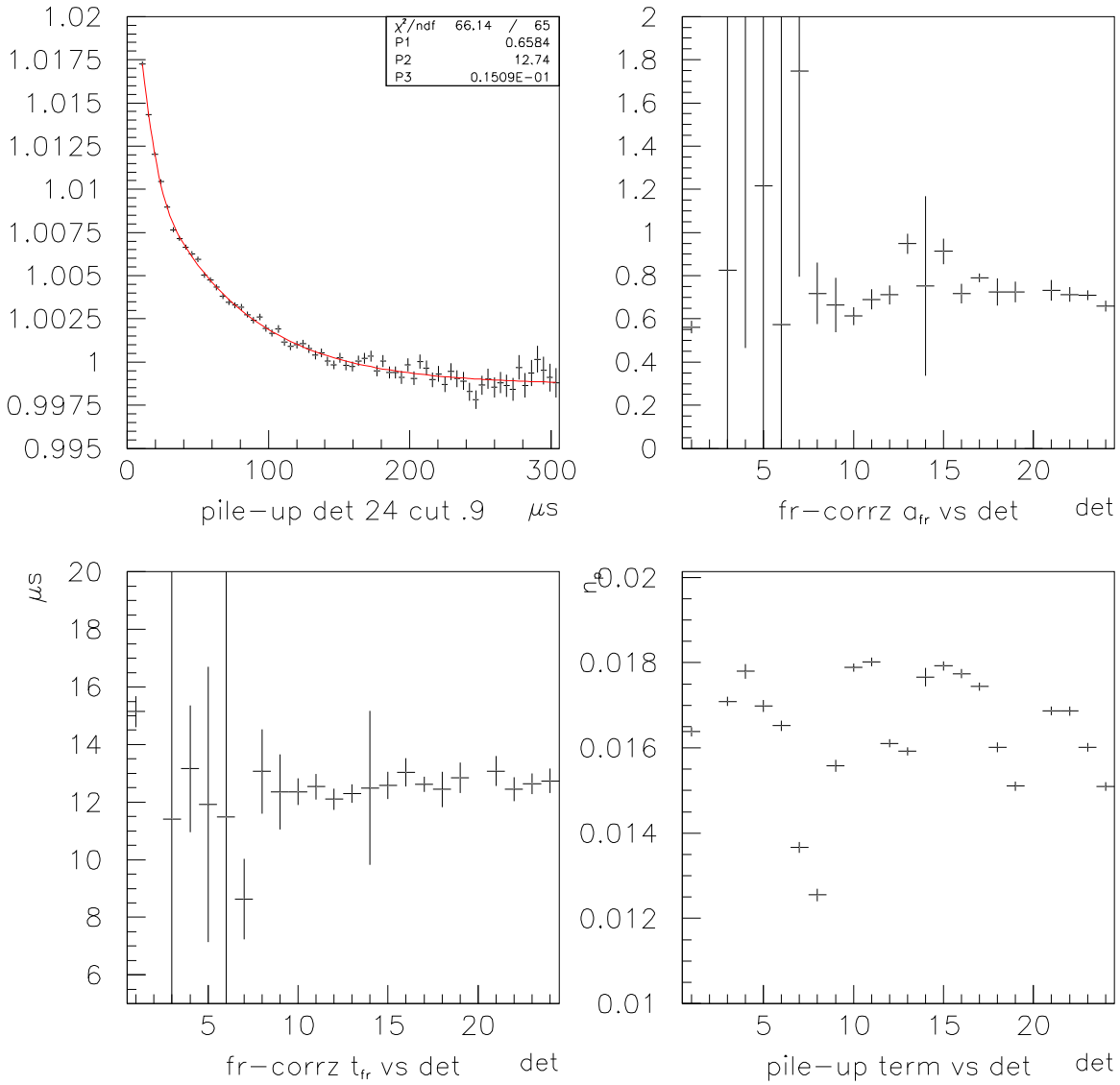

Fig.A6. Results of fitting to pile-up contribution to the average energy (real 1999 data). Top left: an example of fitting detector 24 with a function describing pile-up contribution (Eq. A6). Fit parameters by the detector: a_p (top right), τ_p (bottom left) and pile-up term n_p (bottom right). Detectors 3-7 give greater errors because of late gating. The pile-up fractions found in this study are in a good agreement with the results of fitting to the data (Fig.16b)

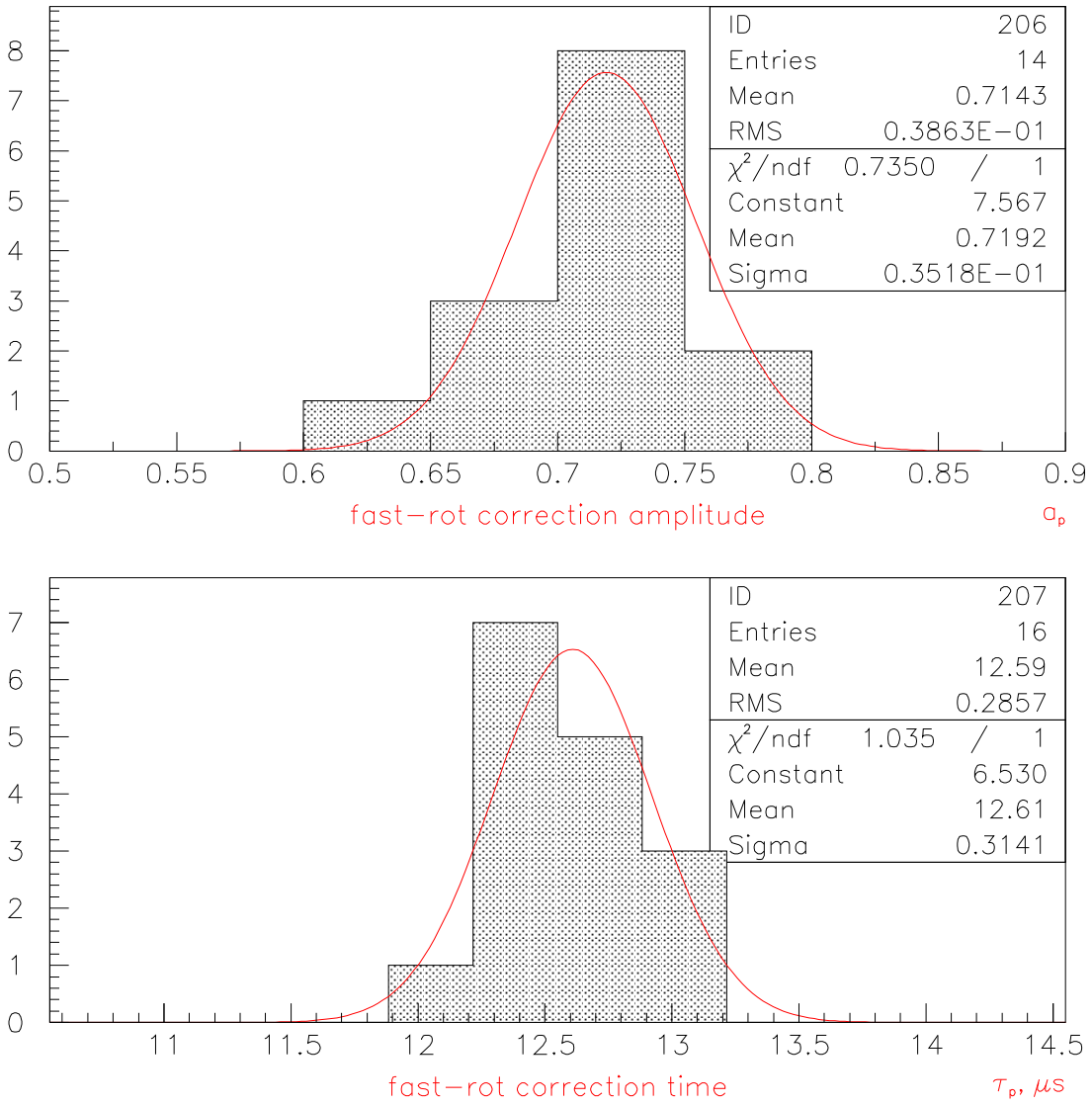

Fig.A7. Distribution of the parameters of fast rotation correction to pile-up: a_p (top) and τ_p (bottom). From fits to real data for detectors 8-24.

Appendix B: Pile-up studies with simulated data

The goal of this study was to reproduce some of the experimental conditions affecting pile-up rate as closely as possible.

At the first stage, a realistic positron distribution was generated. I used double precision random number generator RANMAR [13] and look-up tables for positron number N(E), asymmetry A(E), phase ϕ(E), and fast rotation probability. The look-up tables were provided by Rob and Jim (simulation and fast rotation analysis). Parameters such as R, muon lifetime λ, and the decay rate at the time of injection were fixed. The distributions were produced with two different decay rates, 3 and 4 MHz at the injection time (corresponding to approximately 16.7 and 22.2 muon decays per spill producing a positron with the energy higher than 1.8 GeV at least 40 μs after the injection: slightly higher and lower than the average decay rate observed in the 1999 experiment (Fig.B1)). These studies were repeated with fast rotation "turned" on and off to investigate the contribution to pile-up coming from fast rotation. Approximately 185 million positrons were generated for each combination of conditions. Muon and proton losses, energy-scale changes and betatron oscillation were not taken into the account.

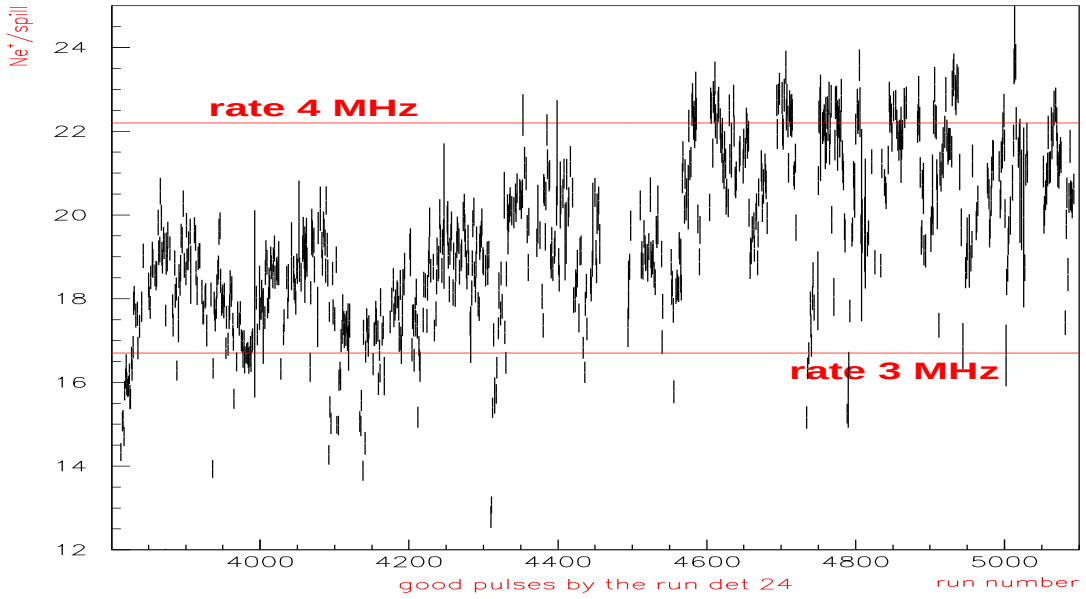

Fig.B1. The average number of high-energy positrons ($E > 1.8$ GeV, $t > 40$ μs) per spill by the run number (in det 24). Estimates of the decay rate at time t=0 are given with the assumption that these positrons constitute 16% of the entire decay spectrum (from Rob's simulation).

The time and energy distribution obtained in the way described above was then converted into fake WFD data, using realistic pulse-shapes for each detector and WFD-phase. The pulse-shape library was the same as the one used in the '99 data production. Following the real WFD algorithm, pulse amplitude in the simulation was rounded down to its integer part, and also cut off at 255 counts should it exceed the WFD pulse height limit. A

random pedestal value, obeying the pedestal distribution seen in the real data, was added to every fake WFD "bin"

On the third stage, the fake WFD data underwent regular `g2off` production and the ntuples similar to the standard production ones were filled in with the information about both generated and detected positron spectra. It was therefore possible to compare two spectra and determine pile-up levels, as a function of positron energy, and energy cut. This study was mostly focused on "doubles", i.e. pile-up pulses to which only two positrons contributed. The occurrence of "triples" is about 2 orders of magnitude less likely.

As illustrated by Fig.B2, the fraction of pulses going into pile-up pairs is practically flat throughout the energy spectrum. Fast rotation, as well, increases the probability of pile-up uniformly for pulses of all energies by about 30%. Since two original pulses (a pile-up pair) form a single pile-up pulse with an energy close to the sum of the two, the relative number of pulses lost to and gained from pile-up differs by the energy bin (Fig.B3). At about 75-80% of the maximal energy these numbers are very close and the net change in the number of detected positrons is negligible. At lower energies, more positrons are lost to pile-up than gained. The opposite is true for the higher energy bins.

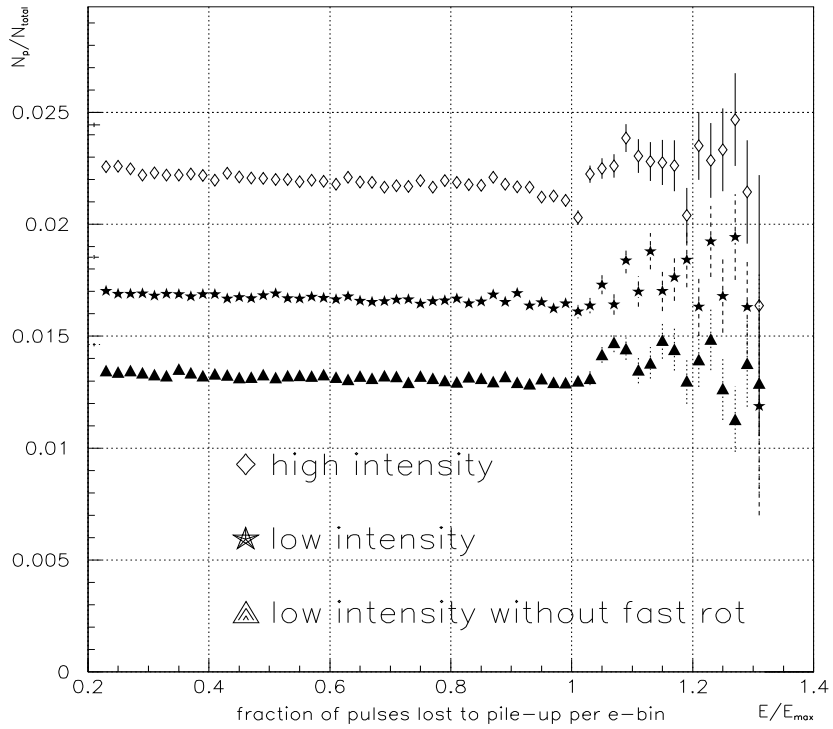

Fig.B2. The fraction of pulses undergoing pile-up is quite sensitive to the decay rate and fast-rotation intensity, but does not vary significantly with the positron energy. On the figure above, the fraction of pulses lost to pile-up is plotted against the normalized positron energy for different simulation conditions: decay rate 4 MHz (higher than the experimental average), 3 MHz (lower than average), and 3 MHz without fast rotation.

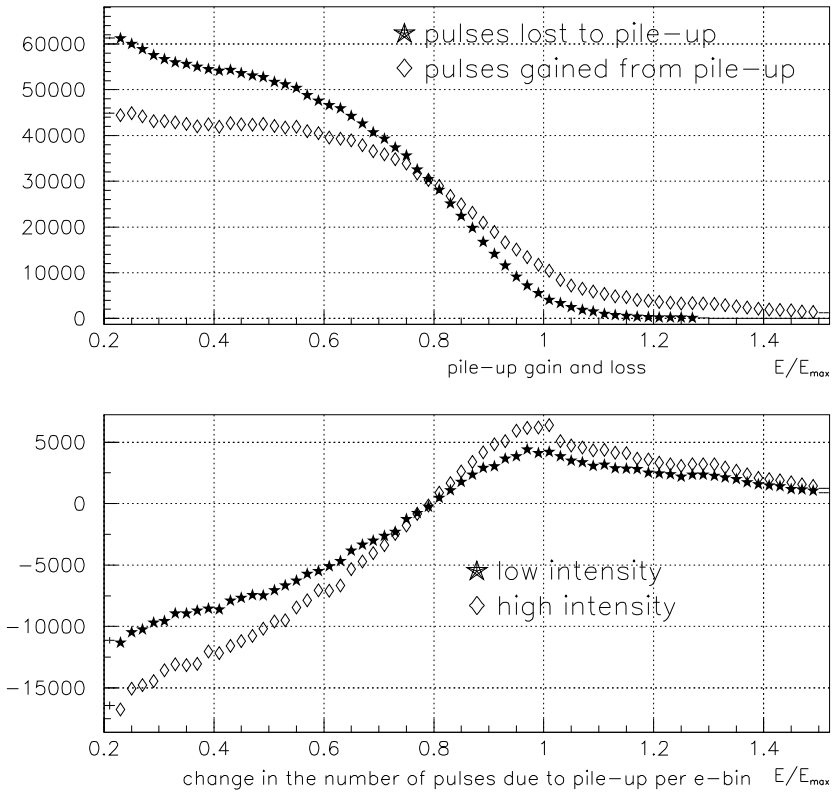

Fig.B3. Positive and negative pile-up. (top) Distribution of the number of positrons lost and gained due to pile-up; (bottom) net change in the number of positrons per energy bin at high and low intensity (4 and 3 MHz rate)

The pile-up fraction (the difference between the number of pulses gained and lost due to pile-up divided by the total number of pulses) grows almost exponentially as a function of low-energy cut for cuts higher than 1.5 GeV (Fig.B4, top part). This however is not exactly the same as the fit parameter n_p in g-2 multi-parameter fitting function (Eq. 2 in main section), the fraction of pile-up pulses at time t=0. If N is the total number of pulses, N_1 is the number of "singles", and N_p is the number of pile-up pulses ("doubles"). Then these parameters are related to the fit parameters in the following way:

$$N_p \simeq \int_0^{t_{stop}} (n_p \cdot N_0 \cdot e^{-2\lambda t} \cdot) dt \simeq \frac{n_p \cdot N_0}{2\lambda} \qquad (B1)$$

$$N_1 \simeq \int_0^{t_{stop}} (N_0 \cdot e^{-\lambda t}) dt \simeq \frac{N_0}{\lambda} \qquad (B2)$$

$$N = N_p + N_1 \qquad (B3)$$

(Fast rotation correction and g-2 wiggle are neglected in Eqs.B1 and B2.) Knowing the

fraction of all pile-up pulses at all times (N_p/N), it is easy to calculate a prediction for n_p:

$$n_p \quad = \quad \frac{2 \cdot (\frac{N_p}{N})}{1 - (\frac{N_p}{N})} \qquad (B4)$$

This prediction is plotted in the bottom part of Fig.B4.

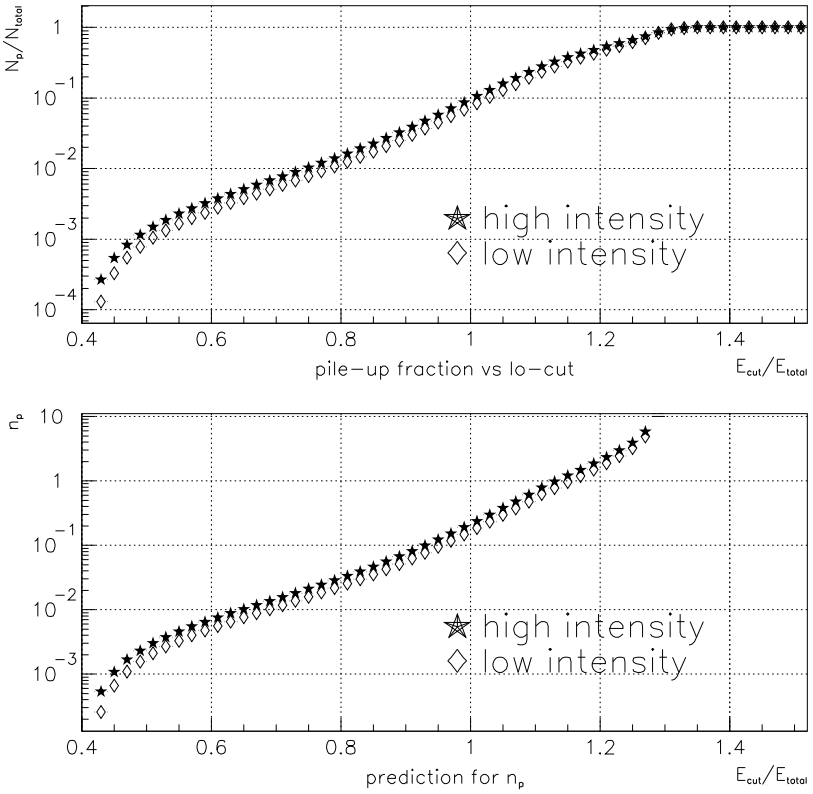

Fig.B4. (Top) fraction of pile-up pulses ($\frac{N_p}{N}$) as a function of lower energy cut (normalized to $E_{max} = 3.1$ GeV; for 4 ("high") and 3 ("low") MHz decay rate); and (bottom) prediction (Eq. B4) for the fit parameter n_p based on the top plot. Prediction agrees very well with the results of fitting to the real data.

Dividing a pile-up time spectrum obtained using a simulation including fast rotation by a "fast-rotation-off" spectrum, one gets a prediction of the inflation of pile-up caused by fast rotation (Fig.B5, top). This inflation was fitted to a 2-parameter function:

$$f_{fr}(t) = 1 + a_p \cdot e^{-\frac{1}{2}(\frac{t}{\tau_p})^2} \qquad (B5)$$

The results are shown in Fig.B5. The values of the pile-up inflation parameters are very close for different lower energy cuts. The difference between the results for different decay rates (3 and 4 MHz) was within a statistical error. For the cut $0.6 \cdot E_{max}$, the parameters of Eq.B5 were found to have the following values: a_p = (0.709 $\pm$ 0.008) and

τ_p = (12.84 $\pm$ 0.17) μs.

This result agrees very well with the one obtained from the energy-scale studies described in Appendix A: a_p = (0.714 $\pm$ 0.038) and τ_p = (12.59 $\pm$ 0.29) μs.

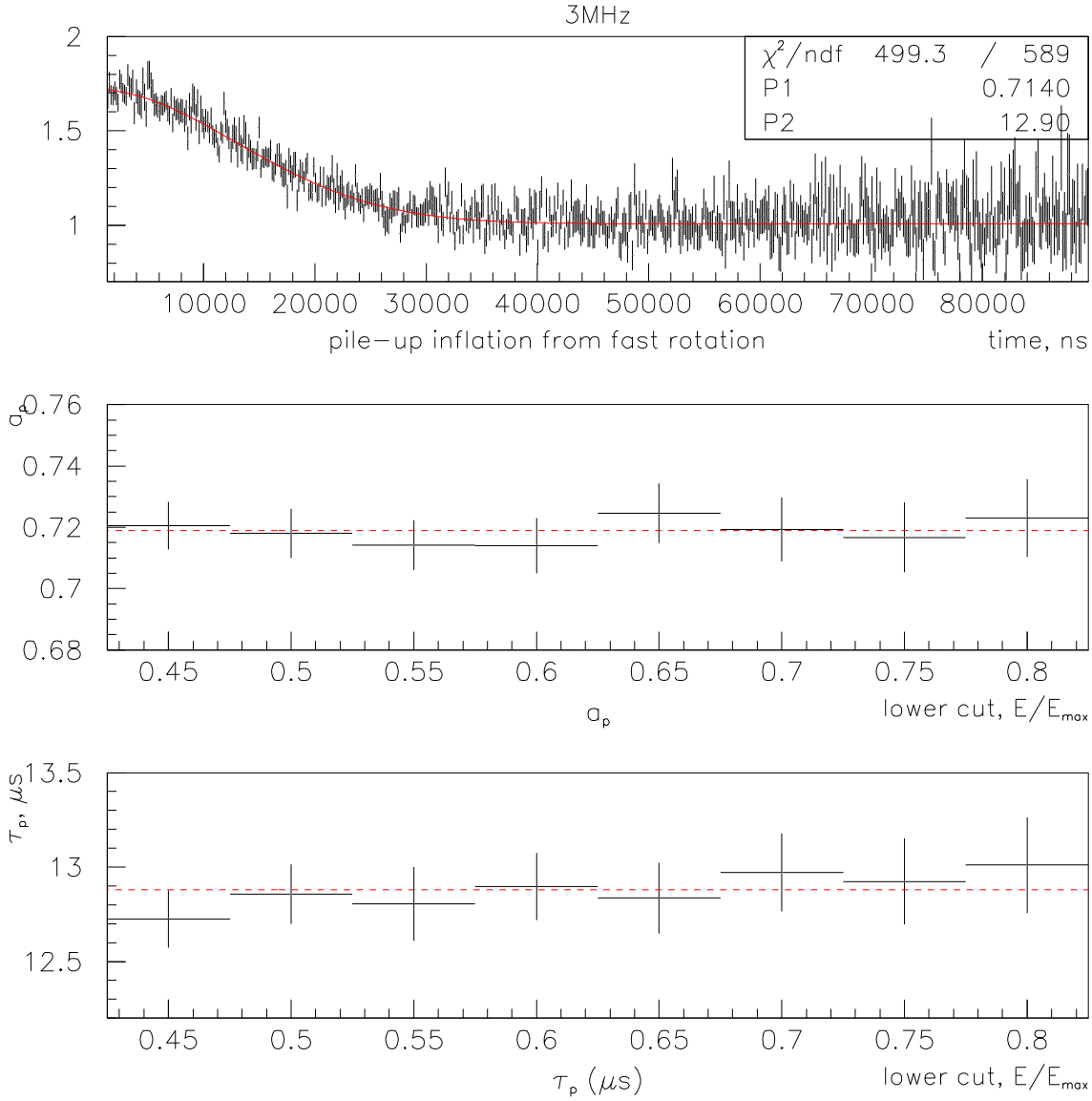

Fig.B5. Results of a 2-parameter fit (Eq.B5) to the pile-up inflation from fast rotation (simulation, decay rate 3 MHz). Top: pile-up inflation for a data set with the lower cut of 60% percent of the maximal positron energy. Middle: inflation amplitude, a_p as a function of lower cut value. Bottom: inflation characteristic time, τ_p as a function of lower cut value.

An attempt to estimate the pile-up phase as a function of cut using the simulation results showed that the pile-up phase is changing rather rapidly, when the asymmetry is small, and is shifting by π rad when the asymmetry is crossing zero. For the cuts of interest (1.8 and 2 GeV), the simulation prediction for the value of asymmetry came out to be higher then the values obtained by fitting the data, therefore it is hard to judge if this simulation can be used to predict the pile-up phase in the real data.

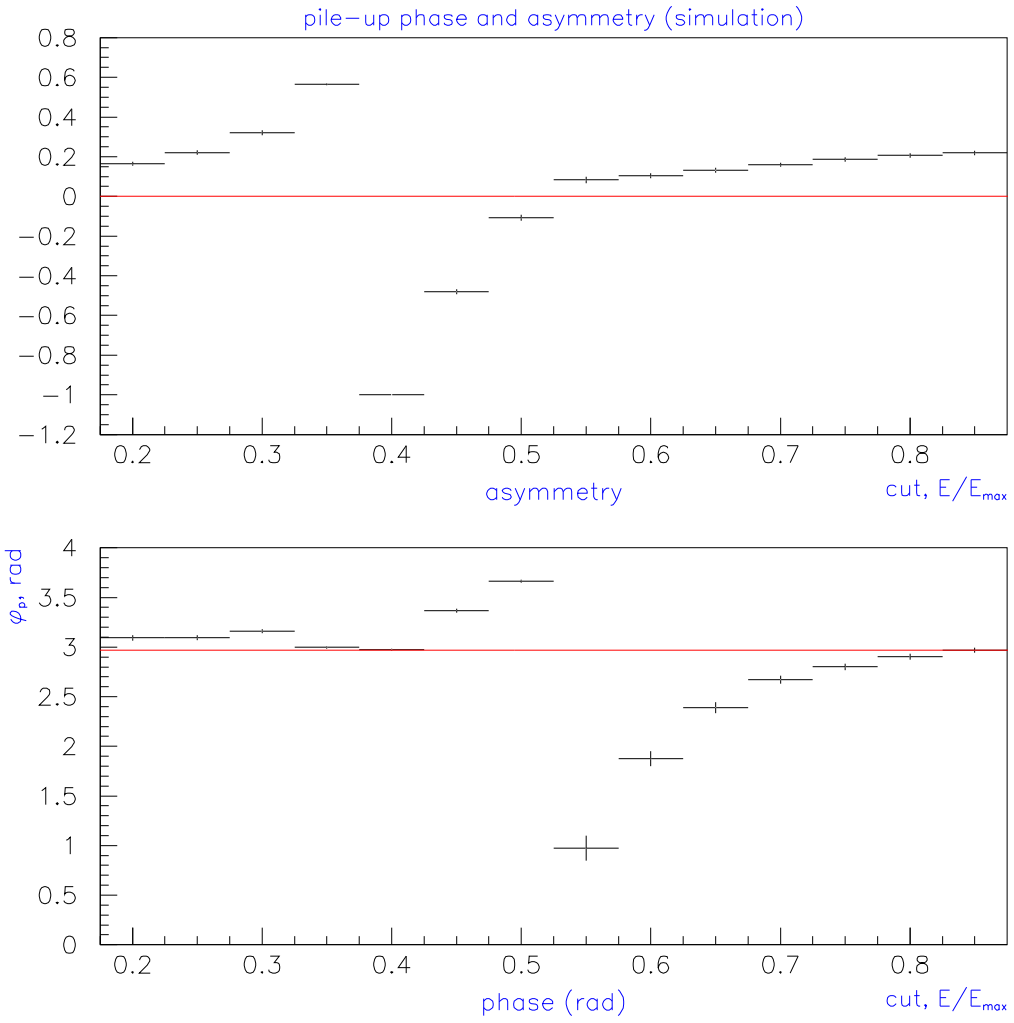

Fig.B6. Pile-up asymmetry (normalized to pile-up fraction) and phase as a function of the energy cut. Pile-up pulses were extracted from simulated data and the distribution fitted to $N(t) = N_0 \cdot e^{-\lambda_p t} \cdot (1 + A_p \cdot \cos[\omega_a t + \phi_p])$. *Asymmetry is singular where pile-up fraction crosses zero (0.35 - 0.4·*E_{max}*). And the phase is singular when the asymmetry crosses zero. G-2 phase was close to 3 rad for all positron energies in this simulation (red line on the bottom plot). The phase difference between the g-2 precession and pile-up is changing dramatically when the pile-up asymmetry is small.*

References

1. I. Logashenko, g-2 note 334.
2. C. Özben, g-2 note 385.
3. C. Özben, g-2 note 347.
4. J. Pretz, g-2 note 353.
5. `MINUIT` Reference Manual, CERN.
6. G. Onderwater and J. Pretz, g-2 note 363.
7. D. Kawall, g-2 note 322.
8. D. Hertzog, private communication.
9. R.Carey, g-2 note 382.
10. C. Özben, Y.Semertzidis, g-2 note 365.
11. S.Redin, g-2 note 387.
12. Y.Semertzidis, presentation at the off-line meeting, BNL, December 14-15, 2000.
13. G. Marsaglia, A. Zaman and W.-W Tsang, **Stat. Prob. Lett 9** (1990), 35
14. Y. Orlov, g-2 note 336.
15. V.Druzhinin, G.Fedotovich, g-2 note 375.
16. S. Redin, g-2 note 342.
17. 0. Rind, private communication.
18. L. Duong, Ratio Fit Results to g2off Data (Draft of g-2 note)